INAUGURAL DISSERTATION

submitted to the

Combined Faculties for Natural Sciences and for Mathematics

of the Ruperto-Carola University of Heidelberg, Germany

for the degree of

Doctor of Natural Sciences

pesented by

Dipl. Biol. Regina Mark

born in Bad Mergentheim

date of oral examination .....

S100-RAGE signaling in the pathogenesis of Head and Neck Squamous Cell Carcinoma

Referees: Prof. Dr. Peter Angel
Prof. Dr. Alexander N.R. Weber

To my parents

Contents

Summary

An aberrant expression of RAGE (receptor for advanced glycation end products) and its ligands, especially the S100-calgranulins has been demonstrated in squamous cell carcinoma of the upper aerodigestive tract. However, while S100-RAGE signaling is commonly linked to the induction and maintenance of a cancer promoting inflammation, the question whether RAGE-signaling is causally linked with neoplastic transformation of keratinocytes in mucosal epithelia has not been addressed so far. The presence of S100-calgranulin positive infiltrating immune cells as well as S100-calgranulin expression in tumor cells was assessed in oropharyngeal squamous cell carcinoma (OPSCC) on tissue microarrays (TMAs) containing tumor biopsies from 188 human patients and compared with the amount of CD66b positive myeloid inflammatory cells on the same TMAs. To address the causal role of S100-RAGE signaling in the onset of oral carcinogenesis, the well established mouse model of 4-nitroquinoline-1-oxide (4-NQO) induced carcinogenesis was used to investigate tumor development in control and RAGE deficient ($Rage^{-/-}$) mice as well as mice deficient in S100a9 ($S100a9^{-/-}$). While patient tumors varied strongly with regard to the amount of S100-calgranulin and CD66b positive immune cells as well as the expression pattern of S100-calgranulins in tumor cells, these features did not correspond with clinico-pathological parameters or prognosis. In the onset of oral and esophageal cancer, driven by 4-NQO induced genotoxic stress and in the absence of an additional inflammatory stimulus, both Rage and S100a9 expression was dispensable for tumor development. In both cohorts, mice developed tumors in the esophagus and tongue with similar incidence rates and comparable multiplicity. Also a detailed analysis of tumor sections by histological and immunohistochemical staining revealed no difference in size or histological architecture of 4-NQO induced lesions, tumor cell proliferation and the number of inflammatory immune cells in the tumor microenvironment. S100a8 and S100a9 were induced upon 4-NQO treatment independent of the presence of RAGE, which may in part be explained by induced transcript and protein levels of the Toll-like receptor 4 (Tlr4) in carcinogen treated tissue, suggesting that signaling via the S100-TLR4 axis may compensate for the lack of RAGE in early stages of tumor development. In summary, these data point out that the impact of S100-RAGE signaling is critically depending on the context. While important in inflammation associated cancer, S100-RAGE signaling is dispensable in cancer caused by genotoxic stress without a promoting inflammation. With regard to therapy and prevention, this illustrates the need of a clear stratification for the presence of a driving inflammation.

Zusammenfasung

Eine aberrante Expression von RAGE (receptor for advanced glycation end products) und seiner Liganden, insbesondere der S100-Calgranuline ist beschrieben für Plattenepithelkarzinome des oberen aerodigestiven Trakts. Während jedoch der S100-RAGE Signalweg gemeinhin verknüpft ist mit dem Auslösen und der Aufrechterhaltung einer tumorfördernden Entzündung, wurde die Frage, ob RAGE abhängige Signalwege kausal mit der neoplastischen Transformation von Keratinozyten in Schleimhäuten zusammenhängen, bisher nie adressiert. Das Vorhandensein S100-Calgranulin positiver inflammatorischer Zellen in Plattenepithelkarzinomen des Oropharynx (OPSCC) wurde analysiert mittels Gewebe- Mikrochips (TMA), welche Gewebeproben von 188 Patienten enthielten und mit der Anzahl CD66b positiver myeloider Entzündungszellen auf den selben TMAs verglichen. Um die kausale Rolle des S100-RAGE Signalwegs in der Entstehung von Kopf-Hals Tumoren auf einer funktionalen Ebene zu adressieren wurde das gut etablierte Maus-Tumormodell der 4-Nitroquinolin-1-Oxid induzierten oralen Karzinogenese verwendet, um Tumorentwicklung in Kontrollen, sowie RAGE defizienten ($Rage^{-/-}$) und S100a9 defizienten ($S100a9^{-/-}$) Mäusen zu ermitteln. Während die Tumore sich stark in der Anzahl der S100-Calgranulin-, als auch der CD66b-positiven Immunzellen sowie den Expressionsmustern der S100-Calgranuline unterschieden, deckten sich diese Beobachtungen nicht mit klinisch-pathologischen Patientenparametern oder der Prognose. In der 4-NQO getriebenen Entstehung von Krebs in der Mundhöhle und der Speiseröhre ohne einen zusätzlichen entzündlichen Stimulus war weder die Expression von RAGE noch von S100a9 notwendig für die Entwicklung eines Tumors. In beiden Kohorten entwickelten die Mäuse mit ähnlichen Inzidenzraten und vergleichbarer Multiplizität Tumore auf Zunge und Ösophagus. Auch eine detaillierte histologische und immunhistochemische Analyse der Gewebeschnitte zeigte keinen Unterschied in der Größe oder histologischen Architektur der 4-NQO induzierten Läsionen, der Tumorzellproliferation und der Anzahl der Entzündungszellen in der Tumor-Mikroumgebung. S100a8 und S100a9 waren nach 4-NQO Behandlung unabhängig von der Gegenwart von RAGE induziert, was teilweise exhilarate werden kann durch die Induktion von Toll-like Rezeptor 4 (Tlr4) auf Transkript- und Proteinebene in Karzinogen-behandeltem Gewebe und darauf hindeutet, dass S100-Tlr4 Signaltransduktion den Verlust von RAGE in frühen Stadien der Tumorentwicklung kompensieren könnte. Zusammenfassend zeigen diese Daten, dass die Bedeutung der S100-RAGE Signalkaskade stark kontextabhängig ist. Während er wichtig ist bei entzündungs-abhängiger Tumorgenese, ist der 100-RAGE Signalweg entbehrlich bei Tumoren welche durch genotoxischen Stress ohne treibende Entzündung verursacht werden. Bezüglich Therapie und Prävention verdeutlicht dies die Notwendigkeit einer klaren Stratifizierung hinsichtlich des Vorhandenseins einer treibenden Entzündung.

Acknowledgements

I would like to say thank you to...

... Prof. Dr. Peter Angel and PD Dr. Jochen Heß for taking me into their labs.

... Prof. Dr. Alexander Weber for helpful suggestions in my advisory committee and for being second examiner in my disputation

... Prof. Dr. Herbert Steinbeisser for stepping in as member of the advisory committee and for being an examiner in my disputation

... PD Dr. Karin Müller-Decker for excellent support with the mouse experiments and for being an examiner in my disputation

... the late Prof. Dr. Angelika Bierhaus, who was a member of the advisory committee and who will always be remembered for her enthusiasm about science.

... my supervisor PD Dr. Jochen Heß for valuable discussion and encouragement and his inexhaustible optimism.

... Ines Kaden, Nataly Henfling, Antje Schuhmann and Ingeborg Vogt for excellent technical assistance as well as well as Angelika Krischke for help with the tissue sectioning.

... the Bosch-lab for taking me in and giving me a new scientific "home" in Heidelberg and Dr. Franz Bosch for sharing valuable experience and insights into the biology of HNSCC.

... Lars Wiechert for introducing me into the lab and sharing of experience and material, especially the *S100a9*$^{-/-}$ mice.

... all my colleagues at dkfz and in the clinic, especially Antje, Ines, Nataly, Pilar, Effie, Dana, Markus and Sonja for creating a great working atmosphere in the lab.

... all the mice that lost their lives in the course of this thesis.

... Ann-Mareen Räthe for sharing scientific ideas, coffee and her friendship.

... my flatmates Sönne, Sabine, Alice and Anne who became close friends on the way and our common special friend Monti.

... my friends, without whom the world would be empty.

... my parents who always encouraged and supported me. And my little sister and best friend, Anna-Maria.

List of Figures

List of Tables

Abbreviations

Abbreviation	Expanded form
° C	Degree Celcius
4-NQO	4-nitroquinoline-1-oxide
AP-1	Activator protein 1
BF	Bright field
Bps	Base pairs
BrdU	Bromodeoxyuridine
CD66b	Cluster of Differentiation 66b
cDNA	Complementary deoxyribonucleic acid
CEACAM8	Carcinoembryonic antigen-related cell adhesion molecule 8
COX	Cyclooxygenase
DAMP	Damage associated molecular pattern
DdH2O	Double destillated water
DF	Dark field
DMBA	Dimethylbenz[a]anthracene
DNA	Deoxyribonucleic acid
DNase	Deoxyribonucleic acid hydrolase
DNTP	Deoxynucleotide triphosphate
E6	HPV early gene 6
E7	HPV early gene 7
EDTA	Ethylene diamine tetraacetic acid
EGFR	Epidermal growth factor receptor
ENT	Ear, nose and throat
EtOH	Ethanol
g	Gram
G-CSF	Granulocyte colony-stimulating factor
GM-CSF	Granulocyte-macrophage colony-stimulating factor
h	hour(s)
H&E	Hematoxilyn & eosin
H_2O_2	Hydrogen peroxide
HKG	House-keeping gene
HMGB1	B1 High-mobility group box 1 protein
HNSCC	Head and neck squamous cell carcinoma
HPV	Human papilloma virus
IHC	Immunhistochemistry
Il	Interleukin
JNK	Janus kinase

Abbreviation	Expanded form
K13	Keratin 13
K13	Cytokeratin 13
K14	Keratin 14
K14	Cytokeratin 14
KCL	Potassium chloride
KDa	Kilo Dalton
M	Metastasis
MAPK	Mitogen-activated protein kinase
Min	Minute(s)
mg	Miligram
ml	Milliliter
mm	Millimeters
mM	Millimolar
mRNA	Messenger RNA
Mrp	Migration inhibitory factor-related protein
µg	Microgram
µL	Microliter
µm	Mikrometer
µM	Mikromolar
N	Nodal stage
n	Number of samples
NaCl	Sodium chloride
NADPH	Nicotinamide adenine dinucleotide phosphate, reduced
NaOH	Sodium Hydroxide
NF- κB	Nuclear factor κ light chain enhancer of activated B cells
o/n	Over night
OCT	Optimal cutting temperature
OPSCC	Oropharyngeal squamous cell carcinoma
OS	Overall survival
p	Probability
p.a.	Pro analysi
PBS	Phosphate buffered saline
PCR	Polymerase
PFS	Progression Free Survival
pH	Pondus hydrogenii
PhD	Philosophiae doctor
PI3K	Phosphoinositide 3-kinase
PS	progression free survival
Pten	Phosphatase and tensin homolog
qRT-PCR	Quantitative real-time PCR
Rage	Receptor for advanced glycation end products
Rage$^{-/-}$	Rage knockout mouse
Rage$^{+/-}$	Heterozygous Rage knockout

Abbreviation	Expanded form
ras	Rat sarcoma
Rb	Retinoblastoma protein
RNA	Ribonucleic acid
RNase	Ribonucleic acid hydrolase
ROS	Reactive oxygen species
rpm	Rounds per minute
rt	Room temparature
S100a9$^{-/-}$	S100a9 knockout mouse
S100a9$^{+/-}$	Heterozygous S100a9 knockout mouse
SCC	Squamous cell carcinoma
SD	Standart deviation
SDS	Sodium dodecylsulfate
sec	second(s)
sRage	Soluble Rage
SSC	Sideward scatter
Stat	Signal transducer and activator of transcription
T	Tumor stage
T_A	Annealing temparature
T_m	melting temparature
TAM	Tumor associated macrophage
TAN	Tumor associated neutrophil
Taq	Thermus aquaticus
TBE	Tris borate EDTA
Tgfbr	Transforming growth factor-beta receptor
TGF-β	Transforming growth factor-beta
TLR	Toll-like receptor
TMA	Tissue Microarray
TNF	Tumor necrosis factor
TNM	Tumour, node, metastasis status
TPA	12-O-tetradecanoyl-phorbol-13-acetate
Tris	Trizma
U	Units
UK	United Kingdom
V	Volt
v/v	Volume to volume
W	Watt
w/v	Weight to volume
WHO	World Health Organisation
wt	Wild type

1 Introduction

1.1 The receptor of advanced glycation end products and its ligands

Encoded by the *Ager* gene, the receptor of advanced glycation end procucts (RAGE) is located within the major histocompatibility complex class III (MHC III) region on human chromosome 6 and in mice on chromosome 17. It belongs to the immunoglobulin superfamily of cell surface receptors and consists of a short cytoplasmic domain, which is proposed to be responsible for signaling, a transmembrane domain and a V-type and two C-type domains at the extracellular part [171, 183, 175]. First characterized 30 years ago [140], RAGE was described and hence named for its ability to bind advanced glycation end products (AGEs). AGEs are produced by non-enzymatic reactions of sugar with free amino groups of cellular proteins, lipids and nucleic acids and accumulate under conditions of metabolic disorders such as Diabetes mellitus [68]. Meanwhile, there is increasing experimental evidence supporting that RAGE can function as a pattern recognition receptor for various ligands (Fig. 1.1), many of which belonging to the group of damage associated molecular patterns (DAMPs) which are released upon cellular stress conditions [175, 58]. Multiple proteins, such as advanced glycation end products (AGEs), S100 proteins, amyloid beta proteins, high mobility group box 1 (HMGB1), and fibrillar protein aggregates trigger intracellular signaling pathways like Ras, MAPK and PI3-Kinase/Akt, JNK/AP-1 or JAK/Stat3 signaling initiated at RAGE and thereby regulate tissue homeostasis and regeneration as well as pro-inflammatory responses in endothelial and epithelial cells, smooth muscle cells, and mononuclear phagocytes [91, 105, 88, 199, 175]. Downstream transcription factors are NF-κB, AP-1 and Stat3, all well described in the context of inflammation and cancer. Signaling via RAGE induces pro-inflammatory me-

diators, including it's ligands S100A8 and S100A9 via NF-κB activation [141]- Containing a NF-κB binding site in it's proximal promoter region, RAGE thus also upregulates it's own expression [120]. Of particular interest in the context of inflammation are members of the S100 protein family. They are small EF-Hand calcium binding proteins with a low molecular weight, named for the 100% solubility in ammonium sulfate of its first described family members S100A1 and S100B [134].

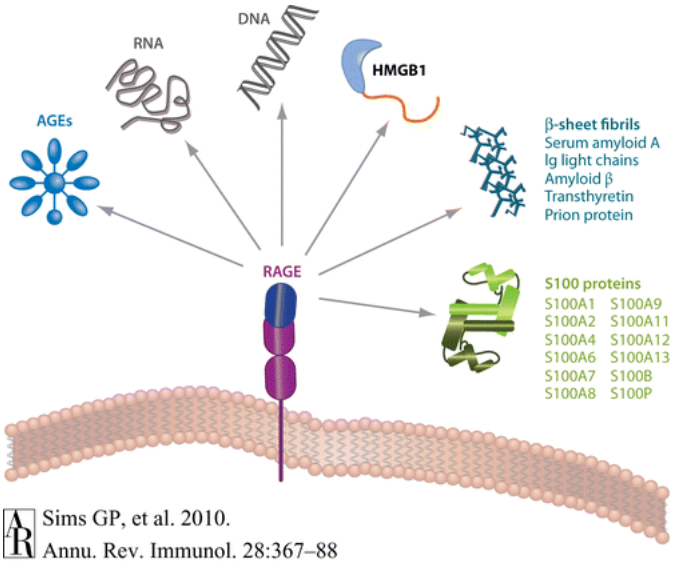

Figure 1.1: The receptor for advanced glycation end products (RAGE) and its ligands. RAGE serves as a pattern recognition receptor for various groups of ligands, such as advanced glycation end products (AGEs), protein aggregates like ß-sheet fibrils, amyloid-ß Protein, several S100-proteins, most importantly S100A8/A9 and high mobility box protein 1 (HMBG1). (Figure taken from Sims et al. 2011 [175]).

The human S100 protein family consists of 25 members with different tissue specific expression patterns; functionally they all have specific tasks [40, 129, 58]. Several S100 Proteins like S100B, S100P, S100A1, S100A2, S100A4, S100A5, S100A6 S100A7 and S100A8/A9, S100A12 and S100A13 are reported to bind RAGE in vivo or in vitro [58]. In the context of inflammation and cancer prominent RAGE ligands among the S100-Proteins are the members of the calgranulin family S100A8 and S100A9 and S100A12.

1.2 RAGE in tissue development and homeostatis

While most studies focusing on RAGE address it's function in inflammation and in the context of human pathologies, little is known so far about the physiologic function of RAGE. No or very low expression levels are detected under physiological conditions in most tissues and cell types, yet during embryonic development RAGE is continuously expressed [24]. In vitro studies showed a contribution of RAGE in axon sprouting in neuronal development [85, 92]. However, RAGE deficient mice do not show any obvious developmental defect and have normal neural development. In general *Rage*$^{-/-}$ mice appear normal and healthy showing no obvious alterations under physiological conditions except a mild pro-inflammatory phenotype [122]. Furthermore, while RAGE expression is downregulated in most organs during development, in the adult lung RAGE is constitutively expressed at high level in the alveolar epithelia [24, 101]. RAGE was proposed to be critically involved in lung development in the embryo and post-natal pulmonary morphogenesis [156]. Interestingly, during lung development, high levels of RAGE expression result in severe lung hyperplasia and subsequently perinatal lethality [186]. Also in the adult lung, RAGE hyper-expression results in alveolar destruction and a persistent inflammatory status [52], arguing that RAGE expression levels need to be tightly controlled during embryonic development. On the other hand, in lung cancer patients pulmonary carcinogenesis is accompanied by a loss of RAGE expression, suggesting a role for RAGE as a tumor suppressor in lung [12]. However, RAGE deficient mice do not display a lung phenotype, the lung develops normally and the animals do not show respiratory problems or histological alterations. The specific role of RAGE in lung epithelia as well as it's physiological role in other tissues therefore remains puzzling.

1.3 RAGE in pathological conditions and cancer

As a DAMP receptor, RAGE may also serve in the clearance of AGEs and other damage associated molecules [66]. Upon stress conditions, damage and inflammation, RAGE is strongly upregulated in various tissues. Elevated levels of RAGE and/or its ligands have been reported under pathological conditions of late diabetic complications, acute and chronic inflammation, neurodegenerative disorders, as well as cancer [158, 18, 119]. While RAGE deficient mice display a mild pro-inflammatory phenotype, the animals were efficiently protected against septic shock in a model of polymicrobial septic peritonitis, [122] and resistant to lethality caused by Listeria monocytogenes infection [125]. Furthermore, RAGE is expressed in myeloid cells and lymphocytes which are recruited at sites of damage and inflammation [19, 31]and has been shown to induce human monocyte survival and differentiation [211].

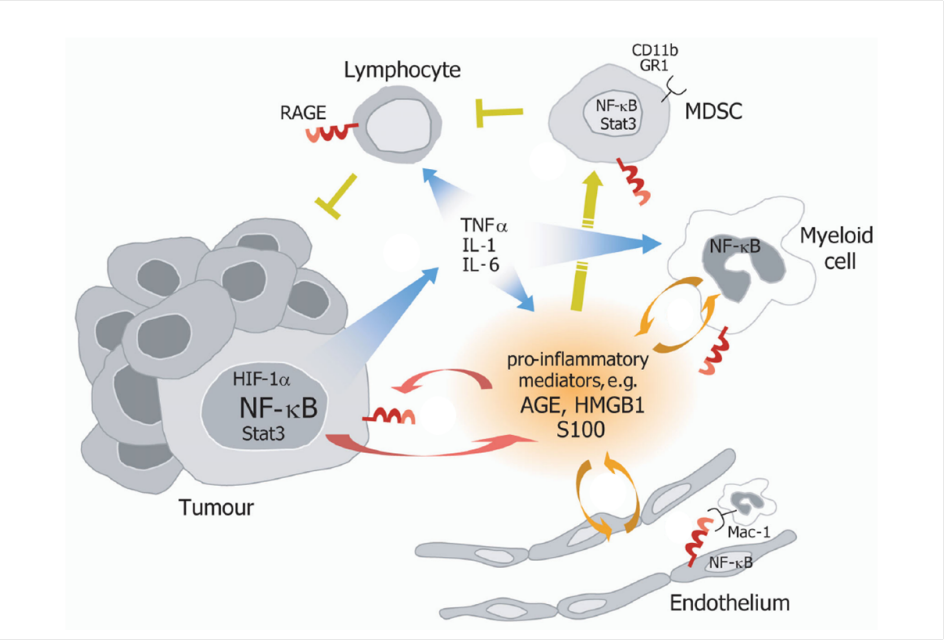

Figure 1.2: The receptor for advanced glycation end products (RAGE) and its ligands. RAGE is expressed on the different cell types of the tumor microenvironment, enabling the crosstalk of there cells via it's ligands (e.g. S100A8/A9) and thus modulating inflammatory reactions. (Figure taken from Riehl et al. 2009 [158])

An association of RAGE with several human malignancies is well documented. RAGE expression is thus linked to gastric cancer [113, 214], malignant neoplaisa of the bile duct [81], pancreatic cancer [194], and prostate cancer [100, 99]. Furthermore functional data from animal experiments as well as observations in human patients associate rage expression with inflammation associated cancer [112, 201, 60, 175]. A persistent tumor promoting inflammation serves as an enabling hallmark in the process of cancer formation [73]. While an anti-tumor immune response reduces or prevents tumor growth, chronic inflammation fuels cancer formation. Damage signals like extracellular S100A8/A9 or HMGB1 are proposed to create an inflammatory feed forward cycle via RAGE as a central modulator, linking inflammatory effector cells as well as epithelial cells and eventually driving the establishment of chronic inflammation (Fig. 1.2) [91, 158]. The role of inflammatory cells of the tumor microenvironment in pro-inflammatory RAGE signaling however is complex. Also, the exact role of immune cells in cancer strongly depends on the composition of immune cell subtypes. In particular intratumoral inflammatory cells of myeloid origin can act as a double edged sword mediating anti-tumor immunity or promotion a pro-tuumorigenic microenvironment [57, 178, 121, 154]. Furthermore the composition of inflammatory cells also depends on the etiology of inflammation associated cancer. While gastric cancer, caused by helibacter pylori infection [46] or hepatocellular carcinoma induced by viral hepatitis [45] present an active infection, chronic inflammation and damage, resulting in necrosis and the release of DAMPs can likewise lead to a sterile, non-infections inflammation and subsequent tumor formation [29, 175].

1.4 Impact of RAGE signaling in mouse tumor models

In inflammation associated cancer (Fig. 1.2) as well as other pro-inflammatory pathological conditions, RAGE functions as a central hub, converting a transient inflammatory stimulus into sustained cellular dysfunction [17, 158]. In the past, the analysis of several genetically-modified mouse models of intestinal and pancreatic cancer provided experimental evidence that ablation of RAGE on genomic level inhibits tumor development and progression [39, 77, 99]. Moreover, RAGE-deficient ($Rage^{-/-}$) mice showed impaired tumorigenesis in chemically induced models of inflammation-driven skin and colon carcinogenesis [60, 201]. Following a DMBA/TPA carcinogenesis protocol RAGE ligands S100a8 and S100a9 were strongly induced in backskin keratinocytes of papillary lesions of wild type mice [60], accompanied by a strong infiltration of S100a8 and S100a9 positive immune cells. While 9,10-dimethyl-1,2-benzanthracene (DMBA) induces ras-mutations in backskin keratinocytes, the inflammatory stimulus provided by the phorbol ester 12-O-tetradecanoylphorbol- 13-acetate (TPA) promotes tumor development. In accordance with the reduction in tumor incidence and multiplicity in these settings $Rage^{-/-}$ mice displayed reduced leukocyte recruitment and cytokine production during the initial phase of tumor promotion, supporting the assumption that RAGE is a key player in the establishment and maintenance of a pro-inflammatory tumor microenvironment [157]. Intriguingly, once activated RAGE-signaling can upregulate both the expression of the receptor itself as well as its ligands, creating an inflammatory feed-forward loop [60].

1.5 Physiologic and pathologic roles of S100-calgranulins

Among the family of S100 proteins, the calgranulins are well described as inflammatory markers and play a distinct role as RAGE ligands in the context of cellular stress conditions and inflammation. While the family of S100-calgranulins consists of three family members, S100A8, S100A9 and S100A12 in humans, rodents lack the expression of S100A12 [155]. S100A12 functions as a dimeric aniparallel homodimer but can also form hexamers under low calcium conditions [136]. Also known as en-RAGE (extracellular newly identified RAGE binding protein) for its binding capacity to the receptor RAGE, S100A12 is implicated in RAGE mediated inflammatory processes [40, 83]. While the main focus of research was on S100A8/A9, little is known about the function of S100A12. It is mainly expressed in neutophilic granuolcytes and to some extend in monocytes[69]. S100A12 is secreted by activated innate immune cells and thus found as a serum marker in inflammatory conditions [132]. Additionally, expression of S100A12 has been described in differentiating mucosal keratinocytes [159].

Also named migration inhibitory factor-related protein 8 (MRP8) and MRP14, S100A8 and S100A9 are well known for their expression in immune cells [207]. In vivo they preferentially form an antiparallel heterodimer, known as calprotectin [37, 40]. While a complete knockout of S100a8 is embryonically lethal [148], S100a9 deficient animals appear phenotypically normal [82]. However, in peripheral leukocytes S100A8 protein stability critically depends on the presence of S100A9, suggesting that ablation of S100A9 may serve as a functional calgranulin knockout in mice [82]. S100A8 and S100A9 are mainly expressed in cells of myeloid origin, especially neutrophils but not in tissue-resident macrophages [115]. Secreted, S100A8 and S100A9 serve as a proinflammatory cytokine presenting danger signals for adjacent cells or immune cells. They mediate neutrophil chemotaxis, macrophage recruitment, leukocyte adhesion and transmigration, and trigger signal transduction via RAGE and Toll like receptor 4 (TLR4) [65, 131, 164]. Extracellular S100A8/A9 can originate from apoptotic neutrophils, but are also actively secreted. As both proteins lack signal peptides for classical secretion by the ER-Golgi pathway, release occurs in a Golgi-independent pathway [152, 182]. As indicated by it's name "calpro-

tectin", at sites of tissue damage and wounding, S100A8/A9 exert important anti-microbial functions [185]. Importantly, apart from their well described extracellular functions as damage signals, inducing signaling via DAMP receptors like RAGE and toll like receptors (TLRs), S100-calgranulins have also intracellular functions, ranging from myeloid cyotoskeletal rearrangement during cell migration to their implication in arachidonic acid metabolism and NADPH-oxidase regulation [59]. The heterodimer of S100a8/S100A9 functions as a coregulator in the formation of reactive oxygen species [21] and is involved in NFkB signaling [104, 141]. Under inflammatory conditions, S100A8/A9 are induced in endothelial and epithelial cells and are secreted by epidermal keratinocytes [213, 102, 182]. Also, induction of S100A8/A9 expression in inflammatory disorders like psoriasis, arthritis, cystic fibrosis, multiple sclerosis, and inflammatory bowel disease is often described. Accordingly, S100A8/A9 as well as S100A12 serum levels are commonly used as inflammatory biomarkers [128]. Furthermore, expression of RAGE ligands S100A8/A9 is detected in a variety of tumors, including colon, prostate and lung cancer as well as HNSCC ([59, 161].

1.6 Head and neck squamous cell carcinoma

The term head and neck cancer relates to a variety of malignant neoplasias of the upper aerodigestive tract. While adenoma and sarcoma only contribute to a minor amount of cases, the vast majority of cases represent squamous cell carcinoma of the head and neck (HNSCC). HNSCC mainly occur at the oral cavity, tongue, larynx and pharynx (Fig. 1.3).

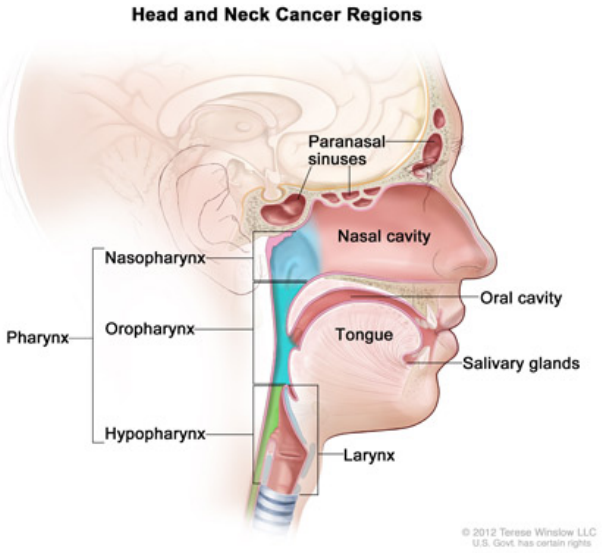

Figure 1.3: Anatomic sites and subunits of the head and neck.
image source: www.cancer.gov/PublishedContent/ Images/ cancertopics/factsheet/ Sites-Types/headandneck-diagram.jpg.

The main risk factors in the western world are alcohol and tobacco consumption, which synergistically account for a large proportion of HNSCC cases [145]. In south-east Asia and India betel quid chewing represents another important risk factor for HNSCC [96]. Although inherited disorders such as Fanconi anemia render a predisposition for the development of the disease [114], they play only a minor role. In oropharyngeal cancer, HPV infection has been shown to not only induce cancer but also form a molecular, epidemiological and clinical distinct subgroup of OPSCC patients [62, 7, 84] and is meanwhile considered an independent risk factor. With around 650.000 new cases each year, HNSCC presents the 6th most common cause for cancer in man worldwide. Roughly three times more men suffer from HNSCC than women. Variations in the

incidence result from different lifestyle habits concerning the main risk factors. (Fig. 1.4) [147, 51, 23, 133]. In Germany, tumors of the oral cavity and pharynx are the 5th most common cancer in the male population. The age standardized rate per 100.000 inhabitants for tumors of the oral cavity and pharynx was 18.7 for men and 5.7 for women, and laryngeal cancer 6.9 and 0.9 [107, 106].

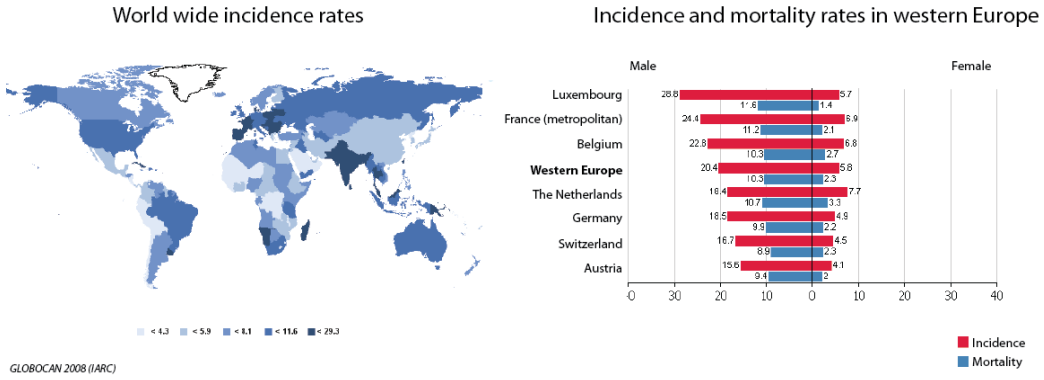

Figure 1.4: Age-standardized incidence rate of head and neck cancer world wide and standardized incidence and mortality rates in western Europe. Included are tumors of the lip, oral cavity, nasopharynx and other pharynx as well as larynx. . Incidence rates for HNSCC are in western Europe rates are age standardized and calculated per 100,000 inhabitants. Data and image source: GLOBOCAN 2008; Cancer Incidence and Mortality Worldwide in 2008 [50]

Only 40-50% of newly diagnosed patients survive 5 years after diagnosis. The prognosis largely depends on the stage when patients are diagnosed with a tumor. While early stage tumors can be treated effectively, the majority of patients present with already advanced stages, often with lymph node involvement [198, 145]. Advanced tumors are mainly treated by surgical resection of the tumor in combination with adjuvant radio- and/or chemotherapy, however in most cases with low clinical benefit. The majority of patients suffer either from tumor recurrence within one to three years following first-line therapy or the formation of secondary tumors, which are often more aggressive and refractory to available treatment options [90].

1.7 Molecular mechanisms of head and neck squamous cell carcinoma

Head and neck squamous cell carcinoma present a heterogeneous disease. Histologically, pathologists differentiate between different types according to the world health organization (WHO) classification of 2005, the conventional, verrucous, basaloid, papillary, spindle cell, acantholytic, adenosquamous and the cuniculatum type [11, 145]. On a molecular level, apart from the obvious stratification into HPV positive and HPV negative tumors, especially within the HPV negative group tumors differ strongly with regard to genetic mutations and transcription profiles [33, 4, 187]. In almost all HNSCC patients p53 and retinoblastoma (Rb) pathways are disrupted. In HPV negative HNSCC, the most common molecular genetic alterations are mutations of p53, overexpression of Cyclin D1, hypermethylation of the p16 promoter and loss of heterozygosity at several chromosomal regions, most importantly 3p, 17p13 and 9p21 [144, 205, 150, 118]. Interestingly, mutations in classical hotspot regions like the PIK3CA gene or RAS proteins are less common in HNSCC. In only about 10 % of cases, PI3-kinase is mutated [151, 163, 108]. Also mutations in the RAS oncogene are often observed among the Indian population but less frequently in HNSCC in the western world [166, 6, 163]. Even though treatment options of many cancer entities have been improved mainly due to the progress in basic and translational cancer research, over the last decades the prognosis for HNSCC patients remains constantly poor. The epithelial growth factor receptor (EGFR) is commonly overexpressed in HNSCC [167, 72], often due to genetic amplification [173], presenting an important therapeutic target for targeted treatment options. Increased EGFR signaling leads to cell cycle progression and enhanced proliferation via the Ras-MAPK, PI3K-PTEN-AKT and phospholipase C pathways [34, 93]. As targeted therapy only EGFR blocking antibodies such as Cetuximab are licensed for therapy of HNSCC, in combination with classical treatment regimen [174]. Various pro-inflammatory cytokines are deregulated in HNSCC tumors. Interleukin (IL) 1-α, IL-6 and IL-8, granulocyte-macrophage colony-stimulating factor (GM-CSF) as well as vascular endothelial growth factor (VEGF) are secreted by HNSCC cell lines and found in HNSCC patient samples [32]. Also, key transcription factors downstream of inflammatory processes like NF-κB and Stat3 have been shown

to play an important role also in HNSCC [127, 180, 117, 3]. The expression of another player in inflammatory reactions as well as human malignancies, Prostaglandin E2 (PGE2), alongside with the expression of Cyclooxygenase-2 (Cox2) was shown to be increased in HNSCC [27, 1, 208]. Chemoprevention using non-steroidal anti-inflammatory drugs (NSAIDs) in the treatment of HNSCC and more recently curcumin (diferuloylmethan) from the *curcuma longa* plant, are under evaluation concerning treatment success in the clinics [5, 2, 35].

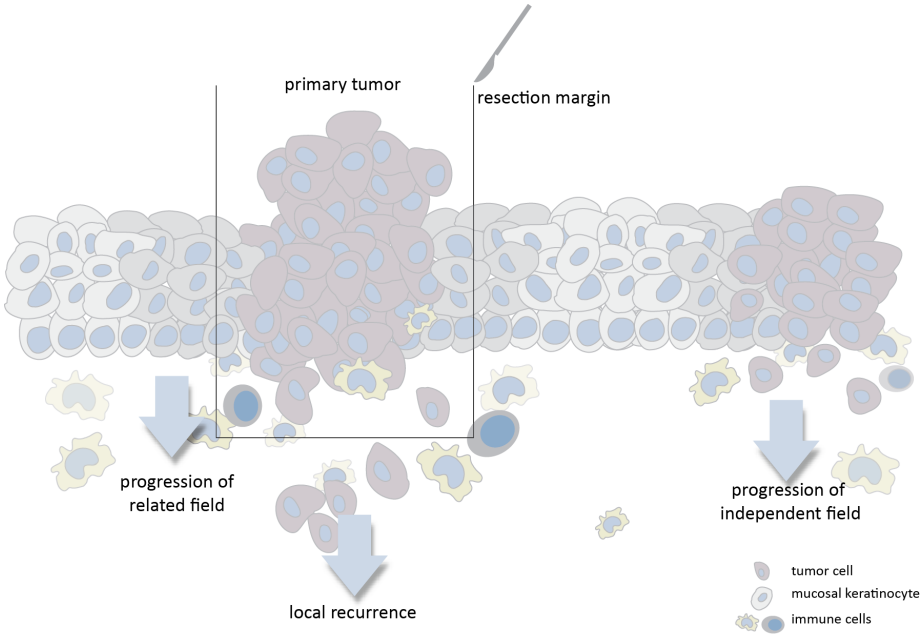

Figure 1.5: Field cancerisation and local relapse.
Fields of genetically altered epithelial cells, originated from clonal expansion of a transformed cell give rise to tumors. After resection, transformed cells from such a field can stay behind as they appear macroscopically and cyctologically normal but with time give rise to secondary tumors. (graphic modified after Leemans et al. 2011 [118])

Similar to other solid tumors, the pathogenesis of HNSCC represents a multistage process, which is characterized by the accumulation of genetic and epigenetic aberrations, which finally lead to squamous hyperplasia and trough advancing stages of dysplasia to invasive squamous cell carcinoma [118]. Already a half century ago the model of field cancerisation was proposed to explain the high rate of local recurrence in patients with HNSCC [177]. Carcinomas arise within large areas of genetically altered cells which arise from

the clonal expansion of a transformed preneoplastic cell (Fig. 1.5). While precancerous lesions such as leukoplakia or erythroplakia are easily recognized by eye in the oral cavity, large areas of the mucosa can be transformed without macroscopically appearing suspicious. Thus, the surgical margin may often retain cells from the previously transformed field, giving rise to a local recurrence or second primary tumor. Furthermore, due to the etiological factors, this concept of field cancerisation is not restricted to one, but often several areas of the mucosal epithelium that become transformed and can in time give rise to neoplastic lesions [26, 191, 118].

1.8 A mouse model for multistage carcinogenesis of oral squamous epithelia using 4-NQO

Despite various advances in the field of cancer therapy, the high morbidity and mortality in HNSCC remains a major challenge for basic and translational cancer research. Therefore preclinical animal models are of fundamental importance in order to better understand the underlying molecular mechanism of the disease. In the past, several animal models have been developed to investigate the cellular and systemic mechanisms of HNSCC. While genetically engineered mouse models are a common tool in biomedical research, for the investigation of HNSCC few proved to be successful. Aberrant activation of Akt in epithelial basal cells induces tumor formation [172] and was used in combination with the epithelial ablation of p53 to study oral carcinogenesis in mice [135]. Classical p53 knockout mice show a high susceptibility to tumor formation, lesions develop spontaneously within 5 months [41], presenting serious limitations regarding their application in HNSCC. However in combination with local DMBA administration, targeted induction of lesions in $p53^{+/-}$ mice presents a model, which recapitulates both tumor formation and the development of metastatic SCC [109]. Conditional activation of PI3K/Akt pathway due to Pten inactivation is not sufficient to efficiently trigger NSCC formation. A novel promising genetic model system was proposed only recently by Bian and colleagues, using a conditional epithelial specific Tgfbr1/Pten double knockout, to reliably generate malignant lesions of the oral mucosa at a high

incidence rate [16]. Furthermore, transgenic mice expressing the HPV-16 early oncogenes E6 [179] and E7 are used to induce cancerous lesions in epithelial cells [78, 179] and therefore also find use as cancer models of HNSCC in combination with chemical induction by 4-NQO [95]. Also, orthotropic mouse model using injection of human tumor cells into the floor of mouth of immunocompromised mice were used to study oral squamous cell carcinoma. Tumors develop rapidly after injection and reach comparatively high tumor volumes [138, 13]. However, concerning etiology and histology of human HNSCC these mouse tumor models only partially reflect the pathophysiological conditions and even more importantly, the lack of a functional immune system is hampering the analysis of anti- and pro-tumorigenic responses of the immune system. HNSCC develops in a multistage process, rising gradually from a transformed cell into full-blown malignant squamous cell carcinoma.

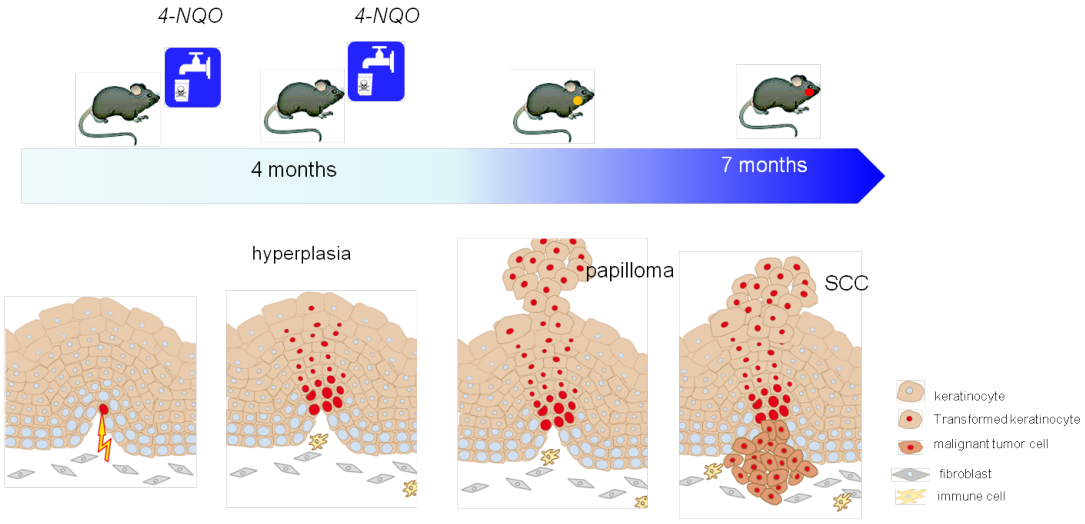

Figure 1.6: Multistep oral carcinogenesis using 4-Nitroquinoline-1-oxide. The mice are treated with 4-Nitroquinoline-1-Oxide (4-NQO) in drinking water for 16 weeks and then observed for another 12 weeks. Within this time, the development of oral mucosal hyperplasia, dysplasia and the development of cancerous lesions is expected.

A well established carcinogen driven animal model is the hamster cheek pouch model using 7,12-dimethylbenzanthracene (DMBA) to induce cancers of the buccal mucosa, which was also applied in mice, rats and non-human primates [47, 63]. However, the cancers developing in this model only partially reflect the situation in human oral carcinogenesis [139]. An elegant mouse tumor model, which reflects the gradual development of oral cancer, takes profit of the carcinogen 4-Nitroquinoline 1-oxide (4-NQO) (Fig. 1.6). 4-NQO can be painted with a brush onto soft palate or tongue or is administered to animals via the drinking water [76, 195]. Within a timeframe of seven months, C57BL/6 mice develop hyperplasia and dysplasia, papillioma and later on also carcinoma, allowing a detailed investigation of oral squamous cell carcinogenesis. Tumor incidence was higher with the carcinogen administration via the drinking water as compared to painting protocol and after 2428 weeks 100 % of animals developed lesions the tongue or in the esophagus [194]. Thus, 4-NQO can be considered both a reliable as well as useful model for oral carcinogenesis.

1.9 The S100-RAGE axis in HNSCC and RAGE as a target for therapy

In head and neck squamous cell carcinoma (HNSCC) it was shown on RNA as well as on protein level, that S100A8 and S100A9 expression is inversely correlated with differentiation in HNSCC [161, 162]. Therefore S100A8/A9 was proposed as a diagnostic marker to better discriminate between healthy and premalignant mucosa and tumor tissue [64, 42]. In vitro, blockage of S100A8 protein in the laryngeal carcinoma cell line hep2 lead to inhibition of metastasis by miR-24 [70]. In the context of head and neck squamous cell carcinoma, both RAGE and its ligands S100A8 and S100A9 have been the focus of several studies. For RAGE, however, available data are controversial, relying on mere descriptive data from expression arrays and immunohistochemical data. However, functional data on the causal link between RAGE function in the pathogenesis and malignant progression of HNSCC are missing. In contrast,

for oral cancer it was shown that RAGE is closely associated with invasive disease [15], supported by another study, where it was shown that RAGE is positively associated with depth of invasion and local recurrence, but not with lymph node metastasis and differentiation [169]. The same group proposed a driving role for RAGE in tumor angiogenesis [168]. On the other hand, a more recent publication suggested a negative correlation between RAGE expression and differentiation, showing a relative reduction of RAGE staining during malignant progression [116]. While obviously cancer-related inflammation is a promising target for therapeutic intervention, it proves a challenge to balance the scales towards an anti-tumorigenic immunity. RAGE as a key molecule in this context appears as a promising target. Aiming at breaking the vicious cycle of S100-RAGE signaling, more and more studies introduce Rage blocking antibodies, soluble RAGE (sRAGE) as a decoy receptor and other RAGE antagonists to as a therapeutic option [87]. In the context of a mouse model for diabetic atherosclerosis application of sRAGE showed beneficial effects [146] and inhibition of RAGE was shown to ameliorate neurotoxicity of amyloid-beta proteins s[188], while in glioma cells, blockage of RAGE suppresses tumor growth and metastasis [192].

1.10 Study design and aims of the study

Even though obviously linked to the pathogenesis and malignant progression of head and neck squamous cell carcinoma, the functional role of the S100-RAGE axis especially under settings of genotoxic conditions versus chronic inflammation remains elusive (sec. 1.6). Thus an important topic, which is addressed in the present S100-RAGE axis and inflammation as a driver for cancer formation was a focus of the study

RAGE function is so far well described in inflammation associated cancer and has been studied extensively in inflammation driven mouse models [60, 201]. On the other hand, little is known about RAGE function in the context of genotoxic stress in the absence extensive inflammatory promotion. Our current

understanding of RAGE focuses mainly on the maintenance of an inflammatory feed forward loop, without explaining whether and how RAGE is involved in the onset and early development of cancer. However, upon genotoxic stress or damage, cells produce stress signals and DAMPs are released from damaged or apoptotic cells and may well activate RAGE early on in carcinogenesis. In skin carcinogenesis, genotoxic stress by sequential DMBA application finally leads to the formation of squamous cell carcinoma (SCC), which again show infiltration by inflammatory cells [202, 49].

To shed further light on the role of S100-RAGE in head and neck squamous cell carcinoma, a patient collective of 188 oropharyngeal squamous cell carcinoma (OPSCC) patients was screened for the distribution of inflammatory cells, addressing the question whether patients can be stratified according to the amount of inflammatory infiltrate as a predictor of clinical outcome. In a more functional approach, RAGE deficient mice [122] were used in a 4-NQO carcinogenesis protocol to address the role of RAGE in the onset and development of oral squamous cell carcinogenesis. Furthermore, mice deficient in S100a9 ($S100a9^{-/-}$) [82] were subjected to the 4-NQO protocol to specifically focus on S100 calgranulins in HNSCC.

The main questions that were addressed are in this study are:

1. Is it possible stratify HNSCC cancer patients according to inflammatory infiltrate to predict behavior?

2. What is the role of the receptor RAGE and it's ligands, calgranulins S100A8 and S100A9 in a 4-NQO model of chemically induced oral squamous cell carcinogenesis?

2 Materials and Methods

2.1 Material

2.1.1 Consumables and equipment

Equipment and consumables	Company
1.5 ml, 2 ml Reaction Tubes	Eppendorf, Hamburg
2 ml Cryotubes	Nunc
Adhesion slides Super Frost® Plus	Menzel-Gläser, Braunschweig
AEC+ Substrate-Chromogen, Ready-to-Use	Dako Cytomation, Hamburg
AlphaMetrix tissue punch	AlphaMetrix Biotech, Rodgau
Autoklave	VX95 Systec GmbH, Wettenberg
Centrifuge 5417R	Eppendorf, Hamburg
Centrifuge Biofuge 13	Hereaus Instruments, Hanau
Centrifuge Varifuge 3.0R	Hereaus Instruments, Hanau
Cover slips (24x36 mm and 24x50 mm)	Knittel, Bielefeld
DAKO Pen Dako A/S	Glostrup, Denmark
disposable scalpel	Feather, Osaka (Japan)
Electrophoresis chamber for agarose gels	Buddenberg, Mannheim
Epi Chem II Darkroom (Gel documentation)	UVP, Upland (CA, USA)
Eppendorf research pipettes	Eppendorf, Hamburg
Filtertips	Biozym Scientific, Oldendorf
Fluoreszenzmikroskope BX50F	Olympus Microscopy, Hamburg
Freezer	Liebherr, Ochsenhausen
freezer -80°C	Harris/Theromo Scientific
Fridge 4°	Liebherr, Ochsenhausen
Hamamatsu NanoZoomer Scanner	Hamamatsu Photonics GmbH

Equipment and consumables	Company
ice-machine	AF20, Scotsman
Kryostat/Microtome blades C35	Feather, Osaka (Japan)
Kryotome 2800 Frigocut	Leica, Nussloch
Microscope BX-50F	Olympus, Hamburg
Microscope IX51	Olympus, Hamburg
Microwave	Robert Bosch GmbH, Stuttgart
Milli-Q	Millipore, Bedford (MA, USA)
MJ Mini Gradient Thermal Cycler	Bio-Rad Laboratories, München
Nanodrop Spectrophotometer, ND-1000	PeqLab, Erlangen
Nuclease free reaction caps (safe-lock)	Eppendorf, Hamburg
PCR stripes (8x0,2ml)	NerbePlus, Wiensen/Luhe
PCR-Thermocycler (Gene Amp System 2400)	Perkin Elmer, Wellesley (MA, USA)
pH-meter	WTW, Weilheim
Pipettes	Gilson-Abimed, Düsseldorf
Pipettips	Micro-Bio-Tec Brand, Giessen
Pipettor Pipetboy acu	Brand, Wertheim
Power supply Power Pac 300/3000	Bio-Rad Laboratories, München
Precision scales	Sartorius, Göttingen
reaction caps (1,5 ml and 2 ml)	Eppendorf, Hamburg
Scales	Sartorius, Göttingen
SC30 (BF camera)	Olympus, Hamburg
steam-cooker	Braun, Kronberg
thermomixer	Eppendorf, Hamburg
Tissue Tek VIP 5 Jr	Sakura, USA
Trucount 15 ml, 50 ml Tubes	Falcon, Greiner, Nunc
Vortex “Reax 2000”	Heidolph, Kehlheim
Water baths	GFL M&S Laborgeräte
XM10 (black/white camera)	Olympus, Hamburg

2.1.2 Glas and plasticware

Equipment	Company
Glass beakers	Fisherbrand, Schwerte
Glass bottles (50 ml-1l)	Schott, Mainz
Glass container for histology,	Schott, Mainz
Graduated cylinder plastic (100 ml – 2 l)	Vitlab, Großostheim
Plastic beakers	Vitlab, Großostheim
Graduated cylinder glas	Brand, Wertheim
Graduated cylinder plastiv	Brand, Wertheim
Erlenmeyer flasks	Brand, Wertheim

2.1.3 Chemicals

Component	Company
10x PCR buffer	Genaxxon, Biberach
Acetic acid	Merck, Darmstadt
Agarose SeaKem GTG	Lonza, USA
β-Mercaptoethanol	Merck, Darmstadt
BCA reagents	Thermo Scientific, USA
Biotyinylated secondary antibody	Vector Laboratories, Burlingame, USA
Boric acid	Roth, Karlsruhe
Bromphenol Blue	Sigma Aldrich, München
ECL reagent solutions	AppliChem, Darmstadt
EDTA	AppliChem, Darmstadt
Eosin	Roth, Karlsruhe
Ethanol p.a.	Merck, Darmstadt
Ethanol, denaturated 99,7%	Roth, Karlsruhe
Eukitt	Kindler, Freiburg
Formaldehyde 37%	Sigma Aldrich, München
Glycerol	AppliChem, Darmstadt
Haematoxylin	AppliChem, Darmstadt
Hematoxylin according to Gill II	Roth, Karlsruhe

Component	Company
GelRed	Biotium, Hayward, CA
Hoechst H33342	Calbiochem/Merck, Darmstadt
Hydrochloric Acid	Merck, Darmstadt
Hydrogen peroxide	Merck, Darmstadt
Isopentan	Roth, Karlsruhe
Isopropanol	Roth, Karlsruhe
MgCl2	Genaxxon, Biberach
Microplate Reader Model 680	Bio-Rad Laboratories, München
Milk powder	Roth, Karlsruhe
MnCl2	Roth, Karlsruhe
N, N, N‘, N‘, Tetramethyl-ethylenediamine (TEMED)	Roth, Karlsruhe
Na2HPO4x2H2O	Merck, Darmstadt
NaH2PO4xH2O	Merck, Darmstadt
Natrium chloride	Roth, Karlsruhe
Natrium-deoxycholat	AppliChem, Darmstadt
NP-40	Sigma Aldrich, München
Nuclease-free water	Gibco/Life Technologies, Darmstadt
Oligo-dT primers	Fermentas, St. Leon-Rot
Paraffin	Vogel, Giessen
Potassium Chloride	Roth, Karlsruhe
Sodium Chloride	Roth, Karlsruhe
Sodium Citrate	Roth, Karlsruhe
Sodium hydroxide	Merck, Darmstadt
Sodiumdodecylsulfate (SDS)	Roth, Karlsruhe
Tris HCl	Roth, Karlsruhe
Tris-base	Roth, Karlsruhe
Triton X-100	AppliChem, Darmstadt
Tween 20	Roth, Karlsruhe
Xylene	Roth, Karlsruhe
Xylene chyanol	Sigma Aldrich, München

2.1.4 Enzymes and fine chemicals

Component	Company
PCR buffer S	Genaxxon, Biberach
Oligo(dT)18	Fermentas, St. Leon-Rot
Taq polymerase	Genaxxon, Biberach
GeneRuler DNA ladder mix	Fermentas St. Leon-Rot
dNTPs	Fermentas, St Leon Roth
Revertaid M-MuLV Buffer	Fermentas, St. Leon-Rot
Revertaid M-MuLV Reverse Transcriptase	Fermentas, St. Leon-Rot
Riboblock RNase inhibitor	Fermentas, Germany

2.1.5 Kits

Kit	Company
RNase-free DNase Set	Qiagen, Hilden
DAB kit	Vector Laboratories, Burlingame, USA
DNaseI Digest Kit	Qiagen, Hilden
ImmPRESS Anti-Rabbit	Vector Laboratories, Burlingame, USA
RNeasy Mini Kit	Qiagen, Hilden
Vectastain Elite-ABC-Peroxidase	Vector Laboratories, Burlingame, USA
Cell proliferation Kit	GE Healthcare Europe, Freiburg

All kits and reagents were used according to the manufacturer's protocol unless otherwise stated.

2.1.6 Buffers and Solutions

Blocking reagent for histology	0.1 % BSA 5 % host serum in PBS
10x Citrat Buffer:	1.8 mM citric acid 8.2 mM sodium citrate
6x DNA loading buffer	0.25 % (v/v) Bromphenol blue 0.25 % (v/v) Xylene Cyanol 30 % (v/v) glycerol
4 % formaldehyde	4 % (v/v) formaldehyde in PBS
Mowiol	6 g glycerol 2.4g Mowiol 4-88 6 ml H2O
10 x PBS	1.5 M NaCl 24 mM KCl 82 mM Na2HPO4 x 2 H2O 17 mM NaH2PO4 x H2O
PCR reaction mix	1.1x PCR buffer S 1.7 mM MgCl2 220 µM dNTPs
tail lysis buffer	50mM Tris (pH 8,0) 100mM NaCl 100mM EDTA 1% SDS
10x TBE	1 M Tris 1 M Boric acid 20 mM EDTA

2.1.7 Primers

Name		Sequence	T_A	Length [Bps]
mHPRT	for	ctggttaagcagtacagcccc	62 °C	380
	rev	caaaagtctggggcgcagc		
mRage	for	acaggcgagggaaggaggtc	58 °C	200
	rev	tttgccatcgggaatcagaag		
mTlr4	for	tcagcaaagtccctgatg	56 °C	183
	rev	ttgagaggtgtgtaagc		

2.1.8 Antibodies

Primary Antibodies

Antigen	Host	Clone	Dilution	Source
BrdU	mouse	BU-1	*	GE Healthcate (RPN202)
Cytokeratin 13, (CK13)	mouse	1C7	1:10	Progen (PC 10523)
Cytokeratin 14 (CK14)	mouse	LL002	1:20	Nova Costa (NCL-LL002)
Loricrin	mouse	polyclonal	1:2000	Covance (RBP 145-P)
Myeloperoxidase Ab-1	rabbit	polyclonal	1:100	Thermo Fisher (RB-373)
mS100a8	goat	polyclonal	1:200	Santa Cruz (Sc-8113)
hS100A8	goat	polyclonal	1:200	Santa Cruz (Sc-8112)
mS100a9	goat	polyclonal	1:200	Santa Cruz (Sc-8115)
hS100A9	goat	polyclonal	1:200	Santa Cruz (Sc-8114)
hS100A12	goat	polyclonal	1:100	Santa Cruz (Sc-8116)
Tlr4	goat	polyclonal	1:100	Santa Cruz (Sc-16240)

* anti-BrdU antibody as part of the GE "Cell proliferation-Kit" was used according to manufacturer's instructions.

Secondary antibodies

Antigen	Host	Label	Dilution	Source
Goat	donkey	Cy3	1:200	Dianova
Rabbit	donkey	Alexa488	1:200	Dianova
Rabbit	goat	biotin	1:500	Vector, (BA-100)
Goat	donkey	polymer	*	Vector, ImmPress anti-Goat
Mouse	donkey	polymer	*	Vector, ImmPress anti-Mouse
Rabbit	donkey	polymer	*	Vector, ImmPress anti-Goat

* polymer coupled secondary Antibody solution was used according to manufacturer's protocol.

2.1.9 Human tissue blocks

Tissue from patients, diagnosed with a squamous cell carcinoma of the orpharynx (OPSCC) and treated at the ENT Department of the University Hospital Heidelberg, Germany, between 1990 and 2008 was used in the context of a previous study [84]. All patients included in the study gave informed consent for the usage of the biopsy material. The study was approved by the Ethics Committee of the Medical Faculty of the University of Heidelberg, study code 176/2002. FFPE tissue with biopsies from routine diagnostic (fixed in formalin and embedded in paraffin according to routine fixation precedures from the institute of pathology) at the Institute of Pathology at the University Hospital Heidelberg were assessed and kindly provided by the pathologist Dr. Christa Flechtenmacher. Only tissue samples of primary tumors were included in the present study.

2.1.10 Software

Software

Program	Distributor
Adobe Acrobat 9.0; Photoshop CS5; Illustrator CS5	Adobe, San Jose, USA
Adobe Photoshop CS5; Illustrator CS5	Adobe, San Jose„ USA
CellSens Dimension 1.5	Olympus, Hamburg
EasyControl 2.04 for Epi Chem II darkroom	UVP, Upland (CA, USA)
Mendeley Desktop 1.7.1	Mendeley Ltd., London, UK
Hamamatsu NanoZoomer (NDP-Viewer)	Hamamatsu Photonics, Herrsching
IBM SPSS Statistics 20	IBM Corporation, Somers NY, USA
Microsoft Office 2007	Microsoft Corp., Unterschleißheim
Microsoft Windows XP	Microsoft Corp., Unterschleißheim
Sigma Plot 11	Systat Software, Erkrath

2.2 Methods

2.2.1 Analyses on human patient samples

2.2.1.1 Data acquisition and selection of patients

In the context of a retrospective study [84], human carcinoma of the oroharynx region were chosen. From originally 188 tumor patients, for whom fresh frozen tumor tissue was available, clinical data were extracted from the electronic patient files of the university hospital Heidelberg and transferred to the laboratory database. Birth date, gender, date of surgery, anatomic region of the tumor, TNM-classification of the tumor, pathological staging, cause of death (tumor dependent/independent) and secondary event were included. Detailed information on alcohol consumption and smoking habits was not available in most cases.The included data mainly refer to general information (yes/no) without quantitative data. The HPV status was analyzed in a separate study [84].

2.2.1.2 Tissue microarray (TMA) production

Tissue microarrays (TMA) enable a high throughput analysis of a large number of tissue samples. A collections of 188 tumor biopsies of patients as well as healthy uvula mucosa were spotted on the tissue microarray. Sections form these biopsies were initially stained by hematoxilyn and eosin (H&E) and examind by the pathologist Dr. med. Christa Flechtenmacher. Punch biopsies from the donor tissue blocks containing patient material (0.6 mm x 3 mm) were transferred into a fresh recipient paraffin block using the AlphaMetrix tissue punch. Several punch biopsies from differet regions of one tumor were included on the TMA to ensure robust data. For better orientation, the TMA contains an asymmetric grid (Fig. 2.1). The recipient block was subsequently incubated at 37° C for one hour. Sectioning was performed with a cryostat at -20° C with sequential 4 µm sections.

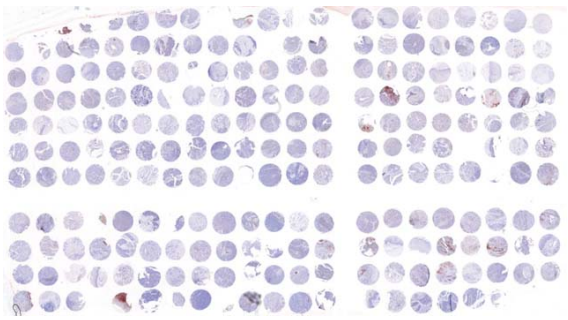

Figure 2.1: Example of a TMA section: overview of TMA018 (stained for CD66b).

2.2.1.3 TMA Scoring

For statistical processing of the data, each spot was scored by eye by at least three independent observers simultaneously. TMAs generally were scored for:

Score A: amount of stained tumor cells (quantity)
Score B: staining intensity in tumor cells (quality)
Score C: localization of cellular proteins or stromal/intratumoral localization of immune cells
Score D: amount of immune cells with positive staining

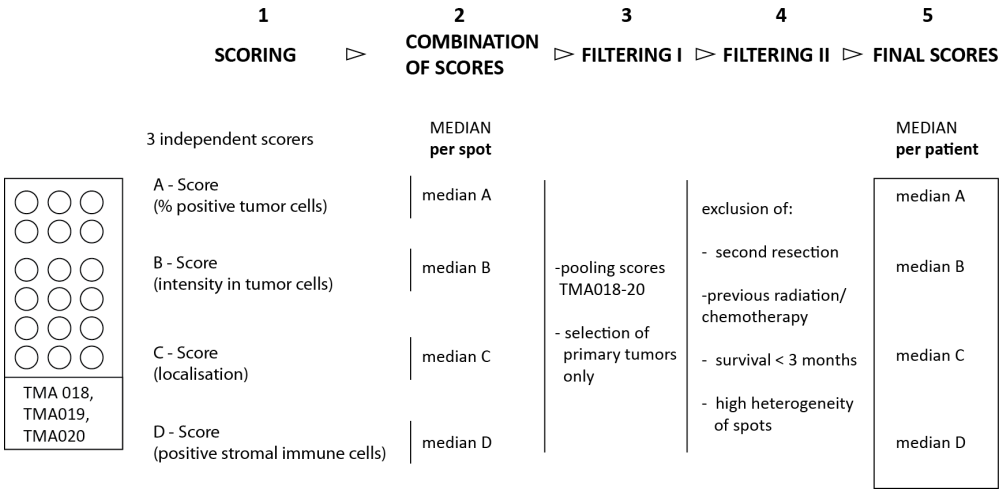

Figure 2.2: TMA scoring system.

(1) TMAs were scored by 3 independent observers simultaneously and the three values per spot were subsequently combined using the median (2); in case of high heterogeneity between the scorers, spots were excluded. (3) Scores from TMA018, TMA019 and TMA020 were aggregated and only primary tumors were selected. (4) Biopsies were filtered for the date of resection and second resections were excluded. Further exclusion criteria were previous chemo/radiation therapy and survival < 3 months after surgery. In case the different spots per patients did not show high heterogeneity (median $>$ standard deviation) scores for spots from the same patient were combined for the final score per patient (5).

Sections were stained for CD66b in order to quantify the amount of CD66b positive immune cells in the tumor microenvironment. Only the C and the D score were used as the protein is expressed only in granulocytes and not in tumor cells. The location score C is used, depending on the protein of interest, to determine intracellular localization of the staining, distribution in stromal cells or the localization of immune cells within the tumor microenvironment. In this study, the location score C was used to differentiate between CD66b positive cells in the tumor stroma and intratumoral CD66b positive cells as well as their amount (Tab. 2.10). The median value per spot for the three observers was determined.

Only primary tumors were included into the analysis and intensity scores from spots of the same patient were subsequently combined using the median. Further filtering excluded biopsies from second resections to exclude alterations in inflammatory parameters as well as patients who received neoadjuvant radiation- or chemotherapy. Furthermore, patients who died within

Table 2.10: TMA scores for CD66b

Score	Intensity	Meaning
C		
Localization of immune cells	1	No intratumoral CD66b positive cells
	2	Few intratumoral CD66b positive cells
	3	Many intratumoral CD66b positive cells
D		
amount of stroma immue cell infiltration	1	No stromal immune cells
	2	Few stromal immune cells
	3	Many stromal immune cells

TMAs were scored for intratumoral CD66b positive cells (C-score) and stromal CD66b positive immune cells (D-Score).

three months after surgery as well as patients were excluded to avoid bias in survival analysis due to complications from treatment regimen. Finally, to aggregate score values per patient from different spots, median and standard deviation were calculated and only patients showing homogeneous scoring values for all spots (median > standard deviation) were considered for further analysis. From originally 188 patient tumors, 153 could be scored for CD66b positive immune cells and used for further analysis.

2.2.1.4 Statistical testing

Statistical analyses were performed using the Sigma Plot statistics package and the IMB SPSS Statistics 20 (statistical packages for social sciences) Software. Differences between groups were assessed by χ^2 (Chi-square) test and unpaired Student's t-test and Wilcoxon signed-rank test. A p-value lower then 0.05 was considered statistically significant.

2.2.1.5 Correlation analysis

The correlation coefficient describes the relationship between two or more variables. For a linear correlation, the correlation coefficient can take on values in a range of "-1" till "+1" where 1 describes a perfect correlation and -1 an inverse correlation. Pearson correlation was used to test for a linear association between normally distributed markers. For other variables, the Spearman's rank correlation was applied.

2.2.1.6 Survival analysis

To assess patient survival, Kaplan-Meyer graphs were used to visualize differences in overall survival (OS) as well as progression free survival (PFS). Patients were grouped according to observed parameters and statistical differences between groups were determined with the log-rank test. Tumor dependent death within the observation period (OS) and progression to secondary event (metastasis, recurrence, secondary tumor) respectively (PFS) were regarded as an event. Patients were censored in case they had not (yet) reached the event. This could be due to either (i) a premature exit from the study ('lost to follow-up'), (ii) tumor independent death or (iii) no progress to event (tumor dependent death; secondary event) within the period of record. Statistical determination of differences between the groups was assessed by Log-Rank test.

2.2.2 Animal Experiments

Rage$^{-/-}$ animals in a C57Bl6 background as described previously (Liliensiek et al., 2004) were used in this study and were housed at the DKFZ animal facility in individually ventilated cages under specific pathogen-free conditions. Temperature (21°C), light cycles and humidity (50-60°) were controlled and kept constant. All experiments were performed with C57Bl6 *wild type*, heterozygous (*Rage*$^{+/-}$) (control group) and homozygous Rage knockout (*Rage*$^{-/-}$) females. The procedures for performing animal experiments were in accordance with the principles and guidelines of the "Arbeitsgemeinschaft der Tierschutzbeauftragten in Baden-Württemberg" and were approved by the German Regional Council, Karlsruhe, Germany under the license number G-21/10.

2.2.2.1 4-NQO treatment of mice

A protocol of 4-nitroquinoline-1-oxide (4-NQO) administration via the drinking water starting at 6 weeks of age. 4-NQO treatment was maintained for 4 months, followed by 2-3 months of observation. The 4-NQO group was treated with 100µg/ml 4-NQO in 2 % polypropylene glycol in the drinking water ad libitum, while the control group received 2 % polypropylene glycol (PPG) only. Weight was controlled regularly and general health state was monitored to be able to terminate the treatment in case of severe side effects. Mice were sacrificed at the end of the observation period or at sign of severe weight loss.

2.2.2.2 In vivo BrdU incorporation

Mice were injected intraperitoneally with 100µl (1µg/µl) BrdU labeling agent per gram body weight according to manufacturer's protocol four hours before sacrificing (cell proliferation kit GE healthcare, Little Chalfornt, UK). BrdU incorporation was quantified on tissue sections by immuohistochemical staining using an anti-BrdU antibody (GE healthcare, cell proliferation kit).

2.2.3 Molecular biological methods

2.2.3.1 Total RNA isolation from tissue

Total RNA from tissues was prepared using the Rneasy Mini Kit (Qiagen). Tissue was cut with the cryostat in 10 µm sections (Leika, 2800 Frigocut) and directly transferred into RLT lysis buffer (Qiagen) containing ß-mercapto ethanol. Tissue was lysed by pipetting and subsequent vortexing. For complete homogenisation, the lysate was then transferred onto QIAshredder columns (Qiagen) and centrifuged for 5 min at 14,000 rpm and 4 °C. RNA was precipitated through addition of equal volumes of 70 % ethanol. The reaction batch was then loaded onto QIAamp RNA extraction columns and processed according to manufacturer's instruction. An additional on column DNase I digest was performed to ensure pure RNA preparation without genomic DNA contamination . For this, 10 µl DNase I stock solution were mixed with 70 µl RDD buffer according to the kit instructions, loaded onto the QIAamp column and incubated for 15 min at room temparature. Samples were washed on column and finally RNA was eluted with 40 µl of $dd\mathrm{H_2O}$.

2.2.3.2 Determination of nucleic acid concentration

Nucleic acid concentration and purity was measured with the Nanodrop Spectophotometer according to manufacturer's instructions at 260 nm. Sample quality and contamination by proteins and aromatic compounds was determined using the OD 260/280 and the OD 260/230 ratio. OD values at 280 nm (absorbance maximum for proteins) and at 260 nm (absorbance maxima for aromatic compounds) should result in an OD 260/230 higher than 2.0 for RNA and a OD 260/280 between 1.8 - 2.0.

2.2.3.3 cDNA synthesis

For cDNA synthesis, 5 µg of DNA were diluted in 35 µl nuclease free water and 0,5 µl Oligo(dT)18 primer (100 µM, Fermentas) were added and incubated at 70 °C for 5 min followed by 5 min at 4 °C. A reaction mix containing 10 µl RevertAidTM buffer, 2 µl dNTP mix, 2 µl RiboLockTM RNase Inhibitor (40 u/µl) and 0,5 µl RevertAidTM M-MuLV reverse transcriptase (200 u/µl, Fermentas) were added and incubated for reverse transcription at 42 °C for 60 min. Obtained cDNA was aliquoted and stored at -20 °C.

2.2.3.4 Polymerase chain reaction (PCR)

Amplification of DNA fragments for semi-quantitative analysis of gene expression or the detection of specific genomic loci was performed on cDNA using polymerase chain reaction (PCR). 3 µl of genomic DNA (10-500 ng) or 15 ng cDNA were mixed with 45 µl OCR reaction mix (10 x PCR buffer S, 1.7 µM $MgCl_2$ (Genaxxon), 220 µM dNTPs (Fermentas)), 20 pmol primer (forward and reverse) and 0,3 µl Taq-polymerase S (200 u/µl; Genaxxon) and ddH2O was added to a final volume of 50 µl. Polymerase chain reaction was performed according to the following protocol:

Denaturation	94 °C	5 min	
Denaturation	94 °C	30 sec	
Primer hybridisation	T_A °C	30 sec	25 - 40 cycles
Elongation	72 °C	45 sec	
Final elongation	72 °C	5 min	
hold	4 °C	∞	

The PCR reaction was analyzed by agarose gel electrophoresis (sec. 2.2.3.5). A complete list with primers, their respective T_A and size of the amplicons is listed in (Tab. 2.6).

2.2.3.5 Agarose gel electrophoresis

Agarose gel electrophoresis was used for the separation of nucleic acid fragments according to their molecular size. DNA fragments migrate through the electric field due to their negative charge; small fragments migrate more quickly than large fragments due to physical interaction with the gel matrix. For fragments between 100 bps and 400 bps a 2 % agarose gel in 1 x TBE buffer was prepared and the intercalating DNA dye GelRed was added in a 1:20,000 ratio before casting of the liquid gel into a gel chamber. Samples were loaded with 6 x loading buffer and electrophoretic separation was performed at 120 V constant for 30 min. Fragment size was determined using a parallel loaded DNA ladder. Bands are visualized under UV light.

2.2.4 Histological methods

2.2.4.1 Tissue fixation and paraffin embedding

Tissues were taken directly after sacrificing of the animals and immediately fixed in 4 % formaldehyde in PBS, pH 7.4 with agitation over night at 4 °C. Samples were subsequently washed in PBS for 30 min at 4 °C, followed by two washing steps in 0.85 % (w/v) NaCl for 30 min. For dehydration, the tissue was incubated in 50 % (v/v) ethanol/ 0.85 % (w/v) NaCl and twice in 70 % (v/v) ethanol for 15 min at room temperature each. Tissue was either further processed using the vacuum infiltration processor Tissue Tek VIP 5 Jr or stored at 4°C. For further processing, samples were transferred in plastic cassettes. The following program was used:

1 x	70 % EtOH	45 min	45° C
1 x	80 % EtOH	45 min	45° C
2 x	90 % EtOH	45 min	45° C
2 x	96 % EtOH	45 min	45° C
2 x	Isopropanol	60 min	45° C
2 x	Xylene	60 min	45° C
4 x	Paraffin	45 min	60° C

Tissues were embedded in paraffin blocks manually. They were taken out the plastic cassettes using tweezers, placed into a metal chill mold in the desired orientation and molded with liquid paraffin. The tissue blocks were down to 4° C and removed from the chill mold once completely solid and kept for storage at room temperature.

2.2.4.2 Preparation of paraffin tissue sections

Paraffin blocks were kept at -20 °C for sectioning and cut in 5 µm sections with the microtome RM2155. Sections were transferred into a waterbath at 40 °C and subsequently mounted onto SuperFrost object slides. Sections were dried at 42 °C o/n and subsequently stored at room temperature.

2.2.4.3 Preparation of cryosections

Tissues were taken directly after sacrificing of the animals and immediately embedded with OCT in plastic molds. Tissues were taken from molds and fixed with OCT on the edging table of the cryotome. 5 µm sections were cut and mounted onto SuperFrost object slides. Cryosections were dried overnight and fixed in aceton at -20 °C. For storage, sections were kept at -80 °C.

2.2.4.4 Hematoxylin and Esosin staining

Staining with hematoxylin and eosin (H&E) is commonly used to assess the histology of tissue sections. Nuclei are stained blue (hematocylin) while intra- and extracellular proteins are stained red (eosin). 5 µm sections from formalin fixed and paraffin-embedded tissues were deparaffinized and rehydrated in a descending ethanol series (100 %, 95 %, 90 %, 80 %, 70 %, 50 % and 30 % (v/v) ethanol in *dd*H2O , 2 min each). Staining with hematoxylin was performed for 8 min, followed by washing in H_2O twice for 2 min. Subsequently, tissue sections were washed in 70 % (v/v)ethanol/0.05 % (v/v) HCl for 20 seconds and in ddH_2O for 10 minutes and then stained in 0.1 % eosin for 3 to 5 minutes. Sections were dehydrated (incubation in 70 %, 90 %, and 100 % (v/v) ethanol), followed by incubation in xylene and subsequent embedding in Eukitt.

2.2.4.5 Immunhistochemical staining

5 µm sections from formalin fixed and paraffin-embedded tissues were deparaffinized and rehydrated as described in (sec. 2.2.4.4), 5 µm cryosections were dried overnight and fixed in aceton at -20 °C. Endogenous peroxidase was blocked with 3 % H_2O_2 for 10 min and heat-mediated antigen retrieval was performed in citrate buffer (pH 6) for 30 min in a steam-cooker. Sections were blocked in horse serum (ImmPress, Vector Laboratories, Burlingame, CA, USA) for 20 min and subsequently incubated with the primary antibody (listed in Tab. 2.7) according to manufacturer's instructions either 2 hours at room temperature or overnight at 4 °C in a wet chamber. Afterwards, sections were washed trice in PBS under agitation for 5 minutes, incubation for 30 min at room temperature with the corresponding, peroxidase coupled secondary antibody (ImmPress) and again washed three time for 5 min each. Subsequently, sections were incubated (1-5 min) with the DAB peroxidase substrate (brown

staining signal) (Vector Laboratries Inc., CA 94010, USA) or AEC substrate (red signal) (Vector Laboratories). Samples were counterstained with hematoxylin and mounted in Evanol or Eukitt (Kindler GmbH, Freiburg, Germany) respectively.

2.2.4.6 Immunofluorescence (IF)

Parraffin-sections were deparaffinized as described above (sec.) and blocked in PBS containing 0.1 % (w/v) BSA and 5 % goat or donkey serum (depending on the species, in which the secondary antibody was produced in). The primary antibody was diluted (Tab. 2.7) in the blocking solution and incubated on the section at 4 °C overnight in a wet chamber. After washing with PBS for 5 min under agitation for 3 times a fluorophore-labeled secondary antibody (Tab. 2.7) was added and incubated on the sections for 30 minutes protected from light in a wet chamber. Sections were rinsed in PBS and incubated with Hoechst H33342 for visualization of nuclei at a 1 : 1000 dilution in PBS in the dark at room temperature for 15 minutes. After a final washing step (3 times, 5 min in PBS, light protected), sections were embedded in Mowiol and stored at 4 °C.

2.2.5 Mikroskopy

Fluorescence labeled Samples were analyzed with an epi-fluorescence microscope (Olympus IX51). Pictures were aquired using the Olympus CellSens Dimension Software. For dark field (DF) images, the XM10 camera system (Olympus) was used, bright field images were taken using the SC30 camera (Olympus).

TMA images were acquired at the Nikon Imaging Center, Heidelberg and only scans of the TMAs were used for the further analysis (Evaluatinon and scoring as well as export of images) with the NDP-Viewer software (Hamamatsu).

3 Results

3.1 Distribution of S100-calgranulin positive immune cells positive immune cells in HNSCC

Even though inflammation is often described in the context of HNSCC [36, 210, 25, 211], our knowledge concerning its correlation with clinical and histopathological charateristics as well as the clinic outcome remains limited. In the past, several clinical and experimental studies demonstrated a functional link between the S100-RAGE signaling axis and the paracrine crosstalk of tumor and immune cells in setting of inflammation associated carcinogenesis [158]. In the context of a previous study (Sonja Funk, unpublished data), Calgranulin expression was assessed in biopsies from OPSCC patients and compared to clinic-pathological features. In this study, the expression of S100A8 an S100A9 as well as S100A12, a third member of the calgranulin protein family, which is absent in rodents was determined. Expression of all three calgranulins was found in normal control mucosa, predominantly in suprabasal and differentiating mucosal keratinocytes. Basal cells of the mucosa were negative for calgranulin expression. Calgranulin staining in tumors varied from no staining to strong staining in almost all tumor cells. In addition to the expected cytoplasmic staining keratinocytes of the normal mucosa showed a prominent nuclear staining, which was also observed in about three quarters of calgranulin positive tumors. Significant correlations between the expression of S100A8 and S100A9, S100A8 and S100A12 and between S100A9 and S100A12 were found. However, S100-calgranulin expression in tumor cells was not linked to patient survival. Furthermore, a large number of tumors showed moderate to high infiltration of S100-calgranulin positive immune cells into the tumor stroma. Even though no significant correlation between the number of S100A9, S100A8 or S100A12 positive immune cells and any clinical outcome was observed, a trend towards a better prognosis for patients with a high number of S100A8 and S100A12 but not S100A9 positive immune cells was

visible (unpublished Data, S. Funk). This may indicate a role for calgranulin positive inflammatory cells, possibly independent of calgranulins staining in tumor cells. Therefore, to assess the distribution of patients with and without inflammatory infiltrate, I determined the percentage of patients with a high number of S100-calgranuline positive immune cells in this OPSCC cohort.

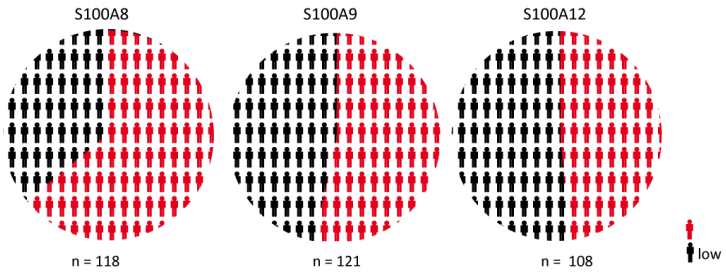

Figure 3.1: Infiltration of S100-calgranulin positive immune cells in the stroma of human OPSCC samples. Patients were stratified according to low (grey curve), high (red curve) and medium (black curve) amount of CD66b positive stromal (A, C) and intratumoral (B, D) immune cells. Overall survival (A, B) and progression free survival (C, D) were determined by Kaplan-Meyer analysis. Lack of statistical significance ($p > 0{,}05$) was assessed by Log-Rank-Test.

64% of patients showed a high number of S100A8 positive infiltrating immune cells, 54% of patients showed high numbers of S100A9 positive stromal cells, whereas high amounts of S100A12 positive stromal cells was observed in 49% of cases (Fig. 3.1). In summary around half of the patients show a high amount of infiltrating, s100A8, S100A9 and S100A12 positive immune cells.

3.2 Human OPSCC samples show a differential pattern of CD66b positive immune cells which correlates with S100-calgranulin positive immune cells

Approximately half of the OPSCC patients display a high amount of S100-calgranulin positive inflammatory infiltrate, however without a clear predictive value concerning clinical outcome. This might be due to the different subtypes and functions of the involved myeloid cells positive for S100-calgranulins. Using a second independent marker specific for granulocytes, the role of myeloid cell infiltration in the tumor microenvironment was assessed in more detail. CD66b, also known as Carcinoembryonic antigen-related cell adhesion molecule 8 (CEACAM 8) is an ahol [84] ctivation marker of human granulocytes and is highly expressed in eosinophils and neutrophils [176, 43]. As CD66b is expected to be expressed on the same cells that are positive for S100-calgranulins, the next focus was on a stratification of human OPSCC patients with regard to CD66b positive cells as a more sepcific inflammatory marker. Quantification of CD66b quantification of CD66b positive immune cells on the same patients (same TMAs) were used to confirm the data on the distribution of calgranulin positive inflammatory immune cells (sec. 3.1). In close collaboration with the ENT department at the University Hospital Essen, tissue microarrays (TMAs) comprised of OPSCC samples from 188 patients, who were treated at the ENT Department of the University Hospital Heidelberg [84] were used for immunohistochemical staining for CD66b-positive immune cells. TMAs were sent to Essen for immunohistochemical staining of CD66b-positive immune cells. The stained sections were scanned in the tissue imaging center at the Bioquant Heidelberg and were analyzed with the NDP Viewer software by three independent observers.

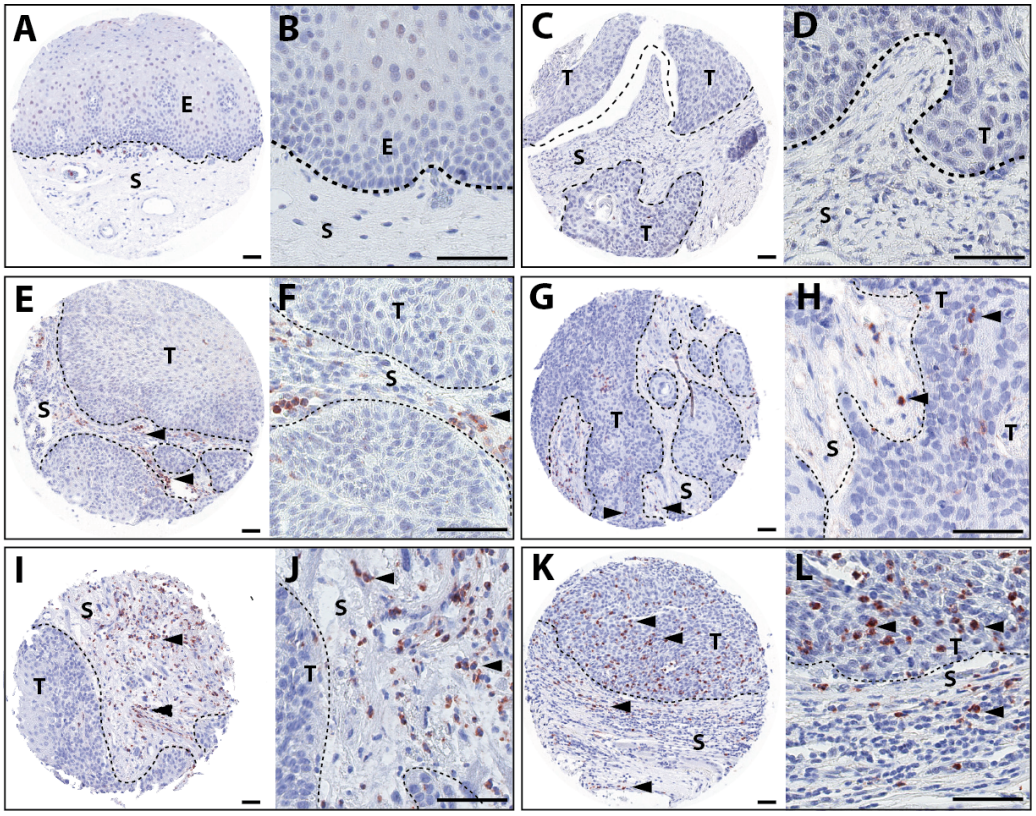

Figure 3.2: Distribution of CD66b positive inflammatory cells in human OPSCC samples. Immunohistochemical staining for CD66b-positive cells was performed on tissue microarrays (TMAs) comprised of human OPSCC samples. Normal mucosa (A and B) served as an internal control. The relative number of CD66b positive cells was scored according to their distribution in the tumor stroma and within the tumor mass. No/low numbers of CD66b positive immune cells C,D; moderate (E,F) and high (I,J) infiltration of stromal CD66b positive immune cells and moderate (G,H) and high (K,L) amount of intratumoral CD66b positive immune cells (red signal, arrows indicate CD66b positive cells). Counterstaining was performed with Hematoxyline. The dotted line separates (S) stroma from (T) tumor mass. Scale bar represents 50 µm.

No CD66b positive cells were observed in the stromal tissue of normal, healthy mucosa (Fig. 3.2 A, B), and almost one third of the tumors did not show any stromal infiltration of CD66b positive cells or CD66b positive cells within the tumor mass (Fig. 3.2 C,D). In contrast, 65% of patients showed moderate to high numbers of stromal CD66b positive infiltrating cells (Fig. 3.2 E and F) and 63% showed moderate to high numbers of intratumoral CD66b positive cells. In 24% of cases, high numbers of both stromal as well as intratumoral CD66b positive cells were observed (Fig. 3.2 G and H, K and L). For statistical

analysis, the relative amount of CD66b positive immune cells in the tumor stroma (Score D, Tab. 2.10) and the presence of intratumoral CD66b positive immune cells (C-Score, Tab. 2.10) was scored by three independent observers without knowledge of the clinic-pathologicalfeatures of the individual patients. Further statistical processing of the data was performed using the IBM SPSS statistics package.

Table 3.1: Correlation of CD66b positive and S100A8, S100A9 and S100A12 stromal and intratumoral immune cells.

		CD66b (C)		CD66b (D)	
		p	ρ	p	ρ
S100A8	A	0,5	-0,068	0,7	-0,039
S100A9		0,2	-0,125	0,2	-0,129
S100A12		0,5	-0,065	0,4	-0,076
S100A8	B	0,4	-0,089	0,6	-0,052
S100A9		0,1	-0,023	0,7	0,040
S100A12		0,1	-0,145	0,6	-0,056
S100A8	C	0,9	0,015	0,3	-0,113
S100A9		0,9	-0,008	0,2	-0,125
S100A12		0,9	0,008	0,6	-0,053
S100A8	D	**0,000**	**0,394****	**0,000**	**0,488****
S100A9		**0,003**	**0,271****	**0,002**	**0,284****
S100A12		**0,008**	**0,257****	**0,002**	**0,301****

Score legend: A number of positive epithelial (tumor) cells, B staining intensity in epithelial cells; C subcellular/histological distribution of the staining signal; D amount of positive stromal immune cells. The correlation coefficient ρ was determined by Spearman's rank Korrelation, statistical significance (p) was determined by χ^2 test.

Since CD66b and S100-calgranulins represent markers for activated granulocytes, a high degree of overlap between of CD66b positive and S100-calgranulin staining in the tumor biopsies was expected. Thus, the expression scores for CD66b (C and D-Score) was compared with data for S100A8, S100A9 and S100A12 from the same TMAs. For all three calgranulins, calgranulin expression in both tumor cells and infiltrating immune cells was determined in a previous study (Sonja Funk, unpublished data) The number of Calgranulin expressing cells (A-score), the staining intensity (B-Score), the subcellular

localization (C-Score) and the number of Calgranulin positive immune cells (D-score) was assessed by three independent observers (internal Data, Sonja Funk). The expression scores for S100A8, S100A9 and S100A12 were then correlated to the expression scores for CD66b. No correlation between the number of CD66b positive stromal (D-Score) and intratumoral (C-Score) immune cells and the number of S100A8, S100A9 and S100A12 positive tumor cells was detected (Tab. 3.1, A-Score). Accordingly, neither for the staining intensity (Tab. 3.1, B) a significant correlation was observed. While not explained in the literature so far, the nuclear localization of the S100-calgranulin staining may hint for the retaining of the protein inside the cell, which may consequently halt the extracellular function of S100-calgranulins as a pro-inflammatory mediator. However, when comparing the number of CD66b positive immune cells, no correlation to the subcellular localization of S100-calgranulins was found (Tab. 3.1, C—Score). In summary, the number of CD66b positive immune cells was independent of Calgranulin staining in the tumor. However, when comparing the number of calgranulin positive immune cells (D-Score) with the number of stromal (D), as well as intratumoral (C) CD66b positive cells, a significant positive correlation was found for all three calgranulins. This observation is shown in representative OPSCC tumor samples as depicted in Figure 19. The highest correlation was observed with the number of S100A8 positive immune cells for both the number of stromal CD66b positive cells (39.2 %) and intratumoral CD66b positive cells (45.3 %). The data suggest, considering that both markers are supposed to detect the same cell compartment and therefore a higher overlap would have been expected, that not all activated myeloid cells detected by CD66b staining are also positive for expression of S100-calgranulins.

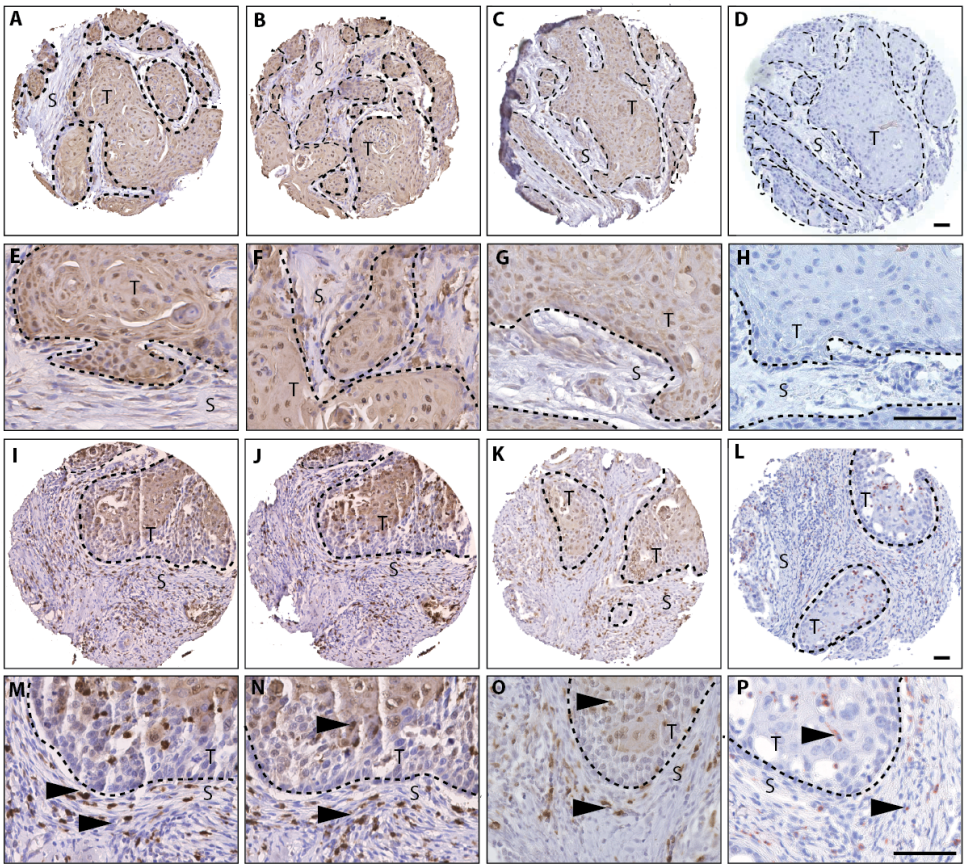

Figure 3.3: Infiltration of S100-calgranulin positive and CD66b positive immune cells in the stroma of human OPSCC samples. No/low numbers of S100a8 (A,E), S100a9 (B,F), S100A12 (C,G) and CD66b (D,H) positive infiltrating cells and moderate/high number of S100a8 (I,M), S100a9 (J,N), S100A12 (K,O) and CD66b (L,P) positive immune cells in tissue samples from human OPSCC patients. Counterstaining was performed with Hematoxyline. The dotted line separates (S) stroma from (T) tumor mass. Scale bar represents 50µm.

Taken together, these data confirm the presence of a strong inflammatory immune cell infiltration in a subgroup of OPSCC patients as detected by four different myeloid markers, S100A8, S100A9, S100A12 and CD66b. However, the abundance of myeloid cell in the tumor or the tumor microenvironment did not correlate with the prognosis or other clinicopathological parameters. Importantly, also no significant correlation between Calgranulin expression in tumor cells and the amount of infiltrating myeloid cells was found.

3.3 The number of CD66b positive myeloid cells in OPSCC samples does not correlate with survival or histopathological parameters

As the compartment of CD66b positive immune cells does not completely overlap with the S100-calgranulin positive cells, the number of CD66b positive stromal cells, as well as the number of CD66b positive cells within the tumor mass were separately tested as prognostic markers in OPSCC. Clinico-pathological patient parameters were compared to the relative amount of both stromal and intratumoral CD66b positive inflammatory infiltrate. Patients were stratified according to high, moderate and low numbers of CD66b positive immune cells. HPV 16 RNA status was included to make sure, that possible differences in inflammatory cell numbers are not simply due to active viral infection. However neither for patient parameters, nor for the clinical features a significant correlation with respect to either stromal or intratumoral CD66b positive cells was observed (Tab. 3.1). Neither tumor size and pathological grading, nor nodal involvement or distant metastasis showed any correlation to the number of CD66b positive immune cells. The same was true when patients were stratified for alcohol and tobacco habits as major risk factors. Most of the patients showed a history of alcohol and tobacco consumption, however, even though both alcohol and tobacco can induce local inflammation, patients were distributed homogeneously regarding CD66b immune cell count. Finally, also the presence of an active HPV virus infection did not show any correlation to the number of CD66b positive cells in the tumor stroma or inside the tumor mass.

Table 3.2: Clinico-pathological characterization of the distribution of stromal and intra- tumoral CD66b positive cells in OPSCC tumors.

		CD66b positive cells							
		intratumoral[2] (C)				stromal[3] (D)			
	total (N = 153)	none	few	many	*p*	none	few	many	*p*
Gender									
Male	114	37	46	31	*0,31*[†]	41	37	36	*0,15*[†]
Female	39	16	17	6		17	16	6	
Age									
≤ 57	74	24	30	20	*0,72*[†]	27	25	21	*0,47*[†]
> 57	79	29	33	17		31	28	21	
Oropharynx region									
Tonsils	73	24	30	19	*0,49*[†]	28	27	18	*0,57*[†]
Base of tongue	29	14	9	6		14	8	7	
Other	51	15	24	12		16	18	17	
Tumor size									
T1-T2	65	17	29	19	*0,36*[†]	20	25	20	*0,47*[†]
T3-T4	86	35	33	18		37	28	21	
Missing[1]	2	1	1			1		1	
Nodal Metastasis									
N0	33	8	14	11	*0,27*[†]	9	12	12	*0,28*[†]
N+	118	44	48	26		48	41	29	
Missing[1]	2	1	1			1	0	1	
Distant Metastasis									
M0	141	50	59	32	*0,34*[#]	55	50	36	*0,38*[#]
M1	7	1	2	4		1	2	4	
Missing[1]	5	2	2	1		2	1	2	
Grading									
GI	7	1	6	0	*0,1*[†]	2	2	3	*0,27*[†]
GII	66	28	23	15		29	17	20	
GIII	56	14	26	16		16	26	14	
Missing[1]	24	10	8	6		11	8	5	
Smoking									
Never	16	7	5	4	*0,47*[†]	7	7	2	*0,12*[†]
Former	18	36	52	27		39	44	32	
Current	115	7	6	5		9	2	7	
Missing[1]	4	3	0	1		3	0	1	
Alcohol consumption									
Never	12	2	8	2	*0,32* [†]	3	6	3	*0,26*[†]
Former	18	6	8	4		10	3	5	
Current	119	42	47	30		42	44	33	
Missing[1]	4	3	0	1		3	0	1	

		CD66b positive cells							
		intratumoral[2] (C)				stromal[3] (D)			
	total (N = 153)	none	few	many	*p*	none	few	many	*p*
HPV 16 status									
non HPV driven	116	36	50	30	*0,17* †	40	41	35	*0,19* †
HPV driven	32	13	13	6		14	12	6	
Missing[1]	5	4	0	1		4	0	1	

1: missing data, no information available; 2: CD66b positive cells within the tumor mass; 3: CD66b positive cells in the tumor stroma #: Fisher's exact test; †: Chi-square-Test

However neither for patient parameters, nor for the clinical features a significant correlation with respect to either stromal or intratumoral CD66b positive cells was observed (Tab. 3.2). Neither tumor size and pathological grading, nor nodal involvement or distant metastasis showed any correlation to the number of CD66b positive immune cells. The same was true when patients were stratified for alcohol and tobacco habits as major risk factors. Most of the patients showed a history of alcohol and tobacco consumption, however, even though both alcohol and tobacco can induce local inflammation, patients were distributed homogeneously regarding CD66b immune cell count. Finally, also the presence of an active HPV virus infection did not show any correlation to the number of CD66b positive cells in the tumor stroma or inside the tumor mass. Overall survival was calculated according to the stratification into patients with low, moderate and high numbers of CD66b positive stromal and CD66b positive intratumoral immune cells. No significant impact of CD66b positive stromal cells (Fig. 3.4, A) on patient outcome was observed . Also the number of CD66b positive immune cells within the tumor mass did not influence patient survival (Fig. 3.4 B). Accordingly, all groups revealed a similar clinical outcome concerning progression-free or overall survival in a Kaplan Meyer analysis (Fig. 3.4C and D).

In summary, the data confirm the presence of an inflammatory tumor microenvironment in a subpopulation of OPSCC patients, but the relative amount of tumor infiltrating or stromal CD66b-positive cells do not correlate with clinicopathological features or the clincial outcome.

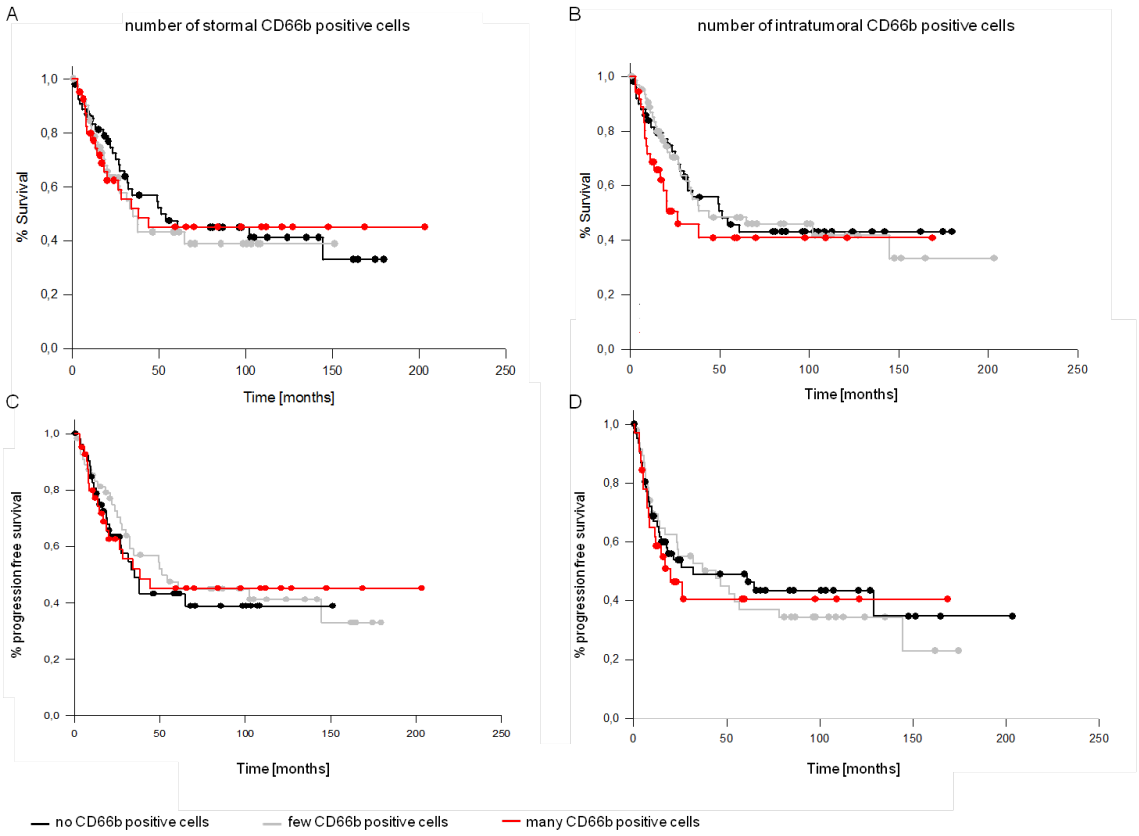

Figure 3.4: Overall and progression-free survival dependent on the number of intratumoral (C - score) and stromal CD66b positive immune cells (D - Score). Patients were stratified according to low (grey curve), high (red curve) and medium (black curve) amount of CD66b positive stromal (A, C) and intratumoral (B, D) immune cells. Overall survival (A, B) and progression free survival (C, D) were determined by Kaplan-Meyer analysis. Lack of statistical significance ($p > 0{,}05$) was assessed by Log-Rank-Test.

3.4 S100a8 and S100a9 are induced in the murine oral mucosa upon 4-NQO treatment

While the analysis of the OPSCC patient cohort revealed no major correlation between the strength of myeloid infiltration and malignant progression or clinical outcome, these data did not exclude the possibility that signaling via the S100-RAGE axis affects neoplastic transformation and early onset of mucosal carcinogenesis in setting of genotoxic stress. Therefore, the role of both S100-clagranulins and RAGE was addressed in the mouse model of 4-NQO induced carcinogenesis. In order to confirm, that 4-NQO treatment induces S100a8 and S100a9 expression in the mucosal epithelium of the tongue and esophagus, *wild type* female mice were treated for 4 months with 4-NQO in the drinking water followed by a 3 months observation period. 4-NQO and Polypropylenglycole (PPG) treated control mice were sacrificed, macroscopically inspected to monitor tumor development and tongue and esophagus tissue specimens were taken for further analysis. Immunohistochemical (IHC) staining was performed on tongue and esophageal formaldehyde-fixed and paraffin embedded (FFPE) tissue sections to determine S100a8 and S100a9 protein expression. IHC staining revealed strong S100a8 and S100a9 protein induction in tissue sections of the tongue and the esophagus from 4-NQO treated animals, as compared to normal mucosa or PPG treated controls (Fig. 3.5, A-D and Fig. 3.5, A and C). Interestingly, a prominent nuclear staining for both calgranulins was observed in keratinocytes of the tongue and the esophagus after 4-NQO treatment, which was absent in basal cells and most prominent in the stratifying layers of the mucosal epithelium (Fig. 3.5, C and D). Moreover, S100a8 and S100a9 positive cells were observed in the stromal tissue of the tongue and esophagus of 4-NQO treated mice. Given their histological appearance and the calgranulin positivity, these cells most likely represent infiltrating immune cells (Fig. 3.5; sec. 3.2, E-F). Notably, only a slight increase in S100a8 and S100a9 positive immune cells was observed upon 4-NQO treatment, suggesting the absence of a strong proinflammatory tumor microenvironmen. Thus hardly any S100a8 and S100a9 positive stromal cells were observed in the PPG treated controls.

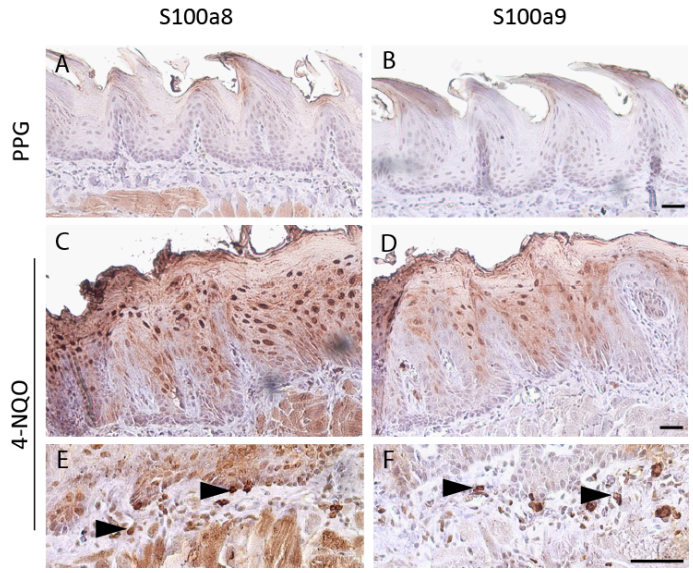

Figure 3.5: S100a8 and S100a9 expression in PPG and 4-NQO treated tongue. No/low numbers of S100a8 (A,E), S100a9 (B,F), S100A12 (C,G) and CD66b (D,H) positive infiltrating cells and moderate/high number of S100a8 (I,M), S100a9 (J,N), S100A12 (K,O) and CD66b (L,P) positive immune cells in tissue samples from human OPSCC patients. Counterstaining was performed with Hematoxyline. The dotted line separates (S) stroma from (T) tumor mass. Scale bar represents 50µm.

3.5 RAGE signaling is dispensable for tumor formation and multiplicity

To address the question whether extracellular S100a8 and S100a9 is implicated in neoplastic transformation of mucosal keratinocytes by the activation of RAGE-dependent signaling, control (wildtype and *Rage*$^{+/-}$) and *Rage*$^{-/-}$ mice were treated with 4-NQO. After 4 months of 4-NQO administration via the drinking water, mice were observed for a maximum of another 3 months and were subsequently sacrificed to analyze tumor development. Both groups showed a similar weight loss during and following 4-NQO administration (as compared to PPG treated control animals Fig. 3.6, A), which was most likely due to reduced food uptake. After an average of 25 weeks the 4-NQO treated mice had to be sacrificed due to massive weight loss whereas the PPG treated control group was kept for the whole observation period. In contrast to the 4-NQO treatment group, *Rage*$^{-/-}$ mice in the PPG treated group showed a slightly increased body weight as compared to wild type and *Rage*$^{+/-}$

mice (Fig. 3.6, B).

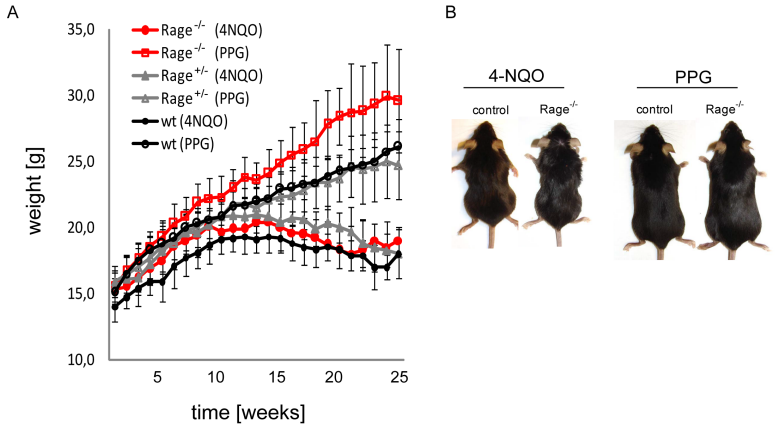

Figure 3.6: Weight loss of wild type, *Rage*$^{+/-}$ and *Rage*$^{-/-}$ mice during and after 4-NQO administration . (A). The filled symbols represent the weight of 4-NQO treated cohorts at the indicated time points, while the empty symbols show weights of the PPG treated mice. Macroscopic inspection of the animals after sacrificing shows decreased body weight compared to the PPG treated animals in the indicated genotypes.

Total RNA was prepared from the tongue of PPG and 4-NQO treated mice and semi-quantitative RT-PCR analysis confirmed RAGE expression only in control animals, which was not affected by 4-NQO administration (Fig. 3.7, A). The presence of neoplastic lesions was determined by macroscopic inspection of the upper aerodigestive tract. In line with previous publications [194] almost all 4-NQO treated control mice developed papillary lesions on the tongue and/or the esophagus, which were visible by eye ($\geq$ 0.5 mm). Tumor incidence on the tongue was 90 % in control mice and 70 % in *Rage*$^{-/-}$ animals , whereas the incidence of esophageal lesions was 75 % in control and 90 % in *Rage*$^{-/-}$ mice (Fig. 3.8, B). Only few lesions were observed on the soft palate and the gingiva (data not shown). The median multiplicity of lesions at the tongue (size between 1 3 mm in diameter) was two per animal, whereas the median multiplicity of lesions at the esophagus (size between 0.5 1 mm in diameter) was 2 3 per animal (Fig. 3.7, D and Fig. 3.8 C). However, no significant difference in tumor multiplicity between 4-NQO treated control and *Rage*$^{-/-}$ animals was observed (Fig. 3.7, C; D and Fig. 3.8, C; D), suggesting that RAGE expression is dispensable for neoplastic transformation of mucosal keratinocytes in a mouse tumor model that is driven by genotoxic stress.

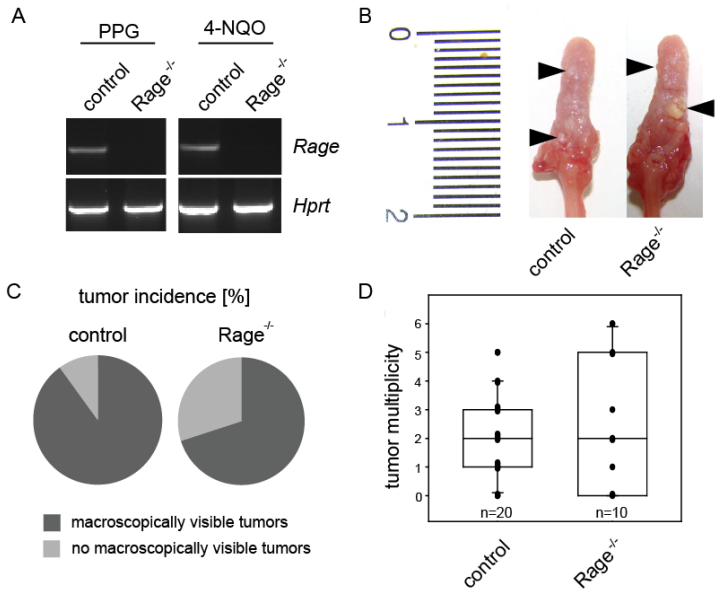

Figure 3.7: 4-NQO-induced tumorigenesis in the tongue of control and *Rage*$^{-/-}$ mice Rage expression was determined by semi-quantitative RT-PCR with cDNA from whole tongue (A). Detection of the *Hprt* amplicon served as control for cDNA quantity and quality. Macroscopic inspection of the tongue (B) revealed no major difference in tumor incidence (90 % in controls and 70 % in *Rage*$^{-/-}$) (C) and no significant difference in the multiplicity (D) between control and Rage-/- mice. n indicates the number of of animals per group; lack of statistical significance ($p > 0.05$) was determined with Wilcoxon signed-rank test.

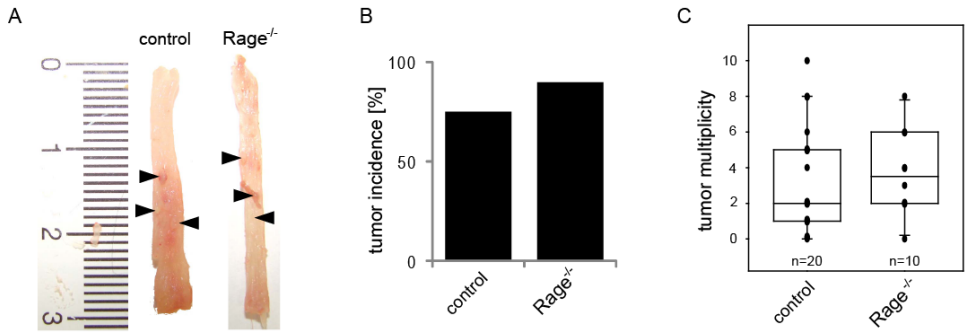

Figure 3.8: 4-NQO-induced tumorigenesis in the esophagus of control and *Rage*$^{-/-}$ mice. Macroscopic inspection of the esophagus (A) revealed similar tumor incidence (B) and no significant difference in tumormultiplicity (C) between control and *Rage*$^{-/-}$ mice. n indicates the number of animals per group; the lack of statistical significance ($p > 0.05$) was determined with Wilcoxon signed-rank test.

3.6 Histology and proliferation of the mucosal epithelia upon 4-NQO treatment

In the past, impaired epidermal hyperplasia and accelerated differentiation was found in papilloma of *Rage*$^{-/-}$ mice as compared to control animals in a chemically induced mouse model of skin carcinogenesis (Gebhardt et al., 2008). Therefore, histology and tissue architecture was addressed on tissue sections of 4-NQO treated *Rage*$^{-/-}$ and control mice. However, histological inspection of H&E stained tongue and esophageal tissue sections derived from 4-NQO treated control and *Rage*$^{-/-}$ mice revealed a similar grade of hyperplasia in both groups as determined by epithelia thickness (Fig. 3.7 A-D, Fig. 3.8 A-D). Moreover, the histological architecture of 4-NQO induced hyperplastic epithelial and dysplastic lesions in both tongue and esophageal tissue was comparable between control and Rage deficient animals (Fig. 3.7, E-F, Fig. 3.8, E-F). The neoplastic lesions represented papillary lesions and no invasive squamous cell carcinoma was observed in both groups.

Next, proliferation of mucosal keratinocytes in hyperplastic tissue and tumor cells in neoplastic lesions was determined by a BrdU incorporation assay. As expected, an increase of proliferative mucosal keratinocytes was detected in the basal layer in 4-NQO treated tongue and esophageal tissues as compared to PPG-treated controls (Fig. 3.9, G-L, Fig. 3.8, G-L). However, no obvious difference in cell proliferation was observed in 4-NQO treated control and *Rage*$^{-/-}$ mice. Furthermore, the number of proliferative tumor cells in the papillary lesions was similar in both groups (Fig. 3.9, I-L; Fig. 3.8, I-L).

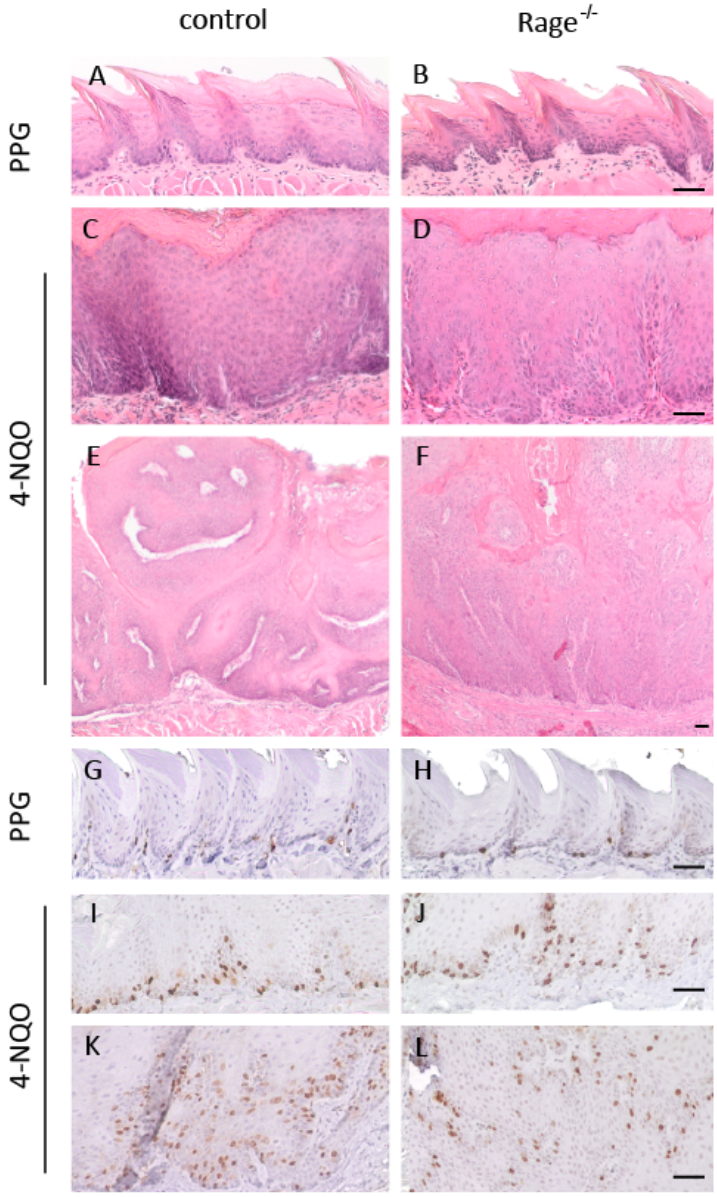

Figure 3.9: Histological staining and determination of keratinocyte proliferation in the tongue. Representative pictures for H&E staining of PPG treated normal tongue (A, B) and 4-NQO induced hyperplastic (E, D) and dysplastic (E, F) tongue epithelium. Keratinocyte proliferation was detected by immunohistochemical staining for BrdU incorporation (brown signal), revealing induced proliferation in 4-NQO treated hyperlastic (I, J) and dysplastic (K, L) tongue compared to PPG treated controls (G, H). Counterstaining with hematoxyline. The scale bar represents 50 µm.

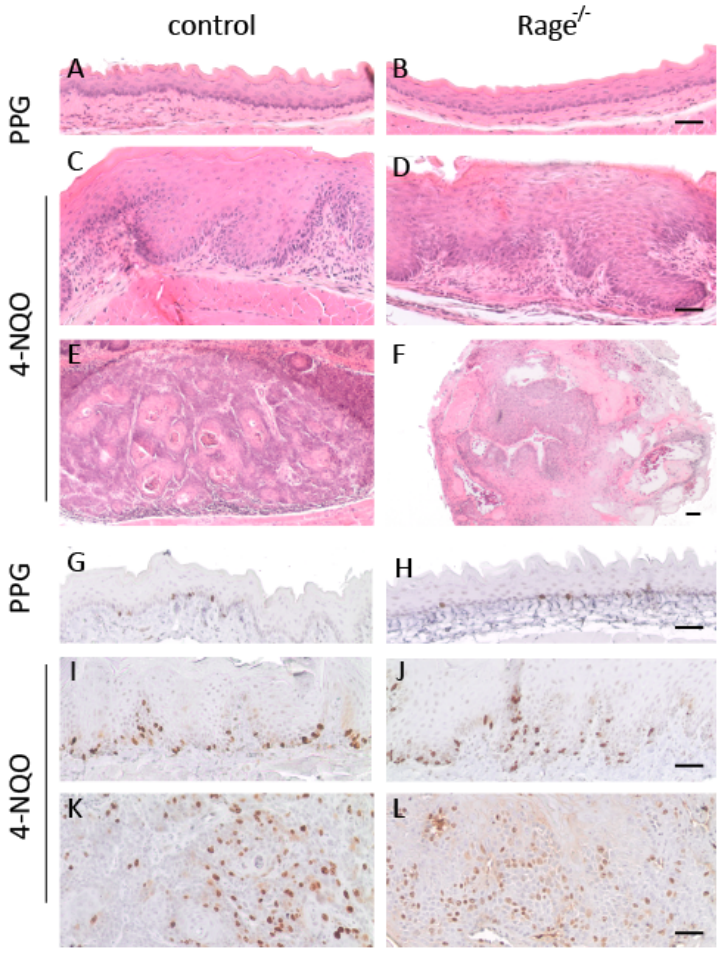

Figure 3.10: Histological staining and determination of keratinocyte proliferation in the esophagus. Representative picture form H&E staining of PPG treated normal esophagus (A, B) and hyperplastic (E, D) as well as dysplastic (E, F) epithelium. Keratinocyte proliferation was determined by immunohistochemical staining for BrdU incorporation (brown signal) in PPG treated controls (G, H) and 4-NQO treated hyperplastic (I, J) and dysplastic (K, L) esophageal epithelial cells. Counterstaining with hematoxyline. The scale bar represents 50 µm.

3.7 Impact of RAGE expression on the number of stromal immune cells and expression of pro-inflammatory mediators

Several studies confirmed an important role of RAGE signaling in the recruitment of inflammatory immune cells, specifically in mouse models of inflammation-associated carcinogenesis [60, 201, 111, 175]. Hence, cryosections of the tongue and the esophagus from PPG or 4-NQO treated control and *Rage*$^{-/-}$ mice were stained for myeloperoxidase (MPO), an established marker for activated monocytes and myeloid cells [149, 123], to monitor the amount of infiltrating immune cells within the stromal tissue. Notably, only a mild increase in the overall number of MPO-positive immune cells in the stroma of 4-NQO induced tumors as compared to PPG treated controls was observed and no difference between control and *Rage*$^{-/-}$ animals (Fig. 3.11, A; B) was found. RAGE ligands S100a8 and S100a9 are well-known proinflammatory mediators that are expressed in myeloid cells of the tumor stroma and induced in keratinocytes under conditions of tissue activation and during tumorigenesis [59, 60, 141]. As shown before (Fig. 3.5) both S100a8 and S100a9 are induced upon 4-NQO treatment in wild type mice. Interestingly, IHC staining of tongue and esophagus tissue sections from Rage deficient and control animals revealed similar expression of the pro-inflammatory mediators S100a9 and S100a8 (shown only for S100a9) in mucosal keratinocytes of hyperplastic tissue and tumor cells of neoplastic lesions upon 4-NQO treatment (Fig. 3.11, C-F and Fig. 3.11, A-F). In line with the data from the MPO staining, comparable amounts of S100a9-positive stromal immune cells (not shown for S100a8) (Fig. 3.11, C-F and Fig. 3.11, C-F) were observed in the tongue and esophagus of 4-NQO treated control and *Rage*$^{-/-}$ mice.

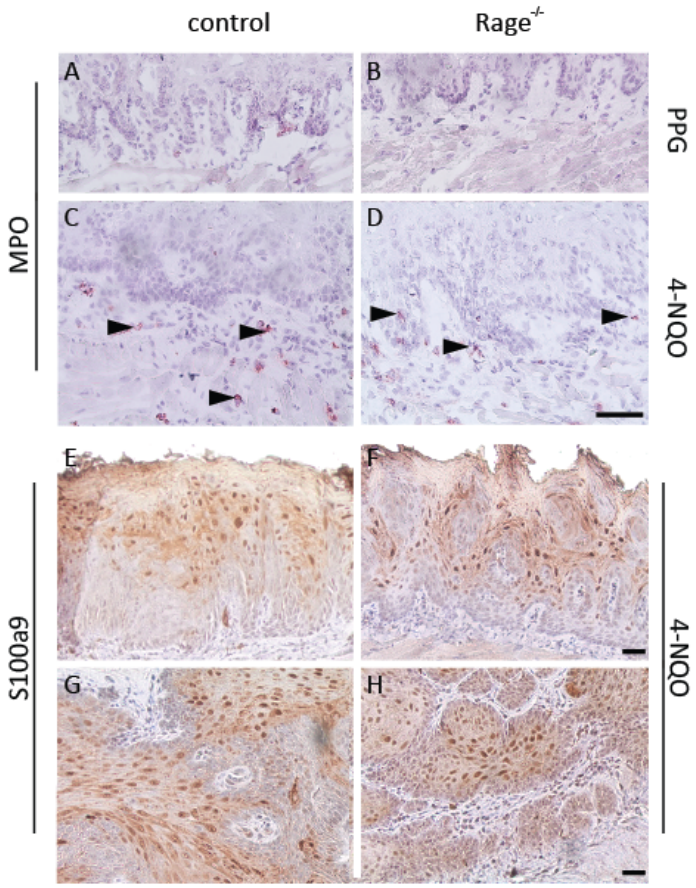

Figure 3.11: Immunohistochemical staining for Myeloperoxidase-positive immune cells and Calgranulin expression. Representative pictures for immunohistochemical staining for Myeloperoxidase (MPO, red signal) shows minor but comparable amounts of infiltrating inflammatory cells in the stroma of 4-NQO treated control (A) and *Rage*$^{-/-}$ (B) mice. Representative picture for immunohistochemical staining of S100a9 expression (brown signal) after 4-NQO shows induced expression in hyperplastic and dysplastic tongues in both wild type (C, E) as well as *Rage*$^{-/-}$ (mice (D, F). Counterstaining with hematoxyline. Scale bar represents 50 µm.

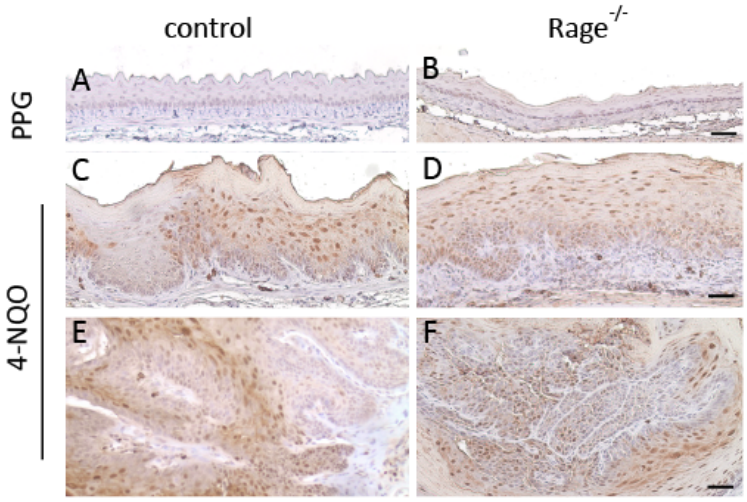

Figure 3.12: S100a9 expression in PPG and 4-NQO treated esophagus of control and *Rage*$^{-/-}$ mice. Representative pictures of immunohistochemical staining for S100a9 (brown signal) shows induced expression in hyperplastic and dysplastic esophageal tissue in both wild type (C, D) as well as *Rage*$^{-/-}$ mice (E, F) as compared to PPG treated tissue(A, B). Counterstaining with hematoxyline. The black bar represents 50µm.

3.8 Expression of the alternative S100a8/S100a9 receptor Tlr4 in 4-NQO induced tumors

Independent of the presence of RAGE, its ligands S100a8 and S100a9 were induced upon 4-NQO treatment in this model (Fig. 3.11, Fig. 3.12). However, RAGE is not the only receptor that is causally linked to the extracellular function of the S100a8 and S100a9. Thus, the question was addressed whether alternative receptors for calgranulins might compensate for the lack of RAGE in the neoplastic transformation of mucosal keratinocytes during 4-NQO induced tumorigenesis. One well-known receptor for S100a8 and S100a9 is the Toll-like receptor 4 (Tlr4), which has been shown to promote tumor growth by S100a9 [44]. Semi-quantitative RT-PCR analysis demonstrated induced Tlr4 transcript levels in 4-NQO treated tongue in both genotypes as compared to tongue tissue of PPG treated controls (Fig. 3.13, A). 4-NQO induced Tlr4 expression was confirmed on protein level by IHC staining of tongue tissue sections from PPG and 4-NQO treated control and *Rage*$^{-/-}$ animals

(Fig. 3.13, B-E). While no staining for Tlr4 was observed in the PPG controls, 4-NQOtreated tongues showed a prominent staining for Tlr4 protein in mucosal keratinocytes, which was independent of the genotype, suggesting that Tlr4 signaling may compensate for the lack of RAGE in the mouse model of 4-NQO induced carcinogenesis.

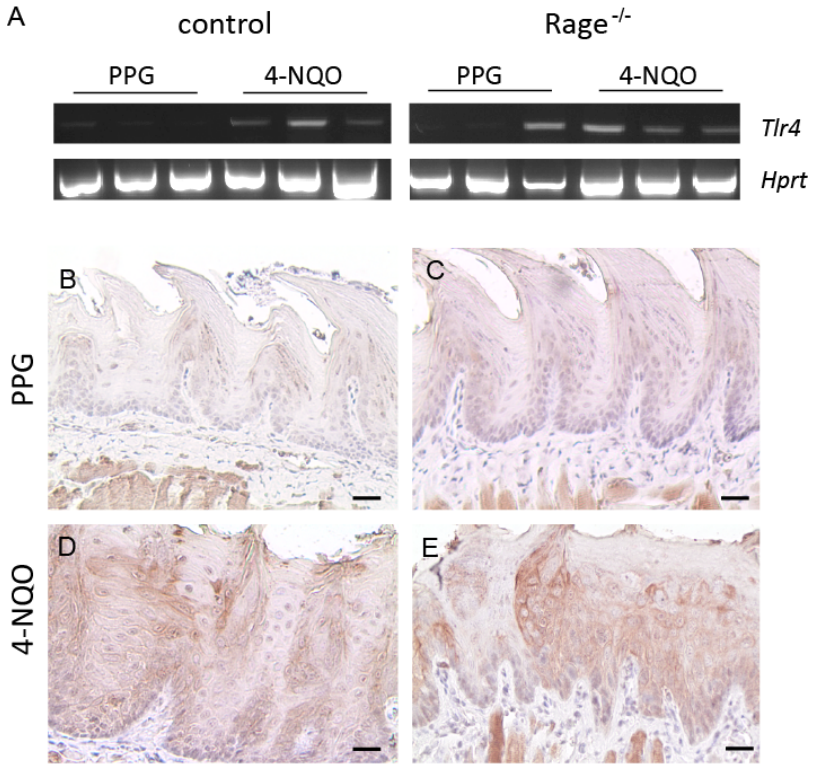

Figure 3.13: 4-NQO induced Tlr4 expression in the tongue of control and *Rage*$^{-/-}$ mice. Tlr4 transcript levels were determined by semi-quantitative RT-PCR with cDNA from whole tongue in three different animals per group (A). Detection of the *Hprt* amplicon served as control for cDNA quality and quantity. Representative pictures of an immunohistochemical staining for Tlr4 protein (brown signal). Comparison between PPG treated tongue (B, C) and 4-NQO treated tongue (D, E) revealed an increased staining for Tlr4 protein after 4-NQO treatment. Counterstaining with hematoxyline. Scale bar represents 50 µm.

3.9 S100a9 deficient mice show ablation of S100a8 expression in myeloid cells but not epidermal keratinocytes

S100a8 and S100a9 were shown to be markedly induced upon 4-NQO treatment, independent of the expression of RAGE. Possibly alternative receptors like TLR4 (sec. 3.8) or an intracellular, RAGE-independent function may account for this observation. Thus, I next focused on the role of the S100-calgranulins in the mouse model of 4-NQO induced tumorigenesis. As a S100a8 knockout is embryonically lethal, S100a9 knockout (*S100a9*$^{-/-}$) mice were used for further analysis. S100a9-/- mice have been postulated to represent a functional knockout of calgranulins, as S100a8 was described to be destabilized upon S100a9 loss [82]. *S100a9*$^{-/-}$ mice as well as heterozygous controls (*S100a9*$^{+/-}$) were treated with 4-NQO over four months with an subsequent observation period on normal drinking water for up to 3 months. The PPG treated animals were sacrificed at the end of the maximal observation time while the 4-NQO treated mice were sacrificed at signs of massive weight loss or general aggravation of the health status. Tissues were taken and further processed for freezing and paraffin embedding. First S100a8 and S100a9 expression was analyzed in FFPE tissue sections of the tongue by immunohistochemical staining. As expected, S100a9 staining was absent in the tongue tissue of *S100a9*$^{-/-}$ mice (Fig. 3.14 D), and in line with the data from the wild type and *Rage*$^{-/-}$ cohort (3.1 and 3.3), tissue sections from tongues of 4-NQO treated controls showed strong S100a9 staining for mucosal keratinocytes as well as stromal immune cells (Fig. 3.14 A+B). No S100a8 positive immune cell in stromal tongue tissue of 4-NQO treated *S100a9*$^{-/-}$ mice was detected (Fig. 3.14 C), raising the question as to whether *S100a9*$^{-/-}$ animals exhibited impaired immune cell activation and infiltration of myeloid cells upon 4-NQO treatment. In order to proof this assumption, cryosections from 4-NQO treated tongue tissue were stained for myeloperoxydase (MPO) a marker for myeloid cells by immunohistochemistry (Fig. 3.14 E and F). MPO positive cells were detected in samples of both 4-NQO treated control as well as *S100a9*$^{-/-}$ animals. The overall number of MPO positive cells was (as already seen in the previous experiments with 4-NQO treated control and *Rage*$^{-/-}$ mice; Fig. 3.11) rather low, supporting the lack of a strong inflammatory reaction.

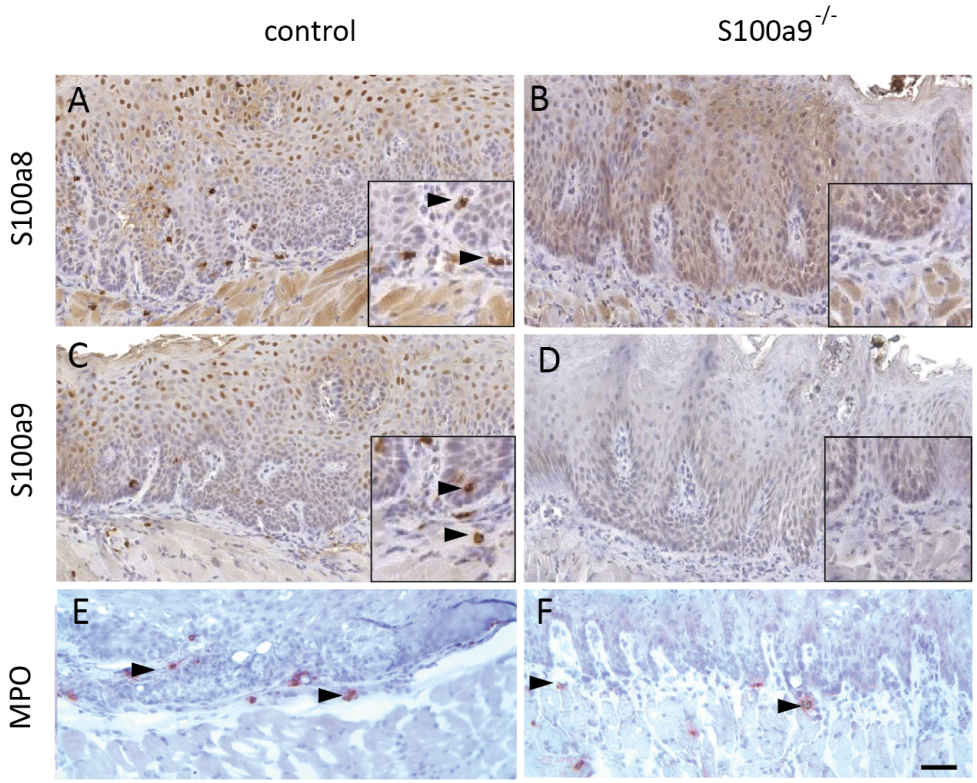

Figure 3.14: Calgranulin expression and stromal immune cell infiltration in *S100a9*$^{-/-}$ mice upon 4-NQO treatment. Representative picture of IHC staining for S100a8 and S100a9 proteins showing prominent expression in mucosal keratinocytes as well as stromal immune cells upon 4-NQO treatment in control mice (A, C). No expression of S100a9 is detected in tongue tissue from 4-NQO treated *S100a9*$^{-/-}$ mice, while a weak staining for S100a8 is detected in mucosal keratinocytes (B, D). Stromal immune cells positive for either S100a8 or S100a9 are not found in 4-NQO treated tissue of S100a9-/- mice, even though myeloperoxidase (MPO) staining showed MPO positive stromal immune cells in both control and S100a9-/- animals (E,F). Scale bar represents 50 µm.

Interestingly, *S100a9*$^{-/-}$ mice show a positive staining for S1008 protein in mucosal keratinocytes of 4-NQO treated tongue (Fig. 3.14 C), which was less prominent and more diffuse as compared to the controls (Fig. 3.14 C and D).

In summary, in consistence to preciously described data [82], a lack of S100a8 protein expression in *S100a9*$^{-/-}$ myeloid cells was observed, yet mucosal keratinocytes still exhibited residual S100a8 protein levels upon 4-NQO treatment.

3.10 Impact of S100a9 deficiency on 4-NQO induced tumorigenesis

In order to address the question whether lack of S100a9 has an impact on tumor incidence and/or tumormultiplicity, *S100a9*$^{-/-}$ deficient mice as well as *S100a9*$^{+/-}$ controls were treated with 4-NQO as described previously. While no obvious difference was measured between PPG-treated control and *S100a9*$^{-/-}$ mice concerning weight, latter animals responded to the 4-NQO treatment with a more severe weight loss as compared to the controls (Fig. 3.15). Consequently, 4-NQOtreated mice were sacrificed due to weight loss already 21 weeks after initiation of the treatment. Two animals in the 4-NQO treated cohort (one out of ten from each group) were found dead in the cage during the observation period and were excluded from the statistical analysis. All PPG treated controls survived until the end of the maximal observation period and were sacrificed after 3 months of observation.

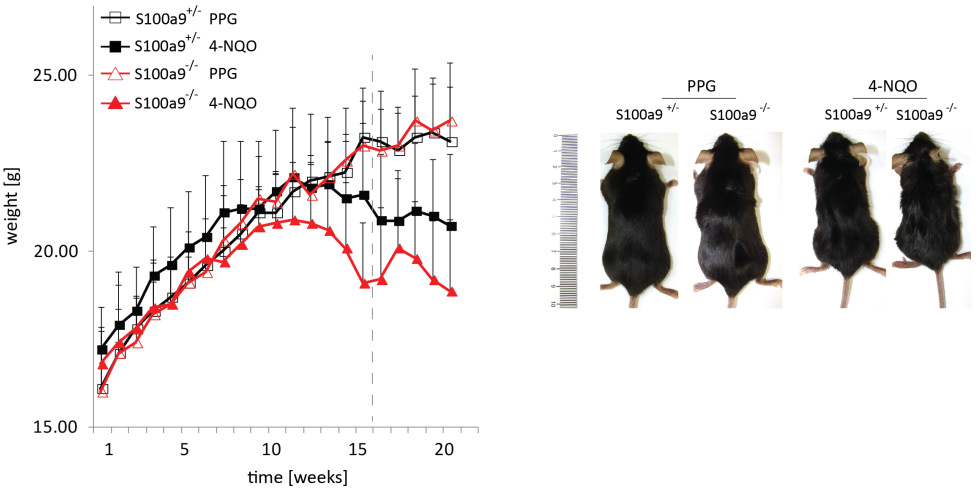

Figure 3.15: Weight loss of *S100a9*$^{-/-}$mice and *S100a9*$^{+/-}$ controls upon 4-NQO treatment. The total weight of PPG and 4-NQO treated *S100a9*$^{-/-}$ and *S100a9*$^{+/-}$ mice was determined at the indicated time points upon initiation of 4-NQO treatment and the quantitative values are shown in the left panel as mean ± standard deviation. The grey dashed line indicates the endpoint of 4-NQO administration. The experiment was terminated at 21 weeks due to massive weight loss due to 4-NQO treatment (right panel).

Inspection of the upper aerodigestive tract revealed macroscopically visible lesions of the tongue and esophagus (Fig. 3.16, A; B). Tumor size was between 0.5 - 2mm for the tongue and 0.5 - 1mm for the esophagus, and as expected 4-NQO treated controls showed a high tumor incidence with 89% in the tongue and 78% in the esophagus. No difference was found for the tumor incidence of the tongue between 4-NQO treated control and *S100a9*$^{-/-}$ mice (89%), but latter animals developed an even higher tumor incidence in the esophagus (100%) (Fig. 3.16, C). However, both genotypes developed a median number of two macroscopically visible lesions at the tongue and two to three tumors at the esophagus without a significant difference. In summary, these data demonstrate no major difference in tumor incidence and multiplicity between *S100a9*$^{-/-}$ and control animals and suggest that S100a9 expression is dispensable for 4-NQO induced tumorigenesis.

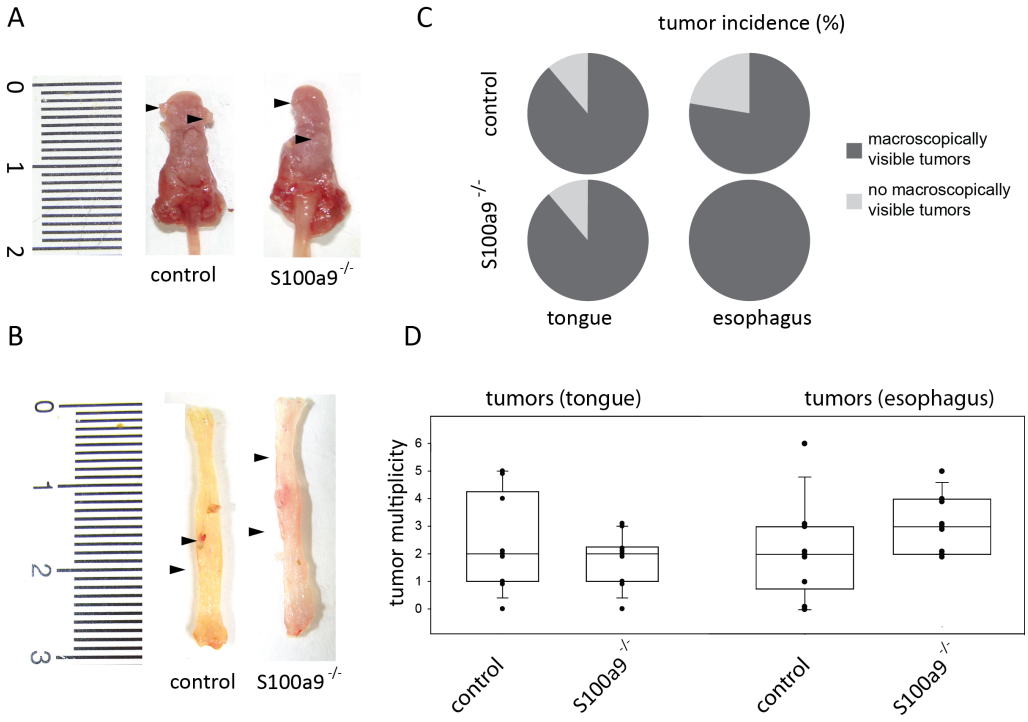

Figure 3.16: 4-NQO induced oral and esophageal carcinogenesis in control and *S100a9*$^{-/-}$ mice. Macroscopic inspection of tongues (A) and esophagi (B) revealed a comparable tumorigenesis upon 4-NQO treatment, and no major difference in tumor incidence (C) and tumor multiplicity (D) was found between control and *S100a9*$^{-/-}$ mice.

3.11 Histology, proliferation and differentiation of 4-NQO treated mucosal tissues from S100a9 deficient and control mice

S100a8 and S100a9 have previously been linked to cutaneous keratinocyte differentiation, as the functional dimer is massively upregulated in psoriatic skin, driving hyperproliferation and abnormal differentiation [14]. Moreover, S100A8/A9 has been shown to promote differentiation of HaCaT keratinocytes in vitro [209].

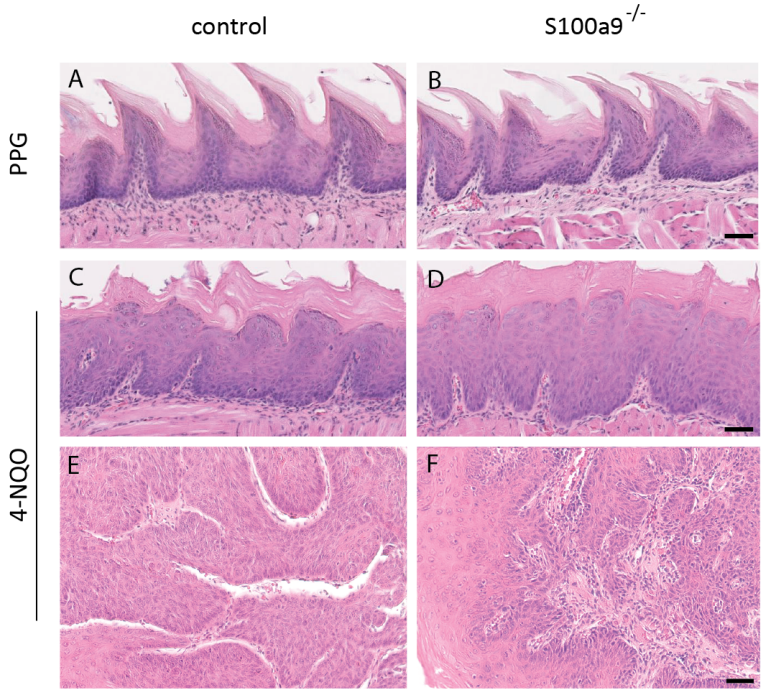

Figure 3.17: 4-NQO induced oral and esophageal carcinogenesis in control and *S100a9$^{-/-}$* mice. Histological staining of tongue specimens derived from 4-NQO treated control and *S100a9$^{-/-}$* mice. Representative pictures for H&E staining of tongue tissue sections from PPG treated normal tongue (A, B) and 4-NQO induced hyperplastic (E, D) and dysplastic (E, F) tongue epithelium. Scale bar represents 50 µm. Macroscopic inspection of tongues (A) and esophagi (B) revealed a comparable tumorigenesis upon 4-NQO treatment, and no major difference in tumor incidence (C) and tumor multiplicity (D) was found between control and *S100a9$^{-/-}$* mice.

Thus, the histological architecture of tongue tissue derived from PPG and 4-NQO treated *S100a9*$^{-/-}$ mice and heterozygous controls was compared on FFPE tissue sections after staining with hematoxyline and eosine (H&E). For both genotypes, prominent hyperplasia of mucosal epithalia and dysplasic lesion were observed following 4-NQO treatment (Fig. 3.17 A-D), and no major difference in the histological architecture of the tissues were visible between 4-NQO treated *S100a9*$^{-/-}$ and control mice (Fig. 3.17 E-F). In line with the data of the Rage cohort no invasive squamous cell carcinoma was observed in both groups. Next, cell proliferation of keratinocytes in hyperplastic mucosal epithelia and tumor cells of neoplastic lesion was determined by IHC detection of BrdU incorporation. Both control and *S100a9*$^{-/-}$ animals showed an increase of BrdU positive cells upon 4-NQO treatment in hyperplastic (Fig. 3.18 C,D) and dysplastic (Fig. 3.18 E,F) tongue tissue as compared to PPG treated controls. However, there was no significant difference between the two genotypes. In summary neither proliferation nor tissue architecture were markedly altered in 4-NQO treated *S100a9*$^{-/-}$ mice as compared to the *S100a9*$^{+/-}$ controls.

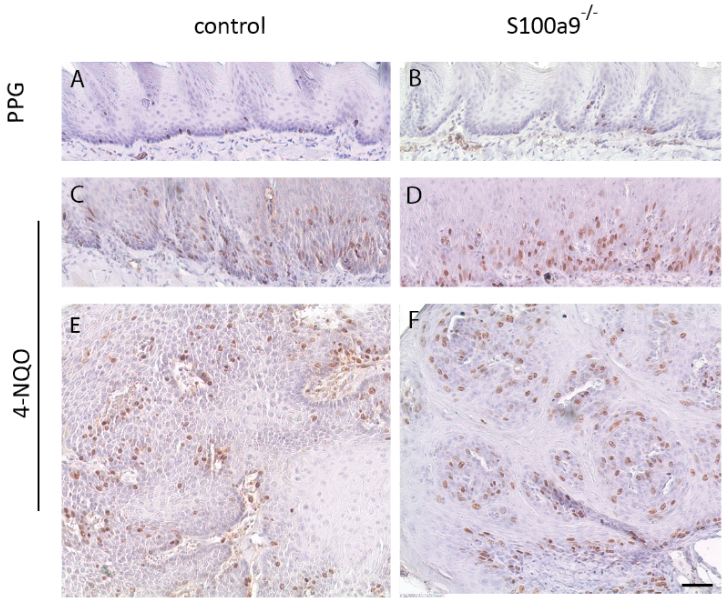

Figure 3.18: Cell proliferation in tissue sections of the tongue uopn 4-NQO treatment.

Cell proliferation was detected by immunohistochemical staining for BrdU incorporation (brown signal) and revealed increased amounts of BrdU positive cells in 4-NQO treated hyperlastic (I, J) and dysplastic (K, L) tongue as compared to PPG treated controls (G, H). Counterstaining was performed with hematoxyline. Scale bar represents 50 µm.

Recently, a correlation between S100A8 and S100A9 expression and the differentiation grade of tumors were demonstrated in human HNSCC [161], suggesting a causal link between calgranulin expression and aberrant differentiation in settings of mucosal tumorigenesis. To proof the assumption, that lack of S100a9 expression is associated with aberrant differentiation, FFPE tissue sections from tongue specimens of 4-NQO treated *S100a9*$^{-/-}$ and control mice were stained by immunohistochemistry for early and intermediate epithelial differentiation markers cytokeration 14 (K14) and cyteokeration 13 (K13) and the late differentiation marker Loricrin. Cytokeratin 14 is a well established marker for basal keratinocytes with proliferative activity, while cytokeratin 13 is preferentially expressed in the suprabasal layer of non-stratifying epithelia.

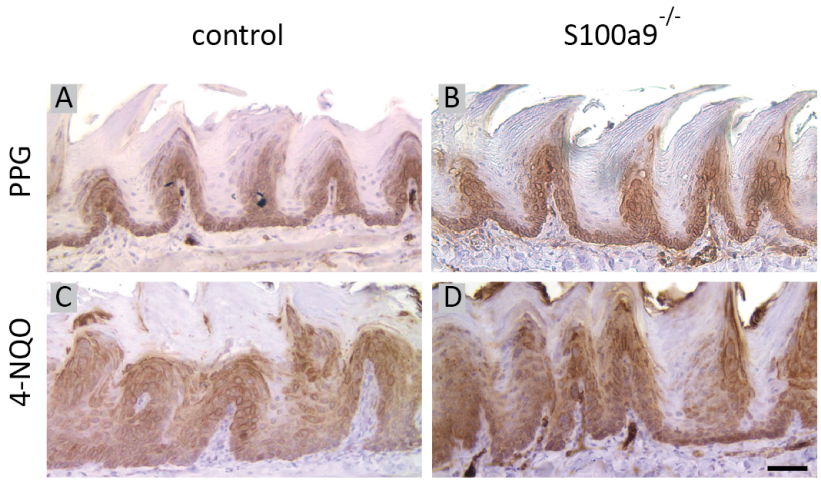

Figure 3.19: Cytokeratin 14 expression in PPG and 4-NQO treated tongue of control and *S100a9*$^{-/-}$ mice.
Cytokeratin 14 expression in PPG and 4-NQO treated tongue of control and *S100a9*$^{-/-}$ mice Keratin 14 is expressed in the basal layer of control and S100a9 deficient tongue epithelia (A,B). After 4-NQO treatment, basal and parabasal expression was detected (C,D). Counterstaining was performed with hematoxyline. Scale bar represents 50 µm.

Cytokeratin 14 expression was detected in the basal layer of the PPG treated tongue epithelium of both genotypes (Fig. 3.19, A;B), and in line with the increase of BrdU positive cells (Fig. 3.18, C;D) showed a broader pattern in basal as well as parabasal keratinocytes after 4-NQO treatment (Fig. 3.19, C;D). However, no obvious difference in staining intensity or the amount of positive cells was found between *S100a9*$^{-/-}$ and control mice. Cytokeratin 13

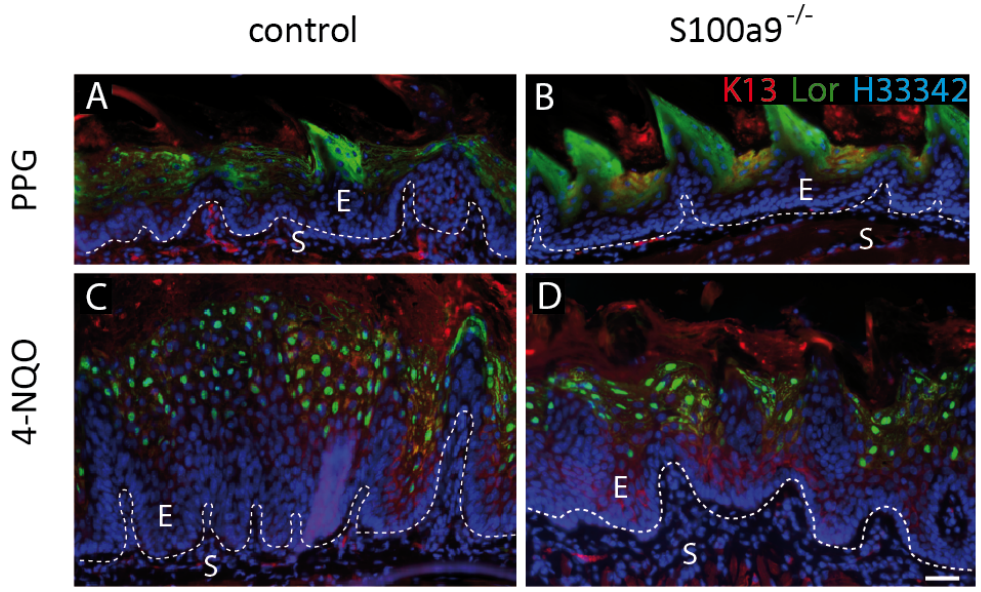

Figure 3.20: Expression of intermediate and late keratinocyte differentiation makers in the tongue of 4-NQO treated control and *S100a9*$^{-/-}$ animals.

(Immunofluorescense staining was performed to detect Cytokeration 13 (K13) (A,B) and Loricrin (C,D) protein expression. Epidermal (E) and stromal compartment (S) are indicated by dashed lines. To compare layering of the two differentiation markers, pictures were merged (E,F); nuclei were visualized with Hoechst H33342 staining (blue signal), K13 (red signal), Loricrin (green signal). The scale bar represents 50 µm.

expression (Fig. 3.20; red signal) was detected by immunofluoreszence ananlysis in the suprabasal and intermediate layers of the tongue epithelium. Again, tissue sections of 4-NQO treated *S100a9*$^{-/-}$ and control tongues revealed a similar staining pattern. Finally, the expression of Loricrin, a well known marker for late keratinocyte differentiation was analyzed, which also exhibited a comparable staining pattern on tissue sections from 4-NQO treated *S100a9*$^{-/-}$ and control mice. (Fig. 3.20; green signal) Altogether, no significant alteration in keratinocyte proliferation and epithelial differentiation was found for *S100a9*$^{-/-}$ mice upon 4-NQO treatment as compared to controls.

4 Discussion

4.1 Calgranulin expression in tumor cells does not coincide with accelerated myeloid cell infiltration in HNSCC

The current concept of the constitution of S100-RAGE signaling contributes in epithelial malignancy is mainly based on preclinical model systems in which RAGE acts as a signaling modulator in the paracrine communication between cancer and immune cells, thereby promoting the establishment and maintenance of a proinflammatory tumor microenvironment (Fig. 1.2). Accordingly, S100A8/A9, which is released by infiltrating immune cells as well as tumor cells, acts via RAGE and thus, while inducing both the expression of the receptor as well as their own expression via NF-κB, fuel this vicious cycle of cancer related inflammation [60, 201, 158, 141].

The analysis of tumor sections from OPSCC patients, however, indicates that in contrary to this model, infiltration of myeloid cells does not necessarily occur in parallel to S100-calgranulin expression in cancer cells. Indeed, distinct subgroups of patients exist with either strong S100-calgranulin expression in tumor cells but no or only minor amounts of S100-calgranulin positive immune cells in the tumor microenvironment, or vice versa. Consequently, no significant overlap linking calgranulin expression in the tumor and inflammatory cells was detected (unpublished data, S. Funk). This finding was further supported by the detection of CD66b-positive immune cells, representing activated granulocytes of the tumor stroma and inside the tumor mass (Fig. 3.2 and Tab. 3.2). Although, a significantly correlation was observed with the number of calgranulin positive immune cells, CD66b-positive granulocytes did not correlate with expression of S100A8, S100A9 or S100A12 in tumor cells, respectively.

Finally, healthy human mucosa shows expression of all three calgranulins in suprabasal as well as differentiated keratinocytes and no staining for either activated CD66b positive granulocytes or S100A8, S100A9 or S100A12 immune cells arguing for an intracellular, possibly inflammation independent mode of action of 100-calgranulins in tissue homeostasis. In line with recent publications [48, 22], this study confirms the presence of a strong tumor infiltration by myeloid cells in numerous HNSCC patients. However, while the amount of tumor infiltrating myeloid cells have been shown to be associated with the clinical outcome of HNSCC patients [75, 204], no significant correlation with clinical and histopathological features or overall survival could be observed. This may in part be due to the complex role inflammatory cells in general and more specific myeloid cells in cancer [66, 56]. Thus, while this study describes two distinct groups of patients (high vs. low levels of myeloid cell infiltration), besides the quantity also the quality of inflammatory cells, which was not covered by the present analysis, critically determines the course of disease. A bias simply caused by the immunemodulatory effect of an active HPV infection in OPSCC seems unlikely, as for S100-calgranulin as well as CD66b positive immune cells no association with HPV infection was observed in this cohort (Tab. 3.2; unpublished Data S. Funk) .

Approximately half of the tumors in is cohort originated from the tonsillar epithelium, 19 % from the base of tongue and 33 % from other anatomical sites within the orophaynx region Tab. 3.2. As much as heterogeneity between different HNSCC patients seems an obvious explanation different behavior and outcome [187], intratumoral heterogeneity of HNSCC tumors might well be an explanation for the lack of statistical significance to some extend [200]. However, by comprising several punches from different areas of one tumor per patient on the tissue microarray, intratumoral heterogeneity with respect to the measured markers could be reduced to a minimal amount. Relative expression levels were scored by three independent observers. For statistical analyses the mean expression score per patient was calculated and tumors with a high divergence between the different spots were excluded from further analysis.

Supporting the observation in human patients, mice treated with 4-NQO showed an induction of S100a8 and S100a9 protein expression in mucosal epithelial and tumor cells without major signs of inflammation (Fig. 3.11). This is observed long after the acute treatment phase with the carcinogen, arguing

for an induction through genotoxic stress. These findings suggest on one hand, that induction and maintenance of high S100A8 and S100A9 expression occurs after genotoxic stress in the absence of further stimulation of an immune reaction, and on the other hand that their expression in keratinocytes does not necessarily result in the establishment of a proinflammatory microenvironment. In this context, S100a8 and S100a9 were found to be significantly upregulated upon UV irradiation in epidermal keratinocytes in response to ROS production, however lacking major inflammatory cell recruitment [67, 130]. Thus S100calgranulin expression might simply be an indicator of stress and epidermal regeneration without necessarily resulting in the induction of an inflammatory milieu.

4.2 S100a8 and S100a9 are induced in 4-NQO driven oral carcinogenesis independent of RAGE

S100-RAGE signaling was identified as a central hub in different inflammation associated cancer models, driving inflammatory reactions and cancer formation. In this context, RAGE deficiency effectively protected from tumor formation in an inflammation driven mouse cancer model of the backskin and in colitis associated colon carcinogenesis [60, 201]. However, little is known so far concerning RAGE function in the absence of a strong inflammatory stimulus. Therefore, *Rage*$^{-/-}$ mice in the 4-NQO model of genotoxic stress driven oral carcinogenesis provide an elegant tool to have a more functional view on RAGE in the onset of oral carcinogenesis in the absence of an actively driving inflammation *in vivo*. 4-NQO treatment induced expression of S100a8 and S1009a proteins in mucosal keratinocytes of both *Rage*$^{-/-}$ mice and control animals (Fig. 3.5, Fig. 3.11 and Fig. 3.12), interestingly with a prominent nuclear staining. Although damage signals induced by 4-NQO may provide an inflammatory stimulus, the 4-NQO treated mice show only mild inflammatory infiltration as shown by MPO positive stomal cells (Fig. 3.11) and S100a8 and S100a9 positive immune cells (Fig. 3.5 and Fig. 3.12) in both *Rage*$^{-/-}$ as

well as control animals. S100-calgranulin secretion in the oral mucosa may be regulated similar to other DAMP signaling molecules like HMGB1, where the effector molecule is retained in the nucleus upon apoptotic cell death, yet gets released to actively induce damage signaling upon severe damage and necrosis and subsequently triggers inflammation [170, 175]. However, the tissue was analyzed long after the 4-NQO treatment phase. Thus, while acute inflammation caused by 4-NQO is described, when the carcinogen is withdrawn, no massive signs of inflammation are expected [76]. S100-calgranulin induction was independent of RAGE expression, in contrast, S100a8 and S100a9 transcript levels were decreased in epidermal keratinocytes of TPA treated backskin from *Rage*$^{-/-}$ mice as compared to *wild type* controls [60]. The latter however relies on the secretion of S100a8/a9 into the tumor microenvironment to efficiently mediate the recruitment of inflammatory immune cells and mediate signaling via RAGE. While 4-NQO efficiently induces S100a8 and S100a9 expression in mucosal keratinocytes it is unlikely that this induction also results in a release of S100a8/a9 and thus enables their extracellular function as RAGE ligands. Possibly, genotoxic stress induced by 4-NQO retains S100a8 and S100a9 in mucosal keratinocytes, while an active inflammatory stimulus leads to the release of the dimer and subsequently the establishment of a RAGE modulated inflammatory feed forward loop. It may therefore well be that the two models represent two distinct modes of action of S100-Calgranulins in cancer.

4.3 RAGE function in cancer - a matter of context?

Looking at the S100-RAGE axis in the context of genotoxic stress on one hand and inflammation driven carcinogenesis on the other, it becomes clear that the current model of S100-calgranulins in cancer as damage mediators and RAGE ligands is not complete. While important for the establishment and maintenance of inflammatory processes and tumor promotion in inflammation associated cancer, the RAGE mediated inflammatory feed forward loop apparently does not play a major role in settings of genotoxic stress or cell damage

without an additional inflammatory stimulus (Fig. 4.1).

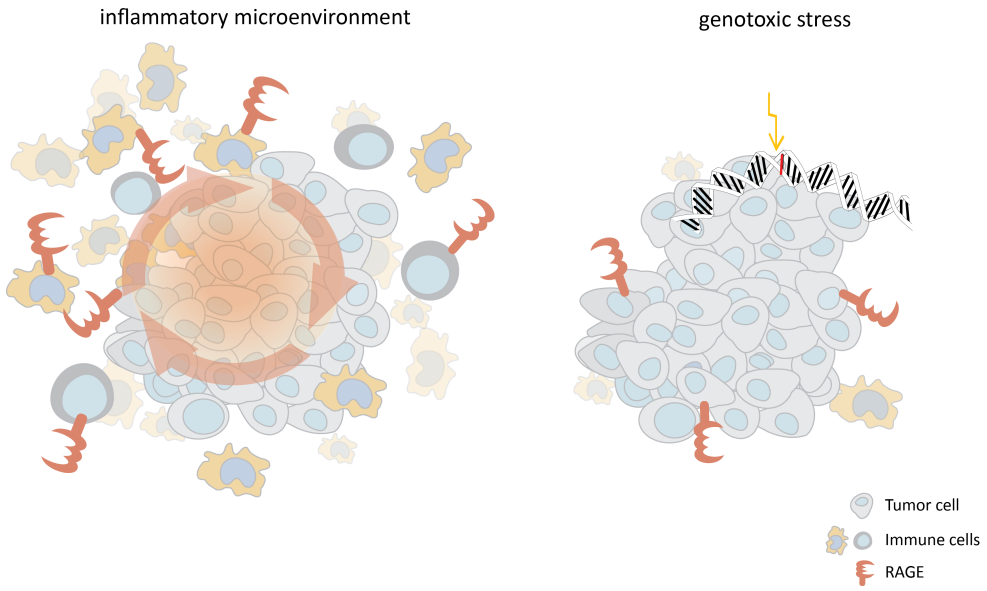

Figure 4.1: Model for the context-dependend role of RAGE in cancers.
RAGE functions as a modulator in inflammation associated cancer, translating extracellular damage signals into a cellular response fueling inflammation (left panel). In cancers driven mainly by genotoxic stress without a distinct inflammatory milieu and in the absence of extracellular DAMPs, RAGE signaling via inflammatory mediators like S100a8/a9 is not playing a major role.

Induction of S100-calgranulin expression in epithelial cells is regarded a sign of stress which consequently leads to the establishment to a RAGE mediated inflammatory feed forward cycle promoting cancer. While this is the case in DBMA/TPA treated backskin, apparently 4-NQO induced damage in the oral mucosa represents a fundamentally different process. While epithelial expression of calgranulins in mucosal keratinocytes is observed regardless of RAGE expression, this expression does not trigger the recruitment of myeloid cells at the site of damage. Therefore, RAGE may not be required as a receptor for S100a8/a9, explaining the lack of a phenotypic difference regarding S100-calgranulin expression in *Rage*$^{-/-}$ mice as compared to *wild type* controls.

4.4 RAGE is dispensable in the onset of oral carcinogenesis in a 4-NQO driven mouse tumor model

Regarding tumor formation, expression of RAGE was dispensable for tumor incidence and multiplicity in the 4-NQO model of mucosal carcinogenesis. While RAGE deficiency was shown to protect from tumor formation in other mouse cancer models [201, 60, 39], in the present setup the loss of RAGE did not seem to influence the onset of oral carcinogenesis. 4-NQO induced lesions develop from Ras transformed cells after the end of the actual carcinogen treatment [76] and thus more relate to protocols of sequential DMBA treatment, which causes HA-*ras* mutations and finally cancer without an additional inflammatory promoter [38]. RAGE deficient mice, however, were never subjected to a sequential DMBA protocol, so a direct comparison is not possible. The employment of *Rage*$^{-/-}$ mice in a sequential DMBA model to more closely mimic 4-NQO carcinogenesis of the oral mucosa would therefore facilitate a direct comparison between *Rage*$^{-/-}$ mice in backskin and oral carcinogenesis, expecting again to see RAGE independent formation of tumors. In line with this, *Rage*$^{-/-}$ mice develop less and smaller tumors in a mouse model of inflammation associated hepatocellular carcinogenesis, while no significant difference was found in a mouse model of diethylnitrosamine (DEN) induced liver cancer, which is characterized by tissue damage and compensatory proliferation, but only minor infiltration of inflammatory immune cells (unpublished data, Tobias Pusterla and Peter Angel).

4.5 RAGE independent intracellular function of calgranulins

S100a8/a9 are mainly described in the context of damage and inflammation and in fact used as serum markers for pathologic inflammatory conditions ([54, 182]. However, far less is known about their intracellular physiologic and pathophysiological function in epithelial and tumor cells. It is commonly assumed, that S100a8/a9, while constitutively expressed in myeloid cells, their expression is induced upon stress signals in other cell types [182]. However, in the normal human mucosa, S100a8, S100a9 and S100A12 are markedly expressed in suprabasal and differentiating keratinocytes (unpublished data, S. Funk) suggesting a potential role for calgranulins in normal mucosal homeostasis. This is in line with the observation that S100-calgranulin expression is lost during malignant progression in HNSCC [161]. Normal mucosa used in this study originated from uvula tissue of patients undergoing surgery for sleep apnea, however data concerning alcohol and tobacco consumption habits were not available, leaving the possibility that S100-calgranulin expression in the non-transformed control mucosa may result from damage through alcohol and tobacco or more generally tissue irritation. Independent of the induction of extracellular signals via RAGE, stress and DNA damage triggers NF-κB activity, which subsequently can induce the expression of S100a8/a9 [141]. NF-κB activation following DNA damage by tobacco smoke in HNSCC patients furthermore confirms the relevance of this pathway [124]. Moreover, overexpression of S100A8 and S100A9 in HaCaT keratinocytes was accompanied by an increase of NF-κB activation [209]. Importantly, Voss and colleagues demonstrated an increase in NF-κB p65 phosphorylation that was independent of the release of S100A8/A9 and its extracellular function. This could explain the paradoxical observation of induced expression of S100a8/a9 in mucosal keratinocytes without simultaneous inflammation and serves as yet another hint that in mucosal keratinocytes S100A8/A9 exert important intracellular functions, contrasting the extracellular role of the complex as a inducer of cell growth in keratinocytes in collaboration with inflammatory cytokines [143]. Several publications describe the intracellular role of S100a8 and S100a9 as inducers of cellular reactive oxygen species (ROS) [158, 9]. The connection of S100A8/A9 with reactive oxygen species and more detailed its impact on

cancer is however not completely understood. While for liver carcinogenesis, a S100A8/A9 mediated increase in ROS was detected, accompanied by enhanced cell survival, proposing a role of S100A8/A9 in ROS-dependent promotion of malignant progression [141], Ghavami and colleagues showed, that S100A8/A9 can induce apoptosis in colon cancer cells *in vitro* in a ROS dependent manner [61]. Furthermore, Also, 4-NQO itself may indirectly interfere with the role of S100A8/A9 in intracellular ROS production as the carcinogen was described to generate reactive oxygen species [153, 8]. Moreover, prominent nuclear staining of calgranulins was visible in human HNSCC Patients [161] as well as after 4-NQO treatment in murine oral mucosa, which further argues for an intracellular mode of action. So far, little is known about the regulation and function of nuclear S100A8 and S100A9. Even though in prostate cancer cells, S100A8 and S100A9 were previously described to be located in the nucleus and nuclear localization in immunohistochemical staining is indeed observed frequently [79, 203]. In addition, for several other members of the S100 protein family like S100A1, S100A2, S100A4, S100A11 and S100A13, nuclear localization has been shown [55, 193, 86, 165]. In the case of S100A4, while it is known to be involved in the regulation of cell cycle progression and differentiation, nuclear localization was linked to metastatic potential in cancer and moreover was shown to mediate invasion and metastasis in esophageal squamous cell carcinoma [53, 214] Another yet unsolved question is the mechanism, by which S100A8 and S100a9 enter the nucleus. Neither protein has a nuclear localization signal, leaving space for speculation on possible shuttling partners and import/export mechanisms.

4.6 Alternative receptors may compensate for the lack of RAGE in 4-NQO treated mice

The RAGE independent induction of S100a8/a9 without simultaneous stromal inflammation upon 4-NQO treatment may be simply attributed to the lack of major levels of secreted S100a8/a9. On the pe hand, it could as well hint to extracellular, yet RAGE independent functions of the heterodimer. Extracellular S100a8 and S100a9 may well trigger alternative receptors, such as Tlr4 [206, 44] and thereby compensate for the lack of RAGE in early stages of neoplastic transformation and tumor growth. While several studies focus on TLR4 expression on immune cells [212, 184], in HNSCC the expression of TLR4 in tumor cells was addressed only in few studies. TLR4 expression in epithelial cells of head and neck tumors was connected to tumor progression and aggressiveness in humans [189, 184]. Szczepanski and colleagues showed TLR4 staining in well differentiated and moderately differentiated HNSCC, supporting the observation of TLR4 expression in lesions induced in the 4-NQO model (Fig. 3.13). The authors also detect TLR4 expression at low levels in normal human mucosa. This may explain the results from mouse tongues on RNA level, showing (mainly faint) signals for TLR4 also in PPG treated tongues, while in the immunohistochemical staining no expression of TLR4 was detected (Fig. 3.13), possibly due to the lack of sensitivity of the antibody. Furthermore, interaction of S100a9 with Tlr4 has recently been demonstrated to promote tumor growth in a model of prostate cancer [98]. Interestingly, impaired tumor growth was found for both Tlr4 and S100a9 knockout mice, but not in Rage deficient mice. Thus, while in literature S100A8/A9 are usually closely connected to RAGE, the extracellular function of S100A8/A9 is not restricted to this receptor. Moreover, only recently binding of S100A9 to the cell surface glycoprotein EMMPRIN [80] was identified to promote metastasis of melanoma cells independent of RAGE. Yet another potential receptor binding to S100a8/a9, though not discussed in the context of canter is the scavenger receptor CD36[103, 28]. Finally the heterodimer can bind to heparin and heparan sulfate glucosamineglycans on the cell membrane [160], in summary, showing up several possible extracellular modes of action of S100a8/a9 that do not require RAGE activation. Importantly, in our study mice were sacrificed due to severe weight loss around three weeks before the planned endpoint of the

experiment hampering the analysis of RAGE function in malignant progression into squamous cell carcinoma. While RAGE is apparently not required in the onset of oral carcinogenesis, no conclusion about its role in malignant progression can be drawn. In this context, RAGE deficient mice showed smaller, mainly low grade lesions in a mouse model of colorectal carcinogenesis in contrast to *wild type* mice, in which invasive adenoma developed [201]. The same was seen for mice deficient in S100a9, while again, as already seen in *wild type* and RAGE deficient mice (Fig. 3.7 and Fig. 3.8), papilloma were observed in the majority of animals (Fig. 3.16), no invasive SCC were found, regardless of the genotype. With regard to S100-calgranulins, this is an important issue keeping in mind that S100-calgranulin expression is lost in advanced stages of human HNSCC and nodal metastasis [161], and concerning the prognosis and treatment of human HNSCC patients. Early stage HNSCC, which is reflected in the present study, can be treated effectively and with a good prognosis. However, patients often present with advanced stages of disease and therefore are facing poor prognosis and limited treatment options [110, 163]. It may therefore well be, that the S100-RAGE signaling axis is not required at early stages of oral carcinogenesis but later on modulate important functions of the tumor microenvironment [158] and become relevant for the maintenance of a pro-tumorigenic milieu. In this context, RAGE antagonists were shown to reduce metastasis and cell growth in pancreatic cancer and glioma and suggested for treatment of pulmonary metastasis [9] In fact, these data relativize the view on s100-RAGE signaling and the function S100 calgranulins in cancer, opening up room for further functional implications and regulatory interactions.

4.7 S100a8 and S100a9 do not affect the onset of oral carcinogenesis

While characterization of the *Rage*$^{-/-}$ mouse in the 4-NQO model of oral carcinogenesis did not reveal a role for the receptor RAGE in the onset of cancer formation, RAGE ligands S100a8 and S100a9 were nevertheless induced in mucosal keratinocytes of tongue and esophagus. It seems however, that the extracellular role of S100a8 and S100a9 as RAGE ligands is either negligible in this setup or that the heterodimer acts in an intracellular and RAGE independent manner. Taking in consideration the obvious heterogeneous, yet fundamentally unclear observation of S100-calgranulin expression in human HNSCC tumors, the logical consequence was to further address S100-calgranulin function in the mouse model. Applying the same protocol of 4-NQO induced oral carcinogenesis to *S100a9*$^{-/-}$ mice however, did not result in an altered response of the S100a9 deficient mice as compared to the controls (Fig. 3.16). As expected, S100a9 protein expression in the tongue epithelium as well as in stromal immune cells is lost in the *S100a9*$^{-/-}$ mice, however it is worth noting that S100a8 expression is still detected in mucosal keratinocytes after 4-NQO treatment Fig. 3.14. Previously, the S100a9 knockout was proposed to be a functional calgranulin knockout due to protein instability of S100a8 in the absence of its dimerization partner S100a9. However, this was only shown for the complex in myeloid cells [82] and in fact, looking at stromal immune cells, while MPO positive cells are visible in the stroma of both genotypes, S100a8 positive immune cells are only seen in the tissue sections of *S100a9*$^{+/-}$ but not in *S100a9*$^{-/-}$ animals Fig. 3.14. In mucosal keratinocytes, S100a8 protein stability is most likely regulated differently as compared to myeloid cells. *In vitro* studies already have shown that murine S100a8 can form homodimers [74, 94]. Furthermore a negative association with S100a3 was reported on expression level [89], while in a yeast-two-hybrid screen, S100a8 was identified as a binding partner for S100A3 and proposed as a molecular switch in S100a8/a9 signaling [141]. Finally, while S100a8 is essential during embryonic development [148], *S100a9*$^{-/-}$ mice develop normally, arguing for a stabilization mechanism of S100a8 in the absence of S100a9 and emphasize an independent role of S100a8. Therefore, it cannot be excluded that residual S100a8 protein expression in mucosal keratinocytes mediates 4-NQO induced carcinogenesis in

S100a9$^{-/-}$ mice. Previous studies showed, that S100a8 and S100a9 expression is down-regulated during malignant progression in HNSCC [161, 162]. In line with these data, in human and less prominent also in 4-NQO challenged mouse mucosal epithelium S100-calgranulin expression was prominent in suprabasal layers but not in the basal keratinocytes of the oral mucosa, (unpublished data S. Funk and Fig. 3.5). Accordingly, it seems plausible that calgranulins are functionally associated with keratinocytes differentiation, and an association of S100A8/A9 expression and differentiation was confirmed *in vitro*, showing that in HaCaT keratinocytes S100A8/A9 expression leads to a reduced proliferation [209]. Furthermore, expression of S100A8/A9 was demonstrated to trigger the expression of epidermal differentiation markers involucrin and fillagrin. Therefore, over all histology, proliferation and differentiation was addressed in *S100a9*$^{-/-}$ mice as compared to *S100a9*$^{+/-}$ controls. Keratinocyte proliferation as measured by BrdU incorporation, however, was induced in both genotypes and keratinocyte differentiation markers Keratin 14, Keratin 13 and Loricrin showed the same expression and distribution in *S100a9*$^{-/-}$ mice as compared to *S100a9*$^{+/-}$ controls. In the present setup no obvious genotype specific alteration in mucosal differentiation markers was observed. Neither in overall expression, nor in the spatial expression pattern (Fig. 3.19 and Fig. 3.20) a significant difference was observed. As already discussed in the context of mucosal carcinogenesis this may be due to the residual expression of S100a8 after 4-NQO treatment which may be sufficient to maintain mucosal differentiation. Also, while *in vitro* data suggest an active part of S100a8/a9 in keratinocyte differentiation [209], this neglects the complex communication of epithelial cells with cells of the underlying connective tissue and immune cells and has so far never been shown *in vivo.* In Summary, these observations in *S100a9*$^{-/-}$ mice support the data from human OPSCC patients, suggesting a diverse role of S100A8/A9 in head and neck cancer, depending on the etiology and the presence of tumor supporting inflammation and that S100A8 and S100A9 are dispensable for the onset of oral carcinogenesis, at least in setting of genotoxic stress. S*S100a9*$^{-/-}$.

4.8 S100 calgranulins, RAGE and oral mucosal homeostasis

As seen previously in *wild type* and *Rage*$^{-/-}$ mice, also *S100a9*$^{-/-}$ mice do not show major signs of inflammatory cell recruitment upon carcinogen treatment. It may, however, well be that while in backskin keratinocytes S100-RAGE signaling is a physiologic response to stress and damage, the maintenance of mucosal functions and tissue homeostasis are not involving S100-RAGE signaling. Also generally, when concluding from data from backskin keratinocytes on their mucosal counterparts, one has to keep in mind also the differences. Depending on the localization, oral mucosal keratinocytes form keratinizing and non keratinizing stratified epithelia. Mucosal keratinocytes show a higher basal level of proliferation and turnover than their counterparts in the skin [181]. While wounds in the oral mucosa do not only heal more quickly and with minimal scar formation as compared to skin, these wounds also show far less infiltration by inflammatory cells and a faster resolution of inflammation [190, 126, 30]. This could explain why only moderate numbers of MPO positive immune cells were visible in the histological sections at the endpoint of the 4-NQO experiment. Also, the oral mucosa continually gets in contact with antigens through food, bacteria and airborne substances. Therefore, what is commonly described as "oral mucosal tolerance" [142] may influence the communication of stromal and epithelial cells and interfere with the damage response in the oral mucosa. Also in this context the expression of S100-calgranulins in normal human mucosa (unpublished data, Sonja funk) claims for a RAGE independent epithelial function of S100-calgranulins in the oral mucosa.

4.9 Easing the rage – what does this mean for therapeutic strategies?

A recent development concerning RAGE in various human disorders including cancer is the use of RAGE blocking antibodies and small molecule drugs that interfere with the pro-inflammatory RAGE signaling axis [20, 197, 137, 9]. However, the role of RAGE is not entirely understood, ranging from a tumor suppressor in lung carcinogenesis [12] to an active driver of pro-tumorigenic inflammation in backskin, liver and colorectal cancer [60, 201] and (Pusterla et al., unpublished data) and malignant progression [9, 192]. Finally, this study suggest, that in a situation driven by a merely genotoxic agent like 4-NQO, the presence of RAGE does not play a major role with respect to the onset of cancer. Both the RAGE deficient animals as well as the control mice developed lesions. Also, no significant augmentation of inflammatory cells in the stromal compartment of 4-NQO treated animals was observed, arguing against a RAGE mediated pro-inflammatory feed forward loop in this model. Also RAGE expression is inversely correlated with the progression of pulmonary carcinogenesis and is regarded a tumor suppressor in the lung [12, 97], and a negative association of RAGE expression and depth of invasion was shown for esophageal cancer, moreover connecting RAGE expression with a better prognosis [196]. Therefore a better understanding of RAGE function in general and specifically a clear stratification for underlying and supporting inflammation, genotoxic stress and further parameters, which may interfere with damage signaling is of vital importance. Furthermore, even though expression of S100-calgranulins greatly varies in human HNSCC tumor samples, as well as inflammation as measured by S100-calgranulin positive stromal immune cells, this does not seem to be correlated with any clinicopathological feature except for tumor grading (unpublished Data, Sonja Funk), [161, 162]. Therefore, it is questionable, whether interference with RAGE signaling will be beneficial for HNSCC patients without clear stratification for inflammation and the induction of pro-inflammatory RAGE ligands like S100calgranulins or HMGB1. It may well be that a subgroup of patients, who show both calgranulin expression in tumor cells as well as a high number of infiltrating inflammatory cells will profit from RAGE-targeted anti-inflammatory therapy. In summary, the data highlight the need for careful stratification of patients with regard to tumor

etiology and the presence of a supportive inflammatory microenvironment as a prerequisite for efficient prevention and therapy of human malignancies, including HNSCC via therapeutic targeting of receptor RAGE. While patients with strong signs of stromal inflammation may well benefit from RAGE targeted therapy, those who do not show an inflammatory tumor microenvironment probably will not profit at all.

4.10 Conclusion and Perspective

The results from the present study point out that S100-calgranulins and the receptor RAGE do not necessarily act together in head and neck cancer and raise awareness for a more differentiated view on the S100-RAGE signaling axis and its molecular components. In the onset of oral and esophageal cancer, driven by genotoxic stress in the absence of an additional inflammatory stimulus, neither Rage expression nor S100a9 expression was essential for the induction and development of cancer. As only papillary lesions were observed in the mice after 4-NQO treatment, the model nicely provides insight in the onset of oral carcinogenesis but does not allow conclusions on malignant progression as no invasive squamous cell carcinoma developed within the observation time. Therefore, while the S100-RAGE axis is dispensable in the onset of oral and esophageal cancer in this model, it may be never the less interesting to address its function in malignant progression. Expanding the S100-RAGE network and looking at TLR4 in the 4-NQO mouse model, possibly also in double knockout animals to better define the impact of the different nodes in the network. Both S100a9/TLR4 as well as Rage/Tlr4 double knockout mice could shed additional light on the complex function of myeloid cells in the tumor stroma. Furthermore, considering the etiology of HNSCC, ethanol as an additional stimulus and potent inducer of tissue damage and inflammation in the 4-NQO model ca should considered to more closely define the role or RAGE in oral cancer. Even after adjustment for smoking, there is a strong association between oral cancer and ethanol consumption [10]. The effect of ethanol in the 4-NQO model was demonstrated in a recent publication, additionally drawing a link to inflammation by associating ethanol consumption to

the activation of the 5-Lox pathway of arachidonic acid metabolism [71]. Also the cellular function of S100-calgranulins would be an interesting starting point for further studies. In both men and mice, nuclear localization was detected in mucosal keratinocytes, raising the obvious question, on the molecular function of nuclear S100A8 and S100A9 in physiological as well as pathophysiological conditions in mucosal epithelia. Conditional, tissue specific knockout of S100a8 and S100a9 via breeding K14-Cre mice to S100a8 or S100a9 mice containing flanking *lox P* sites would provide an elegant tool to address calgranulins in epithelial cells in a more functional approach. Generally, the current view of S100-calgranulins and RAGE acting together in a vicious cycle needs to be carefully revisited. A strict stratification for signals of an inflammatory microenvironment can help to assess the impact of the S100-RAGE axis in a given environment in patients or animals.

Bibliography

[1] A C Abrahao, R M Castilho, C H Squarize, A A Molinolo, D dos Santos-Pinto Jr., and J S Gutkind. A role for COX2-derived PGE2 and PGE2-receptor subtypes in head and neck squamous carcinoma cell proliferation. *Oral Oncol*, 46(12):880–887, 2010.

[2] W M Abuzeid, S Davis, A L Tang, L Saunders, J C Brenner, J Lin, J R Fuchs, E Light, C R Bradford, M E Prince, and T E Carey. Sensitization of head and neck cancer to cisplatin through the use of a novel curcumin analog. *Arch Otolaryngol Head Neck Surg*, 137(5):499–507, 2011.

[3] M Adachi, C Cui, C T Dodge, M K Bhayani, and S Y Lai. Targeting STAT3 inhibits growth and enhances radiosensitivity in head and neck squamous cell carcinoma. *Oral Oncol*, 2012.

[4] N Agrawal, M J Frederick, C R Pickering, C Bettegowda, K Chang, R J Li, C Fakhry, T X Xie, J Zhang, J Wang, N Zhang, A K El-Naggar, S A Jasser, J N Weinstein, L Trevino, J A Drummond, D M Muzny, Y Wu, L D Wood, R H Hruban, W H Westra, W M Koch, J A Califano, R A Gibbs, D Sidransky, B Vogelstein, V E Velculescu, N Papadopoulos, D A Wheeler, K W Kinzler, and J N Myers. Exome sequencing of head and neck squamous cell carcinoma reveals inactivating mutations in NOTCH1. *Science*, 333(6046):1154–1157, 2011.

[5] N Ahmadi, R Goldman, F Seillier-Moiseiwitsch, A M Noone, O Kosti, and B J Davidson. Decreased risk of squamous cell carcinoma of the head and neck in users of nonsteroidal anti-inflammatory drugs. *Int J Otolaryngol*, 2010:424161, 2010.

[6] J A Anderson, J C Irish, and B Y Ngan. Prevalence of RAS oncogene mutation in head and neck carcinomas. *J Otolaryngol*, 21(5):321–326, 1992.

[7] K K Ang, J Harris, R Wheeler, R Weber, D I Rosenthal, P F Nguyen-Tan, W H Westra, C H Chung, R C Jordan, C Lu, H Kim, R Axelrod, C C Silverman, K P Redmond, and M L Gillison. Human papillomavirus and survival of patients with oropharyngeal cancer. *N Engl J Med*, 363(1):24–35, 2010.

[8] Y Arima, C Nishigori, T Takeuchi, S Oka, K Morimoto, A Utani, and Y Miyachi. 4-Nitroquinoline 1-oxide forms 8-hydroxydeoxyguanosine in human fibroblasts through reactive oxygen species. *Toxicol Sci*, 91(2):382–392, 2006.

[9] Thiruvengadam Arumugam, Vijaya Ramachandran, Sobeyda B Gomez, Ann M Schmidt, and Craig D Logsdon. S100P-Derived RAGE Antagonistic Peptide Reduces Tumor Growth and Metastasis. *Clinical cancer research : an official journal of the American Association for Cancer Research*, 18(16):4356–64, July 2012.

[10] V Bagnardi, M Blangiardo, C La Vecchia, and G Corrao. A meta-analysis of alcohol drinking and cancer risk. *Br J Cancer*, 85(11):1700–1705, 2001.

[11] Everson J W Barnes L. Reichart P., Sidransky D. *Classification of Tumors. Pathology and Genetics of Head and Neck Tumors*, volume 6. IARC Press, Lyon, 2005.

[12] B Bartling, H S Hofmann, B Weigle, R E Silber, and A Simm. Down-regulation of the receptor for advanced glycation end-products (RAGE) supports non-small cell lung carcinoma. *Carcinogenesis*, 26(2):293–301, 2005.

[13] A Behren, Y Kamenisch, S Muehlen, C Flechtenmacher, U Haberkorn, H Hilber, J N Myers, Z Bergmann, P K Plinkert, and C Simon. Development of an oral cancer recurrence mouse model after surgical resection. *Int J Oncol*, 36(4):849–855, 2010.

[14] S Benoit, A Toksoy, M Ahlmann, M Schmidt, C Sunderkotter, D Foell, M Pasparakis, J Roth, and M Goebeler. Elevated serum levels of calcium-binding S100 proteins A8 and A9 reflect disease activity and abnormal differentiation of keratinocytes in psoriasis. *Br J Dermatol*, 155(1):62–66, 2006.

[15] U K Bhawal, Y Ozaki, M Nishimura, M Sugiyama, T Sasahira, Y Nomura, F Sato, K Fujimoto, N Sasaki, M A Ikeda, K Tsuji, H Kuniyasu, and Y Kato. Association of expression of receptor for advanced glycation end products and invasive activity of oral squamous cell carcinoma. *Oncology*, 69(3):246–255, 2005.

[16] Y Bian, B Hall, Z J Sun, A Molinolo, W Chen, J S Gutkind, C V Waes, and A B Kulkarni. Loss of TGF-beta signaling and PTEN promotes head and neck squamous cell carcinoma through cellular senescence evasion and cancer-related inflammation. *Oncogene*, 31(28):3322–3332, 2012.

[17] A Bierhaus, P M Humpert, M Morcos, T Wendt, T Chavakis, B Arnold, D M Stern, and P P Nawroth. Understanding RAGE, the receptor for advanced glycation end products. *J Mol Med (Berl)*, 83(11):876–886, 2005.

[18] A Bierhaus and P P Nawroth. Multiple levels of regulation determine the role of the receptor for AGE (RAGE) as common soil in inflammation, immune responses and diabetes mellitus and its complications. *Diabetologia*, 52(11):2251–2263, 2009.

[19] A Bierhaus, D M Stern, and P P Nawroth. RAGE in inflammation: a new therapeutic target? *Curr Opin Investig Drugs*, 7(11):985–991, 2006.

[20] C Bopp, A Bierhaus, S Hofer, A Bouchon, P P Nawroth, E Martin, and M A Weigand. Bench-to-bedside review: The inflammation-perpetuating pattern-recognition receptor RAGE as a therapeutic target in sepsis. *Critical Care*, 12(1), 2008.

[21] A Boyum, K K Skrede, O Myhre, V A Tennfjord, C G Neurauter, H Tolleshaug, E Knudsen, P K Opstad, M Bjoras, and H B Benestad. Calprotectin (S100A8/S100A9) and Myeloperoxidase: Co-Regulators of Formation of Reactive Oxygen Species. *Toxins (Basel)*, 2(1):95–115.

[22] S Brandau, S Trellakis, K Bruderek, D Schmaltz, G Steller, M Elian, H Suttmann, M Schenck, J Welling, P Zabel, and S Lang. Myeloid-derived suppressor cells in the peripheral blood of cancer patients contain a subset of immature neutrophils with impaired migratory properties. *J Leukoc Biol*, 89(2):311–317, 2011.

[23] F Bray, J S Ren, E Masuyer, and J Ferlay. Global estimates of cancer prevalence for 27 sites in the adult population in 2008. *Int J Cancer*, 2012.

[24] J Brett, A M Schmidt, S D Yan, Y S Zou, E Weidman, D Pinsky, R Nowygrod, M Neeper, C Przysiecki, A Shaw, A Migheli, and D Stern. Survey of the Distribution of a Newly Characterized Receptor for Advanced Glycation End-Products in Tissues. *American Journal of Pathology*, 143(6):1699–1712, 1993.

[25] C Brocks, H Graefe, H Frenzel, R Pries, and B Wollenberg. Isolation of human myeloid dendritic cells from tumor tissue and peripheral blood. *In Vivo*, 20(2):239–242, 2006.

[26] J Califano, P van der Riet, W Westra, H Nawroz, G Clayman, S Piantadosi, R Corio, D Lee, B Greenberg, W Koch, and D Sidransky. Genetic progression model for head and neck cancer: implications for field cancerization. *Cancer Res*, 56(11):2488–2492, 1996.

[27] M Camacho, X Leon, M T Fernandez-Figueras, M Quer, and L Vila. Prostaglandin E(2) pathway in head and neck squamous cell carcinoma. *Head Neck*, 30(9):1175–1181, 2008.

[28] D L Cecil, C T G Appleton, M D Polewski, J S Mort, A M Schmidt, A Bendele, F Beier, and R Terkeltaub. The Pattern Recognition Receptor CD36 Is a Chondrocyte Hypertrophy Marker Associated with Suppression of Catabolic Responses and Promotion of Repair Responses to Inflammatory Stimuli. *J Immunol*, 182(8):5024–5031, 2009.

[29] Grace Y Chen and Gabriel Nuñez. Sterile inflammation: sensing and reacting to damage. *Nature reviews. Immunology*, 10(12):826–37, December 2010.

[30] L Chen, Z H Arbieva, S J Guo, P T Marucha, T A Mustoe, and L A DiPietro. Positional differences in the wound transcriptome of skin and oral mucosa. *BMC Genomics*, 11, 2010.

[31] Y L Chen, E M Akirav, W Chen, O Henegariu, B Moser, D Desai, J M Shen, J C Webster, R C Andrews, A M Mjalli, R Rothlein, A M Schmidt, R Clynes, and K C Herold. RAGE ligation affects T cell activation and controls T cell differentiation. *J Immunol*, 181(6):4272–4278, 2008.

[32] Z Chen, P S Malhotra, G R Thomas, F G Ondrey, D C Duffey, C W Smith, I Enamorado, N T Yeh, G S Kroog, S Rudy, L McCullagh, S Mousa, M Quezado, L L Herscher, and C Van Waes. Expression of proinflammatory and proangiogenic cytokines in patients with head and neck cancer. *Clin Cancer Res*, 5(6):1369–1379, 1999.

[33] C H Chung, J S Parker, G Karaca, J Y Wu, W K Funkhouser, D Moore', D Butterfoss, D Xiang, A Zonation, X Y Yin, W W Shockley, M C Weissler, L G Dressler, C G Shores, W G Yarbrough, and C M Perou. Molecular classification of head and neck squamous cell carcinomas using patterns of gene expression. *Cancer Cell*, 5(5):489–500, 2004.

[34] F Ciardiello and G Tortora. Epidermal growth factor receptor (EGFR) as a target in cancer therapy: understanding the role of receptor expression and other molecular determinants that could influence the response to anti-EGFR drugs. *Eur J Cancer*, 39(10):1348–1354, 2003.

[35] C A Clark, Y Rong, X Rong, S Shah, H Barham, and C O Nathan. Curcumin inhibits HNSCC by modulating the Akt/mTOR pathway. *Oral Oncol*, pages 94–95, 2009.

[36] L M Coussens and Z Werb. Inflammation and cancer. *Nature*, 420(6917):860–867, 2002.

[37] I Dale, M K Fagerhol, and I Naesgaard. Purification and Partial Characterization of a Highly Immunogenic Human-Leukocyte Protein, the L1-Antigen. *European Journal of Biochemistry*, 134(1):1–6, 1983.

[38] J DiGiovanni. Multistage carcinogenesis in mouse skin. *Pharmacol Ther*, 54(1):63–128, 1992.

[39] J DiNorcia, M K Lee, D N Moroziewicz, M Winner, P Suman, F Bao, H E Remotti, Y S Zou, S F Yan, W Qiu, G H Su, A M Schmidt, and J D Allendorf. RAGE gene deletion inhibits the development and progression of ductal neoplasia and prolongs survival in a murine model of pancreatic cancer. *J Gastrointest Surg*, 16(1):104–12; discussion 112, 2012.

[40] R Donato. S100: a multigenic family of calcium-modulated proteins of the EF-hand type with intracellular and extracellular functional roles. *International Journal of Biochemistry & Cell Biology*, 33(7):637–668, 2001.

[41] L A Donehower, M Harvey, B L Slagle, M J McArthur, C A Montgomery Jr., J S Butel, and A Bradley. Mice deficient for p53 are developmentally normal but susceptible to spontaneous tumours. *Nature*, 356(6366):215–221, 1992.

[42] O Driemel, U Murzik, N Escher, C Melle, A Bleul, R Dahse, T E Reichert, G Ernst, and F von Eggeling. Protein profiling of oral brush biopsies: S100A8 and S100A9 can differentiate between normal, premalignant, and tumor cells. *Proteomics Clinical Applications*, 1(5):486–493, 2007.

[43] A M Eades-Perner, J Thompson, H van der Putten, and W Zimmermann. Mice transgenic for the human CGM6 gene express its product, the granulocyte marker CD66b, exclusively in granulocytes. *Blood*, 91(2):663–672, 1998.

[44] J M Ehrchen, C Sunderkotter, D Foell, T Vogl, and J Roth. The endogenous Toll-like receptor 4 agonist S100A8/S100A9 (calprotectin) as innate amplifier of infection, autoimmunity, and cancer. *J Leukoc Biol*, 86(3):557–566, 2009.

[45] H B El-Serag and K L Rudolph. Hepatocellular carcinoma: epidemiology and molecular carcinogenesis. *Gastroenterology*, 132(7):2557–2576, 2007.

[46] P B Ernst and B D Gold. The disease spectrum of Helicobacter pylori: the immunopathogenesis of gastroduodenal ulcer and gastric cancer. *Annu Rev Microbiol*, 54:615–640, 2000.

[47] J W Eveson. Animal models of intra-oral chemical carcinogenesis: a review. *J Oral Pathol*, 10(3):129–146, 1981.

[48] G Falconieri, M A Luna, S Pizzolitio, G DeMaglio, V Angione, and M Rocco. Eosinophil-rich squamous carcinoma of the oral cavity: a study of 13 cases and delineation of a possible new microscopic entity. *Annals of Diagnostic Pathology*, 12(5):322–327, 2008.

[49] A Farnoush and I C Mackenzie. Sequential histological changes and mast cell response in skin during chemically-induced carcinogenesis. *J Oral Pathol*, 12(4):300–306, 1983.

[50] J Ferlay, D M Parkin, and E Steliarova-Foucher. Estimates of cancer incidence and mortality in Europe in 2008. *Eur J Cancer*, 46(4):765–781, 2010.

[51] J Ferlay, H R Shin, F Bray, D Forman, C Mathers, and D M Parkin. Estimates of worldwide burden of cancer in 2008: GLOBOCAN 2008. *Int J Cancer*, 127(12):2893–2917, 2010.

[52] S Fineschi, G De Cunto, F Facchinetti, M Civelli, B P Imbimbo, C Carnini, G Villetti, B Lunghi, S Stochino, D L Gibbons, A Hayday,

G Lungarella, and E Cavarra. RAGE Contributes to Postnatal Pulmonary Development and Adult Lung Maintenance Program in Mice. *Am J Respir Cell Mol Biol*, 2012.

[53] K Flatmark, K B Pedersen, J M Nesland, H Rasmussen, G Aamodt, S O Mikalsen, K Bjornland, O Fodstad, and G M Maelandsmo. Nuclear localization of the metastasis-related protein S100A4 correlates with tumour stage in colorectal cancer. *J Pathol*, 200(5):589–595, 2003.

[54] D Foell, M Frosch, C Sorg, and J Roth. Phagocyte-specific calcium-binding S100 proteins as clinical laboratory markers of inflammation. *Clin Chim Acta*, 344(1-2):37–51, 2004.

[55] C Franz, I Durussel, J A Cox, B W Schafer, and C W Heizmann. Binding of Ca2+ and Zn2+ to human nuclear S100A2 and mutant proteins. *Journal of Biological Chemistry*, 273(30):18826–18834, 1998.

[56] Z G Fridlender and S M Albelda. Tumor-associated neutrophils: friend or foe? *Carcinogenesis*, 33(5):949–955, 2012.

[57] Z G Fridlender, J Sun, S Kim, V Kapoor, G Cheng, L Ling, G S Worthen, and S M Albelda. Polarization of tumor-associated neutrophil phenotype by TGF-beta: "N1" versus "N2" TAN. *Cancer Cell*, 16(3):183–194, 2009.

[58] G Fritz. RAGE: a single receptor fits multiple ligands. *Trends Biochem Sci*, 36(12):625–632, 2011.

[59] C Gebhardt, J Nemeth, P Angel, and J Hess. S100A8 and S100A9 in inflammation and cancer. *Biochem Pharmacol*, 72(11):1622–1631, 2006.

[60] Christoffer Gebhardt, Astrid Riehl, Moritz Durchdewald, Julia Németh, Gerhard Fürstenberger, Karin Müller-Decker, Alexander Enk, Bernd Arnold, Angelika Bierhaus, Peter P Nawroth, Jochen Hess, and Peter Angel. RAGE signaling sustains inflammation and promotes tumor development. *The Journal of experimental medicine*, 205(2):275–85, February 2008.

[61] S Ghavami, C Kerkhoff, M Los, M Hashemi, C Sorg, and F Karami-Tehrani. Mechanism of apoptosis induced by S100A8/A9 in colon cancer cell lines: the role of ROS and the effect of metal ions. *J Leukoc Biol*, 76(1):169–175, 2004.

[62] M L Gillison, W M Koch, R B Capone, M Spafford, W H Westra, L Wu, M L Zahurak, R W Daniel, M Viglione, D E Symer, K V Shah, and D Sidransky. Evidence for a causal association between human papillomavirus and a subset of head and neck cancers. *J Natl Cancer Inst*, 92(9):709–720, 2000.

[63] I B Gimenez-Conti and T J Slaga. The hamster cheek pouch model of carcinogenesis and chemoprevention. *Adv Exp Med Biol*, 320:63–67, 1992.

[64] H E Gonzalez, M Gujrati, M Frederick, Y Henderson, J Arumugam, P W Spring, K Mitsudo, H W Kim, and G L Clayman. Identification of 9 genes differentially expressed in head and neck squamous cell carcinoma. *Arch Otolaryngol Head Neck Surg*, 129(7):754–759, 2003.

[65] A Gonzalez-Lopez, A Aguirre, I Lopez-Alonso, L Amado, A Astudillo, M S Fernandez-Garcia, M F Suarez, E Batalla-Solis, E Colado, and G M Albaiceta. MMP-8 deficiency increases TLR/RAGE ligands S100A8 and S100A9 and exacerbates lung inflammation during endotoxemia. *PLoS One*, 7(6):e39940, 2012.

[66] J Greten, I Kreis, K Wiesel, E Stier, A M Schmidt, D M Stern, E Ritz, R Waldherr, and P P Nawroth. Receptors for advance glycation end-products (AGE) - expression by endothelial cells in non-diabetic uraemic patients. *Nephrol Dial Transplant*, 11(5):786–790, 1996.

[67] M A Grimbaldeston, C L Geczy, N Tedla, J J Finlay-Jones, and P H Hart. S100A8 induction in keratinocytes by ultraviolet A irradiation is dependent on reactive oxygen intermediates. *Journal of Investigative Dermatology*, 121(5):1168–1174, 2003.

[68] A Gugliucci. Glycation as the glucose link to diabetic complications. *J Am Osteopath Assoc*, 100(10):621–634, 2000.

[69] F Guignard, J Mauel, and M Markert. Identification and characterization of a novel human neutrophil protein related to the S100 family. *Biochem J*, 309 (Pt 2:395–401, 1995.

[70] Y Guo, W N Fu, H Chen, C Shang, and M Zhong. miR-24 functions as a tumor suppressor in Hep2 laryngeal carcinoma cells partly through down-regulation of the S100A8 protein. *Oncol Rep*, 27(4):1097–1103, 2012.

[71] Yizhu Guo, Xin Wang, Xinyan Zhang, Zheng Sun, and Xiaoxin Chen. Ethanol promotes chemically induced oral cancer in mice through activation of the 5-lipoxygenase pathway of arachidonic acid metabolism. *Cancer prevention research (Philadelphia, Pa.)*, 4(11):1863–72, November 2011.

[72] T Hama, Y Yuza, Y Saito, O uchi J, S Kondo, M Okabe, H Yamada, T Kato, H Moriyama, S Kurihara, and M Urashima. Prognostic significance of epidermal growth factor receptor phosphorylation and mutation in head and neck squamous cell carcinoma. *Oncologist*, 14(9):900–908, 2009.

[73] D Hanahan and R A Weinberg. Hallmarks of cancer: the next generation. *Cell*, 144(5):646–674, 2011.

[74] C A Harrison, M J Raftery, J Walsh, P Alewood, S E Iismaa, S Thliveris, and C L Geczy. Oxidation regulates the inflammatory properties

of the murine S100 protein S100A8. *Journal of Biological Chemistry*, 274(13):8561–8569, 1999.

[75] Evelyn Hartmann, Barbara Wollenberg, Simon Rothenfusser, Moritz Wagner, Daniela Wellisch, Brigitte Mack, Thomas Giese, Olivier Gires, Stefan Endres, and Gunther Hartmann. Identification and functional analysis of tumor-infiltrating plasmacytoid dendritic cells in head and neck cancer. *Cancer research*, 63(19):6478–87, October 2003.

[76] B L Hawkins, B W Heniford, D M Ackermann, M Leonberger, S A Martinez, and F J Hendler. 4NQO carcinogenesis: a mouse model of oral cavity squamous cell carcinoma. *Head Neck*, 16(5):424–432, 1994.

[77] J Heijmans, N V Buller, E Hoff, A A Dihal, T van der Poll, M A van Zoelen, A Bierhaus, I Biemond, J C Hardwick, D W Hommes, V Muncan, and G R van den Brink. Rage signalling promotes intestinal tumourigenesis. *Oncogene*, 2012.

[78] R Herber, A Liem, H Pitot, and P F Lambert. Squamous epithelial hyperplasia and carcinoma in mice transgenic for the human papillomavirus type 16 E7 oncogene. *J Virol*, 70(3):1873–1881, 1996.

[79] A Hermani, B De Servi, S Medunjanin, P A Tessier, and D Mayer. S100A8 and S100A9 activate MAP kinase and NF-kappaB signaling pathways and trigger translocation of RAGE in human prostate cancer cells. *Exp Cell Res*, 312(2):184–197, 2006.

[80] T Hibino, M Sakaguchi, S Miyamoto, M Yamamoto, A Motoyama, J Hosoi, T Shimokata, T Ito, R Tsuboi, and N H Huh. S100A9 is a novel ligand of EMMPRIN that promotes melanoma metastasis. *Cancer Res*, 2012.

[81] Kenro Hirata, Moriatsu Takada, Yasuyuki Suzuki, and Yoshikazu Kuroda. Expression of receptor for advanced glycation end products (RAGE) in human biliary cancer cells. *Hepatogastroenterology*, 50(53):1205–1207, 2003.

[82] Josie A R Hobbs, Richard May, Kiki Tanousis, Eileen McNeill, Margaret Mathies, Christoffer Gebhardt, Robert Henderson, Matthew J Robinson, and Nancy Hogg. Myeloid cell function in MRP-14 (S100A9) null mice. *Molecular and cellular biology*, 23(7):2564–76, April 2003.

[83] M A Hofmann, S Drury, C Fu, W Qu, A Taguchi, Y Lu, C Avila, N Kambham, A Bierhaus, P Nawroth, M F Neurath, T Slattery, D Beach, J McClary, M Nagashima, J Morser, D Stern, and A M Schmidt. RAGE mediates a novel proinflammatory axis: a central cell surface receptor for S100/calgranulin polypeptides. *Cell*, 97(7):889–901, 1999.

[84] D Holzinger, M Schmitt, G Dyckhoff, A Benner, M Pawlita, and F X Bosch. Viral RNA Patterns and High Viral Load Reliably Define

Oropharynx Carcinomas with Active HPV16 Involvement. *Cancer Res*, 72(19):4993–5003, 2012.

[85] O Hori, J Brett, T Slattery, R Cao, J Zhang, J X Chen, M Nagashima, E R Lundh, S Vijay, D Nitecki, and Et al. The receptor for advanced glycation end products (RAGE) is a cellular binding site for amphoterin. Mediation of neurite outgrowth and co-expression of rage and amphoterin in the developing nervous system. *Journal of Biological Chemistry*, 270(43):25752–25761, 1995.

[86] H L Hsieh, B W Schafer, J A Cox, and C W Heizmann. S100A13 and S100A6 exhibit distinct translocation pathways in endothelial cells. *Journal of Cell Science*, 115(15):3149–3158, 2002.

[87] B I Hudson, L G Bucciarelli, T Wendt, T Sakaguchi, E Lalla, W Qu, Y Lu, L Lee, D M Stern, Y Naka, R Ramasamy, S D Yan, S F Yan, V D'Agati, and A M Schmidt. Blockade of receptor for advanced glycation endproducts: a new target for therapeutic intervention in diabetic complications and inflammatory disorders. *Arch Biochem Biophys*, 419(1):80–88, 2003.

[88] B I Hudson, A Z Kalea, M Del Mar Arriero, E Harja, E Boulanger, V D'Agati, and A M Schmidt. Interaction of the RAGE cytoplasmic domain with diaphanous-1 is required for ligand-stimulated cellular migration through activation of Rac1 and Cdc42. *Journal of Biological Chemistry*, 283(49):34457–34468, 2008.

[89] L Hummerich, R Muller, J Hess, F Kokocinski, M Hahn, G Furstenberger, C Mauch, P Lichter, and P Angel. Identification of novel tumour-associated genes differentially expressed in the process of squamous cell cancer development. *Oncogene*, 25(1):111–121, 2006.

[90] K D Hunter, E K Parkinson, and P R Harrison. Profiling early head and neck cancer. *Nat Rev Cancer*, 5(2):127–135, 2005.

[91] H J Huttunen, C Fages, and H Rauvala. Receptor for advanced glycation end products (RAGE)-mediated neurite outgrowth and activation of NF-kappaB require the cytoplasmic domain of the receptor but different downstream signaling pathways. *Journal of Biological Chemistry*, 274(28):19919–19924, 1999.

[92] H J Huttunen, J Kuja-Panula, G Sorci, A L Agneletti, R Donato, and H Rauvala. Coregulation of neurite outgrowth and cell survival by amphoterin and S100 proteins through receptor for advanced glycation end products (RAGE) activation. *Journal of Biological Chemistry*, 275(51):40096–40105, 2000.

[93] N E Hynes and H A Lane. ERBB receptors and cancer: the complexity of targeted inhibitors. *Nat Rev Cancer*, 5(5):341–354, 2005.

[94] K Ishikawa, A Nakagawa, I Tanaka, M Suzuki, and J Nishihira. The structure of human MRP8, a member of the S100 calcium-binding protein family, by MAD phasing at 1.9 angstrom resolution. *Acta Crystallographica Section D-Biological Crystallography*, 56:559–566, 2000.

[95] S Jabbar, K Strati, M K Shin, H C Pitot, and P F Lambert. Human papillomavirus type 16 E6 and E7 oncoproteins act synergistically to cause head and neck cancer in mice. *Virology*, 407(1):60–67, 2010.

[96] J H Jeng, M C Chang, and L J Hahn. Role of areca nut in betel quid-associated chemical carcinogenesis: current awareness and future perspectives. *Oral Oncol*, 37(6):477–492, 2001.

[97] R Jing, M Cui, J Wang, and H Wang. Receptor for advanced glycation end products (RAGE) soluble form (sRAGE): a new biomarker for lung cancer. *Neoplasma*, 57(1):55–61, 2010.

[98] E Kallberg, T Vogl, D Liberg, A Olsson, P Bjork, P Wikstrom, A Bergh, J Roth, F Ivars, and T Leanderson. S100A9 Interaction with TLR4 Promotes Tumor Growth. *PLoS One*, 7(3):e34207, 2012.

[99] R Kang, T Loux, D Tang, N E Schapiro, P Vernon, K M Livesey, A Krasinskas, M T Lotze, and H J Zeh 3rd. The expression of the receptor for advanced glycation endproducts (RAGE) is permissive for early pancreatic neoplasia. *Proc Natl Acad Sci U S A*, 109(18):7031–7036, 2012.

[100] R Kang, D Tang, N E Schapiro, K M Livesey, A Farkas, P Loughran, A Bierhaus, M T Lotze, and H J Zeh. The receptor for advanced glycation end products (RAGE) sustains autophagy and limits apoptosis, promoting pancreatic tumor cell survival. *Cell Death and Differentiation*, 17(4):666–676, 2010.

[101] F Katsuoka, Y Kawakami, T Arai, H Imuta, M Fujiwara, H Kanma, and K Yamashita. Type II alveolar epithelial cells in lung express receptor for advanced glycation end products (RAGE) gene. *Biochem Biophys Res Commun*, 238(2):512–516, 1997.

[102] A B Katz and L B Taichman. A partial catalog of proteins secreted by epidermal keratinocytes in culture. *J Invest Dermatol*, 112(5):818–821, 1999.

[103] C Kerkhoff, C Sorg, N N Tandon, and W Nacken. Interaction of S100A8/S100A9 - Arachidonic acid complexes with the scavenger receptor CD36 may facilitate fatty acid uptake by endothelial cells. *Biochemistry*, 40(1):241–248, 2001.

[104] Claus Kerkhoff, Wolfgang Nacken, Malgorzata Benedyk, Marie Claire Dagher, Claudia Sopalla, and Jacques Doussiere. The arachidonic acid-binding protein S100A8/A9 promotes NADPH oxidase activation by interaction with p67phox and Rac-2. *FASEB journal : official publica-*

tion of the Federation of American Societies for Experimental Biology, 19(3):467–9, March 2005.

[105] J Y Kim, H K Park, J S Yoon, S J Kim, E S Kim, K S Ahn, D S Kim, S S Yoon, B K Kim, and Y Y Lee. Advanced glycation end product (AGE)-induced proliferation of HEL cells via receptor for AGE-related signal pathways. *Int J Oncol*, 33(3):493–501, 2008.

[106] Robert Koch-instituts. *Krebs in Deutschland Häufigkeiten und Trends Gesundheitsberichterstattung des Bundes Beiträge zur Gesundheitsberichterstattung des Bundes Krebs in Deutschland Häufigkeiten und Trends*, volume 7. Robert Koch-Institut (Hrsg.) und Gesellschaft der epidemiologischen Krebsregister in Deutschland e.V. (Hrsg.), 2010.

[107] Robert Koch-instituts. Krebs in Deutschland 2007/2008., 2012.

[108] K Kozaki, I Imoto, A Pimkhaokham, S Hasegawa, H Tsuda, K Omura, and J Inazawa. PIK3CA mutation is an oncogenic aberration at advanced stages of oral squamous cell carcinoma. *Cancer Sci*, 97(12):1351–1358, 2006.

[109] T K Ku, D C Nguyen, M Karaman, P Gill, J G Hacia, and D L Crowe. Loss of p53 expression correlates with metastatic phenotype and transcriptional profile in a new mouse model of head and neck cancer. *Mol Cancer Res*, 5(4):351–362, 2007.

[110] S K Kundu and M Nestor. Targeted therapy in head and neck cancer. *Tumour Biol*, 33(3):707–721, 2012.

[111] H Kuniyasu, Y Chihara, and T Takahashi. Co-expression of receptor for advanced glycation end products and the ligand amphoterin associates closely with metastasis of colorectal cancer. *Oncol Rep*, 10(2):445–448, 2003.

[112] Hiroki Kuniyasu, Yoshitomo Chihara, and Hideaki Kondo. Differential effects between amphoterin and advanced glycation end products on colon cancer cells. *International journal of cancer. Journal international du cancer*, 104(6):722–7, May 2003.

[113] Hiroki Kuniyasu, Naohide Oue, Atsuko Wakikawa, Hideo Shigeishi, Norimasa Matsutani, Kazuya Kuraoka, Reiko Ito, Hiroshi Yokozaki, and Wataru Yasui. Expression of receptors for advanced glycation end-products (RAGE) is closely associated with the invasive and metastatic activity of gastric cancer. *The Journal of pathology*, 196(2):163–70, February 2002.

[114] D I Kutler, A D Auerbach, J Satagopan, P F Giampietro, S D Batish, A G Huvos, A Goberdhan, J P Shah, and B Singh. High incidence of head and neck squamous cell carcinoma in patients with Fanconi anemia. *Arch Otolaryngol Head Neck Surg*, 129(1):106–112, 2003.

[115] E Lagasse and I L Weissman. Mouse Mrp8 and Mrp14, 2 Intracellular Calcium-Binding Proteins Associated with the Development of the Myeloid Lineage. *Blood*, 79(8):1907–1915, 1992.

[116] R Landesberg, V Woo, L Huang, M Cozin, Y Lu, C Bailey, W Qu, C Pulse, and A M Schmidt. The expression of the receptor for glycation endproducts (RAGE) in oral squamous cell carcinomas. *Oral Surg Oral Med Oral Pathol Oral Radiol Endod*, 105(5):617–624, 2008.

[117] T L Lee, X P Yang, B Yan, J Friedman, P Duggal, L Bagain, G Dong, N T Yeh, J Wang, J Zhou, A Elkahloun, C Van Waes, and Z Chen. A novel nuclear factor-kappa B gene signature is differentially expressed in head and neck squamous cell carcinomas in association with TP53 status. *Clinical Cancer Research*, 13(19):5680–5691, 2007.

[118] C R Leemans, B J Braakhuis, and R H Brakenhoff. The molecular biology of head and neck cancer. *Nat Rev Cancer*, 11(1):9–22, 2011.

[119] B Leuner, M Max, K Thamm, C Kausler, Y Yakobus, A Bierhaus, S Sel, B Hofmann, R E Silber, A Simm, and N Nass. RAGE influences obesity in mice. Effects of the presence of RAGE on weight gain, AGE accumulation, and insulin levels in mice on a high fat diet. *Z Gerontol Geriatr*, 45(2):102–108, 2012.

[120] J Li and A M Schmidt. Characterization and functional analysis of the promoter of RAGE, the receptor for advanced glycation end products. *Journal of Biological Chemistry*, 272(26):16498–16506, 1997.

[121] Y W Li, S J Qiu, J Fan, J Zhou, Q Gao, Y S Xiao, and Y F Xu. Intratumoral neutrophils: a poor prognostic factor for hepatocellular carcinoma following resection. *J Hepatol*, 54(3):497–505, 2011.

[122] B Liliensiek, M A Weigand, A Bierhaus, W Nicklas, M Kasper, S Hofer, J Plachky, H J Grone, F C Kurschus, A M Schmidt, S D Yan, E Martin, E Schleicher, D M Stern, G G Hammerling, P P Nawroth, and B Arnold. Receptor for advanced glycation end products (RAGE) regulates sepsis but not the adaptive immune response. *J Clin Invest*, 113(11):1641–1650, 2004.

[123] K M Lin and G E Austin. Functional activity of three distinct myeloperoxidase (MPO) promoters in human myeloid cells. *Leukemia*, 16(6):1143–1153, 2002.

[124] X Liu, S Togo, M Al-Mugotir, H Kim, Q Fang, T Kobayashi, X Wang, L Mao, P Bitterman, and S Rennard. NF-kappaB mediates the survival of human bronchial epithelial cells exposed to cigarette smoke extract. *Respir Res*, 9:66, 2008.

[125] E C Lutterloh, S M Opal, D D Pittman, J C Keith Jr., X Y Tan, B M Clancy, H Palmer, K Milarski, Y Sun, J E Palardy, N A Parejo, and N Kessimian. Inhibition of the RAGE products increases survival in

experimental models of severe sepsis and systemic infection. *Critical Care*, 11(6):R122, 2007.

[126] K Mak, A Manji, C Gallant-Behm, C Wiebe, D A Hart, H Larjava, and L Hakkinen. Scarless healing of oral mucosa is characterized by faster resolution of inflammation and control of myofibroblast action compared to skin wounds in the red Duroc pig model. *Journal of Dermatological Science*, 56(3):168–180, 2009.

[127] F R Mangone, M M Brentani, S Nonogaki, M D Begnami, A H Campos, F Walder, M B Carvalho, F A Soares, H Torloni, L P Kowalski, and M H Federico. Overexpression of Fos-related antigen-1 in head and neck squamous cell carcinoma. *Int J Exp Pathol*, 86(4):205–212, 2005.

[128] A C Manolakis, A N Kapsoritakis, E K Tiaka, and S P Potamianos. Calprotectin, calgranulin C, and other members of the s100 protein family in inflammatory bowel disease. *Dig Dis Sci*, 56(6):1601–1611, 2011.

[129] I Marenholz, C W Heizmann, and G Fritz. S100 proteins in mouse and man: from evolution to function and pathology (including an update of the nomenclature). *Biochem Biophys Res Commun*, 322(4):1111–1122, 2004.

[130] C Marionnet, F Bernerd, A Dumas, F Verrecchia, K Mollier, D Compan, B Bernard, M Lahfa, J Leclaire, C Medaisko, B Mehul, S Seite, A Mauviel, and L Dubertret. Modulation of gene expression induced in human epidermis by environmental stress in vivo. *J Invest Dermatol*, 121(6):1447–1458, 2003.

[131] M M McCormick, F Rahimi, Y V Bobryshev, K Gaus, H Zreiqat, H Cai, R S Lord, and C L Geczy. S100A8 and S100A9 in human arterial wall. Implications for atherogenesis. *Journal of Biological Chemistry*, 280(50):41521–41529, 2005.

[132] B Meijer, R B Gearry, and A S Day. The role of S100A12 as a systemic marker of inflammation. *Int J Inflam*, 2012:907078, 2012.

[133] G A Meijer. GLOBOCAN 1: Cancer incidence and mortality worldwide. *Journal of Clinical Pathology*, 53(2):164, 2000.

[134] B W Moore. A soluble protein characteristic of the nervous system. *Biochem Biophys Res Commun*, 19(6):739–744, 1965.

[135] M Moral, C Segrelles, M F Lara, A B Martinez-Cruz, C Lorz, M Santos, R Garcia-Escudero, J Lu, K Kiguchi, A Buitrago, C Costa, C Saiz, J L Rodriguez-Peralto, F J Martinez-Tello, M Rodriguez-Pinilla, M Sanchez-Cespedes, M Garin, T Grande, A Bravo, J DiGiovanni, and J M Paramio. Akt activation synergizes with Trp53 loss in oral epithelium to produce a novel mouse model for head and neck squamous cell carcinoma. *Cancer Res*, 69(3):1099–1108, 2009.

[136] O V Moroz, A A Antson, G N Murshudov, N J Maitland, G G Dodson, K S Wilson, I Skibshoj, E M Lukanidin, and I B Bronstein. The three-dimensional structure of human S100A12. *Acta Crystallogr D Biol Crystallogr*, 57(Pt 1):20–29, 2001.

[137] S Muller-Krebs, L P Kihm, T Madhusudhan, B Isermann, J Reiser, M Zeier, and V Schwenger. Human RAGE antibody protects against AGE-mediated podocyte dysfunction. *Nephrology Dialysis Transplantation*, 27(8):3129–3136, 2012.

[138] J N Myers, F C Holsinger, S A Jasser, B N Bekele, and I J Fidler. An orthotopic nude mouse model of oral tongue squamous cell carcinoma. *Clin Cancer Res*, 8(1):293–298, 2002.

[139] J M Nauta, J L Roodenburg, P G Nikkels, M J Witjes, and A Vermey. Comparison of epithelial dysplasia–the 4NQO rat palate model and human oral mucosa. *Int J Oral Maxillofac Surg*, 24(1 Pt 1):53–58, 1995.

[140] M Neeper, A M Schmidt, J Brett, S D Yan, F Wang, Y C E Pan, K Elliston, D Stern, and A Shaw. Cloning and Expression of a Cell-Surface Receptor for Advanced Glycosylation End-Products of Proteins. *Journal of Biological Chemistry*, 267(21):14998–15004, 1992.

[141] Julia Németh, Ilan Stein, Daniel Haag, Astrid Riehl, Thomas Longerich, Elad Horwitz, Kai Breuhahn, Christoffer Gebhardt, Peter Schirmacher, Meinhard Hahn, Yinon Ben-Neriah, Eli Pikarsky, Peter Angel, and Jochen Hess. S100A8 and S100A9 are novel nuclear factor kappa B target genes during malignant progression of murine and human liver carcinogenesis. *Hepatology (Baltimore, Md.)*, 50(4):1251–62, October 2009.

[142] N Novak, J Haberstok, T Bieber, and J P Allam. The immune privilege of the oral mucosa. *Trends Mol Med*, 14(5):191–198, 2008.

[143] T Nukui, R Ehama, M Sakaguchi, H Sonegawa, C Katagiri, T Hibino, and N H Huh. S100A8/A9, a key mediator for positive feedback growth stimulation of normal human keratinocytes. *J Cell Biochem*, 104(2):453–464, 2008.

[144] O G Opitz, Y Suliman, W C Hahn, H Harada, H E Blum, and A K Rustgi. Cyclin D1 overexpression and p53 inactivation immortalize primary oral keratinocytes by a telomerase-independent mechanism. *J Clin Invest*, 108(5):725–732, 2001.

[145] S I Pai and W H Westra. Molecular pathology of head and neck cancer: implications for diagnosis, prognosis, and treatment. *Annu Rev Pathol*, 4:49–70, 2009.

[146] L Park, K G Raman, K J Lee, Y Lu, L J Ferran Jr., W S Chow, D Stern, and A M Schmidt. Suppression of accelerated diabetic atherosclerosis

by the soluble receptor for advanced glycation endproducts. *Nat Med*, 4(9):1025–1031, 1998.

[147] D M Parkin, F Bray, J Ferlay, and P Pisani. Global cancer statistics, 2002. *CA Cancer J Clin*, 55(2):74–108, 2005.

[148] R J Passey, E Williams, A M Lichanska, C Wells, S Hu, C L Geczy, M H Little, and D A Hume. A null mutation in the inflammation-associated S100 protein S100A8 causes early resorption of the mouse embryo. *J Immunol*, 163(4):2209–2216, 1999.

[149] G S Pinkus and J L Pinkus. Myeloperoxidase: a specific marker for myeloid cells in paraffin sections. *Mod Pathol*, 4(6):733–741, 1991.

[150] M L Poeta, J Manola, M A Goldwasser, A Forastiere, N Benoit, J A Califano, J A Ridge, J Goodwin, D Kenady, J Saunders, W Westra, D Sidransky, and W M Koch. TP53 mutations and survival in squamous-cell carcinoma of the head and neck. *N Engl J Med*, 357(25):2552–2561, 2007.

[151] W Qiu, F Schonleben, X Li, D J Ho, L G Close, S Manolidis, B P Bennett, and G H Su. PIK3CA mutations in head and neck squamous cell carcinoma. *Clin Cancer Res*, 12(5):1441–1446, 2006.

[152] A Rammes, J Roth, M Goebeler, M Klempt, M Hartmann, and C Sorg. Myeloid-related protein (MRP) 8 and MRP14, calcium-binding proteins of the S100 family, are secreted by activated monocytes via a novel, tubulin-dependent pathway. *Journal of Biological Chemistry*, 272(14):9496–9502, 1997.

[153] D Ramotar, E Belanger, I Brodeur, J Y Masson, and E A Drobetsky. A yeast homologue of the human phosphotyrosyl phosphatase activator PTPA is implicated in protection against oxidative DNA damage induced by the model carcinogen 4-nitroquinoline 1-oxide. *Journal of Biological Chemistry*, 273(34):21489–21496, 1998.

[154] H L Rao, J W Chen, M Li, Y B Xiao, J Fu, Y X Zeng, M Y Cai, and D Xie. Increased intratumoral neutrophil in colorectal carcinomas correlates closely with malignant phenotype and predicts patients' adverse prognosis. *PLoS One*, 7(1):e30806, 2012.

[155] T Ravasi, K Hsu, J Goyette, K Schroder, Z Yang, F Rahimi, L P Miranda, P F Alewood, D A Hume, and C Geczy. Probing the S100 protein family through genomic and functional analysis. *Genomics*, 84(1):10–22, 2004.

[156] P R Reynolds, S D Kasteler, M G Cosio, A Sturrock, T Huecksteadt, and J R Hoidal. RAGE: developmental expression and positive feedback regulation by Egr-1 during cigarette smoke exposure in pulmonary epithelial cells. *American Journal of Physiology-Lung Cellular and Molecular Physiology*, 294(6):L1094–L1101, 2008.

[157] Astrid Riehl, Tobias Bauer, Benedikt Brors, Hauke Busch, Regina Mark, Julia Németh, Christoffer Gebhardt, Angelika Bierhaus, Peter Nawroth, Roland Eils, Rainer König, Peter Angel, and Jochen Hess. Identification of the Rage-dependent gene regulatory network in a mouse model of skin inflammation. *BMC genomics*, 11:537, January 2010.

[158] Astrid Riehl, Julia Németh, Peter Angel, and Jochen Hess. The receptor RAGE: Bridging inflammation and cancer. *Cell communication and signaling : CCS*, 7:12, January 2009.

[159] M J Robinson and N Hogg. A comparison of human S100A12 with MRP-14 (S100A9). *Biochem Biophys Res Commun*, 275(3):865–870, 2000.

[160] M J Robinson, P Tessier, R Poulsom, and N Hogg. The S100 family heterodimer, MRP-8/14, binds with high affinity to heparin and heparan sulfate glycosaminoglycans on endothelial cells. *Journal of Biological Chemistry*, 277(5):3658–3665, 2002.

[161] M Roesch Ely, M Nees, S Karsai, I Magele, R Bogumil, S Vorderwulbecke, A Ruess, A Dietz, M Schnolzer, and F X Bosch. Transcript and proteome analysis reveals reduced expression of calgranulins in head and neck squamous cell carcinoma. *Eur J Cell Biol*, 84(2-3):431–444, 2005.

[162] M Roesch-Ely, M Nees, S Karsai, A Ruess, R Bogumil, U Warnken, M Schnolzer, A Dietz, P K Plinkert, C Hofele, and F X Bosch. Proteomic analysis reveals successive aberrations in protein expression from healthy mucosa to invasive head and neck cancer. *Oncogene*, 26(1):54–64, 2007.

[163] S M Rothenberg and L W Ellisen. The molecular pathogenesis of head and neck squamous cell carcinoma. *J Clin Invest*, 122(6):1951–1957, 2012.

[164] C Ryckman, K Vandal, P Rouleau, M Talbot, and P A Tessier. Proinflammatory activities of S100: proteins S100A8, S100A9, and S100A8/A9 induce neutrophil chemotaxis and adhesion. *J Immunol*, 170(6):3233–3242, 2003.

[165] M Sakaguchi, M Miyazaki, M Takaishi, Y Sakaguchi, E Makino, N Kataoka, H Yamada, M Namba, and N H Huh. S100C/A11 is a key mediator of Ca2+-induced growth inhibition of human epidermal keratinocytes. *Journal of Cell Biology*, 163(4):825–835, 2003.

[166] D Saranath, S E Chang, L T Bhoite, R G Panchal, I B Kerr, A R Mehta, N W Johnson, and M G Deo. High frequency mutation in codons 12 and 61 of H-ras oncogene in chewing tobacco-related human oral carcinoma in India. *Br J Cancer*, 63(4):573–578, 1991.

[167] D Saranath, R G Panchal, R Nair, A R Mehta, V D Sanghavi, and M G Deo. Amplification and overexpression of epidermal growth factor receptor gene in human oropharyngeal cancer. *Eur J Cancer B Oral Oncol*, 28B(2):139–143, 1992.

[168] T Sasahira, T Kirita, U K Bhawal, M Ikeda, A Nagasawa, K Yamamoto, and H Kuniyasu. The expression of receptor for advanced glycation end products is associated with angiogenesis in human oral squamous cell carcinoma. *Virchows Arch*, 450(3):287–295, 2007.

[169] T Sasahira, T Kirita, U K Bhawal, K Yamamoto, H Ohmori, K Fujii, and H Kuniyasu. Receptor for advanced glycation end products (RAGE) is important in the prediction of recurrence in human oral squamous cell carcinoma. *Histopathology*, 51(2):166–172, 2007.

[170] P Scaffidi, T Misteli, and M E Bianchi. Release of chromatin protein HMGB1 by necrotic cells triggers inflammation. *Nature*, 418(6894):191–195, 2002.

[171] A M Schmidt, S D Yan, S F Yan, and D M Stern. The multiligand receptor RAGE as a progression factor amplifying immune and inflammatory responses. *J Clin Invest*, 108(7):949–955, 2001.

[172] C Segrelles, J Lu, B Hammann, M Santos, M Moral, J L Cascallana, M F Lara, O Rho, S Carbajal, J Traag, L Beltran, A B Martinez-Cruz, R Garcia-Escudero, C Lorz, S Ruiz, A Bravo, J M Paramio, and J DiGiovanni. Deregulated activity of Akt in epithelial basal cells induces spontaneous tumors and heightened sensitivity to skin carcinogenesis. *Cancer Res*, 67(22):10879–10888, 2007.

[173] J J C Sheu, C H Hua, L Wan, Y J Lin, A T Lai, H C Tseng, N Jinawath, M H Tsai, N W Chang, C F Lin, C C Lin, L J Hsieh, T L Wang, I M Shih, and F J Tsai. Functional Genomic Analysis Identified Epidermal Growth Factor Receptor Activation as the Most Common Genetic Event in Oral Squamous Cell Carcinoma. *Cancer Res*, 69(6):2568–2576, 2009.

[174] D M Shin, N J Donato, R Perez-Soler, H J Shin, J Y Wu, P Zhang, K Lawhorn, F R Khuri, B S Glisson, J Myers, G Clayman, D Pfister, J Falcey, H Waksal, J Mendelsohn, and W K Hong. Epidermal growth factor receptor-targeted therapy with C225 and cisplatin in patients with head and neck cancer. *Clin Cancer Res*, 7(5):1204–1213, 2001.

[175] G P Sims, D C Rowe, S T Rietdijk, R Herbst, and A J Coyle. HMGB1 and RAGE in inflammation and cancer. *Annu Rev Immunol*, 28:367–388, 2010.

[176] K M Skubitz, K D Campbell, and A P N Skubitz. CD66a, CD66b, CD66c, and CD66d each independently stimulate neutrophils. *J Leukoc Biol*, 60(1):106–117, 1996.

[177] D P Slaughter, H W Southwick, and W Smejkal. Field cancerization in oral stratified squamous epithelium; clinical implications of multicentric origin. *Cancer*, 6(5):963–968, 1953.

[178] G Solinas, G Germano, A Mantovani, and P Allavena. Tumor-associated

macrophages (TAM) as major players of the cancer-related inflammation. *J Leukoc Biol*, 86(5):1065–1073, 2009.

[179] S Song, H C Pitot, and P F Lambert. The human papillomavirus type 16 E6 gene alone is sufficient to induce carcinomas in transgenic animals. *J Virol*, 73(7):5887–5893, 1999.

[180] C H Squarize, R M Castilho, V Sriuranpong, D S Pinto Jr., and J S Gutkind. Molecular cross-talk between the NFkappaB and STAT3 signaling pathways in head and neck squamous cell carcinoma. *Neoplasia*, 8(9):733–746, 2006.

[181] Christopher A Squier. Human oral mucosa : development, structure, and function, 2011.

[182] G Srikrishna. S100A8 and S100A9: new insights into their roles in malignancy. *J Innate Immun*, 4(1):31–40, 2012.

[183] G Srikrishna, H J Huttunen, L Johansson, B Weigle, Y Yamaguchi, H Rauvala, and H H Freeze. N -Glycans on the receptor for advanced glycation end products influence amphoterin binding and neurite outgrowth. *J Neurochem*, 80(6):998–1008, 2002.

[184] K Starska, E Forma, M Brys, E Glowacka, I Lewy-Trenda, M Lukomski, and W M Krajewska. The expression of TLR pathway molecules in peripheral blood mononuclear cells and their relationship with tumor invasion and cytokine secretion in laryngeal carcinoma. *Advances in Medical Sciences*, 57(1):124–135, 2012.

[185] M Steinbakk, C F Naess-Andresen, E Lingaas, I Dale, P Brandtzaeg, and M K Fagerhol. Antimicrobial actions of calcium binding leucocyte L1 protein, calprotectin. *Lancet*, 336(8718):763–765, 1990.

[186] J A Stogsdill, M P Stogsdill, J L Porter, J M Hancock, A B Robinson, and P R Reynolds. Embryonic overexpression of receptors for advanced glycation end-products by alveolar epithelium induces an imbalance between proliferation and apoptosis. *Am J Respir Cell Mol Biol*, 47(1):60–66, 2012.

[187] N Stransky, A M Egloff, A D Tward, A D Kostic, K Cibulskis, A Sivachenko, G V Kryukov, M S Lawrence, C Sougnez, A McKenna, E Shefler, A H Ramos, P Stojanov, S L Carter, D Voet, M L Cortes, D Auclair, M F Berger, G Saksena, C Guiducci, R C Onofrio, M Parkin, M Romkes, J L Weissfeld, R R Seethala, L Wang, C Rangel-Escareno, J C Fernandez-Lopez, A Hidalgo-Miranda, J Melendez-Zajgla, W Winckler, K Ardlie, S B Gabriel, M Meyerson, E S Lander, G Getz, T R Golub, L A Garraway, and J R Grandis. The mutational landscape of head and neck squamous cell carcinoma. *Science*, 333(6046):1157–1160, 2011.

[188] E Sturchler, A Galichet, M Weibel, E Leclerc, and C W Heizmann.

Site-specific blockade of RAGE-Vd prevents amyloid-beta oligomer neurotoxicity. *J Neurosci*, 28(20):5149–5158, 2008.

[189] M J Szczepanski, M Czystowska, M Szajnik, M Harasymczuk, M Boyiadzis, A Kruk-Zagajewska, W Szyfter, J Zeromski, and T L Whiteside. Triggering of Toll-like receptor 4 expressed on human head and neck squamous cell carcinoma promotes tumor development and protects the tumor from immune attack. *Cancer Res*, 69(7):3105–3113, 2009.

[190] A M Szpaderska, J D Zuckerman, and L A DiPietro. Differential injury responses in oral mucosal and cutaneous wounds. *J Dent Res*, 82(8):621–626, 2003.

[191] M P Tabor, B J Braakhuis, J E van der Wal, P J van Diest, C R Leemans, R H Brakenhoff, and J A Kummer. Comparative molecular and histological grading of epithelial dysplasia of the oral cavity and the oropharynx. *J Pathol*, 199(3):354–360, 2003.

[192] A Taguchi, D C Blood, G del Toro, A Canet, D C Lee, W Qu, N Tanji, Y Lu, E Lalla, C Fu, M A Hofmann, T Kislinger, M Ingram, A Lu, H Tanaka, O Hori, S Ogawa, D M Stern, and A M Schmidt. Blockade of RAGE-amphoterin signalling suppresses tumour growth and metastases. *Nature*, 405(6784):354–360, 2000.

[193] K Takenaga, H Nakanishi, K Wada, M Suzuki, O Matsuzaki, A Matsuura, and H Endo. Increased expression of S100A4, a metastasis-associated gene, in human colorectal adenocarcinomas. *Clin Cancer Res*, 3(12 Pt 1):2309–2316, 1997.

[194] X H Tang, B Knudsen, D Bemis, S Tickoo, and L J Gudas. Oral cavity and esophageal carcinogenesis modeled in carcinogen-treated mice. *Clin Cancer Res*, 10(1 Pt 1):301–313, 2004.

[195] J Tanuma, H Shisa, H Hiai, S Higashi, Y Yamada, T Kamoto, Y Hirayama, H Matsuuchi, and M Kitano. Quantitative trait loci affecting 4-nitroquinoline 1-oxide-induced tongue carcinogenesis in the rat. *Cancer Res*, 58(8):1660–1664, 1998.

[196] T Tateno, S Ueno, K Hiwatashi, M Matsumoto, H Okumura, T Setoyama, Y Uchikado, M Sakoda, F Kubo, S Ishigami, H Shinchi, and S Natsugoe. Expression of receptor for advanced glycation end products (RAGE) is related to prognosis in patients with esophageal squamous cell carcinoma. *Ann Surg Oncol*, 16(2):440–446, 2009.

[197] V Thallas-Bonke, M T Coughlan, A L Tan, B E Harcourt, P E Morgan, M J Davies, L A Bach, M E Cooper, and J M Forbes. Targeting the AGE-RAGE axis improves renal function in the context of a healthy diet low in AGE content. *Nephrology (Carlton)*, 2012.

[198] G R Thomas, H Nadiminti, and J Regalado. Molecular predictors of

clinical outcome in patients with head and neck squamous cell carcinoma. *Int J Exp Pathol*, 86(6):347–363, 2005.

[199] F Toure, J M Zahm, R Garnotel, E Lambert, N Bonnet, A M Schmidt, F Vitry, J Chanard, P Gillery, and P Rieu. Receptor for advanced glycation end-products (RAGE) modulates neutrophil adhesion and migration on glycoxidated extracellular matrix. *Biochem J*, 416(2):255–261, 2008.

[200] S C Tremmel, K Gotte, S Popp, S Weber, K Hormann, C R Bartram, and A Jauch. Intratumoral genomic heterogeneity in advanced head and neck cancer detected by comparative genomic hybridization. *Cancer Genet Cytogenet*, 144(2):165–174, 2003.

[201] O Turovskaya, D Foell, P Sinha, T Vogl, R Newlin, J Nayak, M Nguyen, A Olsson, P P Nawroth, A Bierhaus, N Varki, M Kronenberg, H H Freeze, and G Srikrishna. RAGE, carboxylated glycans and S100A8/A9 play essential roles in colitis-associated carcinogenesis. *Carcinogenesis*, 29(10):2035–2043, 2008.

[202] V Turusov, N Day, L Andrianov, and D Jain. Influence of dose on skin tumors induced in mice by single application of 7,12-dimethylbenz(a)anthracene. *J Natl Cancer Inst*, 47(1):105–111, 1971.

[203] M Uhlen, P Oksvold, L Fagerberg, E Lundberg, K Jonasson, M Forsberg, M Zwahlen, C Kampf, K Wester, S Hober, H Wernerus, L Bjorling, and F Ponten. Towards a knowledge-based Human Protein Atlas. *Nat Biotechnol*, 28(12):1248–1250, 2010.

[204] Ravindra Uppaluri, Gavin P Dunn, and James S Lewis. Focus on TILs: prognostic significance of tumor infiltrating lymphocytes in head and neck cancers. *Cancer immunity*, 8:16, January 2008.

[205] V M van Houten, M P Tabor, M W van den Brekel, J A Kummer, F Denkers, J Dijkstra, R Leemans, I van der Waal, G B Snow, and R H Brakenhoff. Mutated p53 as a molecular marker for the diagnosis of head and neck cancer. *J Pathol*, 198(4):476–486, 2002.

[206] T Vogl, K Tenbrock, S Ludwig, N Leukert, C Ehrhardt, M A van Zoelen, W Nacken, D Foell, T van der Poll, C Sorg, and J Roth. Mrp8 and Mrp14 are endogenous activators of Toll-like receptor 4, promoting lethal, endotoxin-induced shock. *Nat Med*, 13(9):1042–1049, 2007.

[207] Thomas Vogl, Stephan Ludwig, Matthias Goebeler, Anke Strey, Irmgard S Thorey, Rudolf Reichelt, Dirk Foell, Volker Gerke, Marie P Manitz, Wolfgang Nacken, Sabine Werner, Clemens Sorg, and Johannes Roth. MRP8 and MRP14 control microtubule reorganization during transendothelial migration of phagocytes. *Blood*, 104(13):4260–8, December 2004.

[208] B H A von Rahden, H J Stein, F Puhringer, I Koch, R Langer, G Piontek, J R Siewert, H Hofler, and M Sarbia. Coexpression of cyclooxyge-

nases (COX-1, COX-2) and vascular endothelial growth factors (VEGF-A, VEGF-C) in esophageal adenocarcinoma. *Cancer Res*, 65(12):5038–5044, 2005.

[209] A Voss, G Bode, C Sopalla, M Benedyk, G Varga, M Bohm, W Nacken, and C Kerkhoff. Expression of S100A8/A9 in HaCaT keratinocytes alters the rate of cell proliferation and differentiation. *FEBS Lett*, 585(2):440–446, 2011.

[210] S G Wan, C Taccioli, Y Jiang, H Chen, K J Smalley, K Huang, X P Liu, J L Farber, C M Croce, and L Y Fong. Zinc deficiency activates S100A8 inflammation in the absence of COX-2 and promotes murine oral-esophageal tumor progression. *Int J Cancer*, 129(2):331–345, 2011.

[211] L C Wang, L Thomsen, R Sutherland, C B Reddy, S M Tijono, C J Chen, C E Angel, P R Dunbar, and L M Ching. Neutrophil influx and chemokine production during the early phases of the antitumor response to the vascular disrupting agent DMXAA (ASA404). *Neoplasia*, 11(8):793–803, 2009.

[212] C A Wild, S Brandau, M Lindemann, R Lotfi, T K Hoffmann, S Lang, and C Bergmann. Toll-like Receptors in Regulatory T Cells of Patients With Head and Neck Cancer. *Arch Otolaryngol Head Neck Surg*, 136(12):1253–1259, 2010.

[213] T Yen, C A Harrison, J M Devery, S Leong, S E Iismaa, T Yoshimura, and C L Geczy. Induction of the S100 chemotactic protein, CP-10, in murine microvascular endothelial cells by proinflammatory stimuli. *Blood*, 90(12):4812–4821, 1997.

[214] H Y Zhang, X Z Zheng, X H Wang, X Y Xuan, F Wang, and S S Li. S100A4 mediated cell invasion and metastasis of esophageal squamous cell carcinoma via the regulation of MMP-2 and E-cadherin activity. *Mol Biol Rep*, 39(1):199–208, 2012.